THE OHIO STATE UNIVERSITY

JOINT SERVICES ELECTRONICS PROGRAM

Eighteenth Annual Report

L. Peters, Jr.

The Ohio State University

ElectroScience Laboratory

Department of Electrical Engineering
Columbus, Ohio 43212

Annual Report 721563-8
Contract No. N00014-89-J-1007
December 1995

Department of the Navy
Office of Naval Research
800 North Quincy Street
Arlington, Virginia 22217

A. Approved for public release; Distribution is unlimited

NOTICES

When Government drawings, specifications, or other data are used for any purpose other than in connection with a definitely related Government procurement operation, the United States Government thereby incurs no responsibility nor any obligation whatsoever, and the fact that the Government may have formulated, furnished, or in any way supplied the said drawings, specifications, or other data, is not to be regarded by implication or otherwise as in any manner licensing the holder or any other person or corporation, or conveying any rights or permission to manufacture, use, or sell any patented invention that may in any way be related thereto.

50272-101

REPORT DOCUMENTATION PAGE	1. REPORT NO.	2.	3. Recipient's Accession No.

4. Title and Subtitle Joint Services Electronics Program - Eighteenth Annual Report	5. Report Date December 1995 6.
7. Author(s) Leon Peters, Jr.	8. Performing Org. Rept. No. 721563-8
9. Performing Organization Name and Address The Ohio State University ElectroScience Laboratory 1320 Kinnear Road Columbus, OH 43212	10. Project/Task/Work Unit No. 11. Contract(C) or Grant(G) No. (C) N00014-89-K-1007 (G)
12. Sponsoring Organization Name and Address Department of the Navy, Office of Naval Research 800 North Quincy Street Arlington, Virginia 22217	13. Report Type/Period Covered Annual Report 14.

15. Supplementary Notes

16. Abstract (Limit: 200 words)

17. Document Analysis a. Descriptors

b. Identifiers/Open-Ended Terms

c. COSATI Field/Group

18. Availability Statement	19. Security Class (This Report)	21. No. of Pages
A. Approved for public release; Distribution is unlimited.	Unclassified	138
	20. Security Class (This Page) Unclassified	22. Price

(See ANSI-Z39.18) *See Instructions on Reverse* OPTIONAL FORM 272 (4-77)
Department of Commerce

Contents

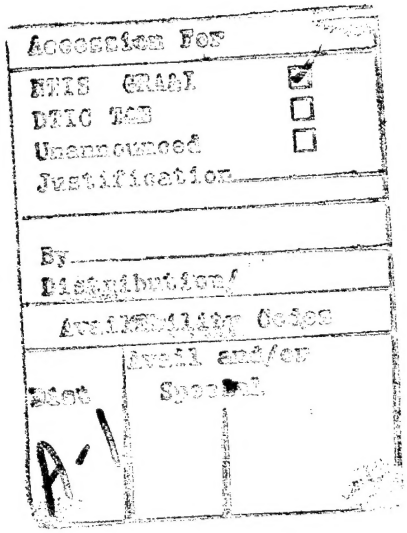

List of Figures

I. DIRECTOR'S OVERVIEW

This report represents the eighteenth annual summary of The Ohio State University Joint Services Electronics Program (JSEP). Prof. Kouyoumjian has been elected to the National Academy of Engineering. His citation denoted the development of the Uniform Theory of Diffraction. This research was supported by JSEP.

There have been a total of 39 Ph.D. and 29 M.Sc. degrees in Electrical Engineering obtained under partial JSEP sponsorship. There are currently 8 Ph.D. and 3 M.Sc. students being partially supported under JSEP.

As may be seen in the Annual Report Appendix, 14 reprints have been included for the period September 1994 to September 1995. In addition, 10 papers have already been accepted for publication in the coming year, an additional 6 papers have been submitted, and finally, 16 papers are in preparation.

II. DESCRIPTION OF SPECIAL ACCOMPLISHMENTS AND TECHNOLOGY TRANSITION

The transfer of the compact range and target identification technology initiated under JSEP support for time domain studies continues to make large advances. The large compact reflector and a modern radar of our design at ASD, Wright Patterson Air Force Base (WPAFB) has been the subject of our updated evaluation techniques resulting in substantial improvement in its operation, especially for lower frequencies. WPAFB is interested in operating at much lower frequencies than originally intended which has required a complete re-evaluation of their system at lower frequencies. This led to significant stray signal errors that cannot be solved by conventional methods, such as using 12-foot absorber. As a result of our theoretical JSEP studies, we have shown that much thinner material can be built and used to solve the WPAFB problems. An even more advanced compact range has been designed for NASA, Langley and is expected to be built this coming year. It was specifically designed for measurements as low as 300 MHz. This new range will fit in a room $40' \times 40' \times 80'$ instead of the previously required $120' \times 120' \times 360'$. The cost savings in this case are enormous.

New absorbers and feeds have been designed which are to be incorporated in the NASA and WPAFB ranges.

We continue to assist Rockwell (Tulsa) to update their RCS facilities. Our latest pulsed/CW radar system has been installed at Rockwell during the previous year. This work is on a subcontract to the ESL from the Air Force. These and other advances were only possible because of the initial JSEP support. This continues to be a case where a small investment of basic research funds have been leveraged to generate much larger support and have achieved major contributions for DoD. This has also led to OSU-ESL involvement in the study of Ultra Wide Band radar systems.

The Compact Range Technology has also resulted in an antenna for the detection of anti-personnel mines. This is a small reflector antenna which has a secondary focus in the vicinity of the ground. The extent of the focussed spot has been evaluated using the Gaussian Beam representation (see Diffraction Work Unit) for the fields of a reflector antenna and the analysis shows the spot size to be maintained for a substantial region. This is clearly the most successful antenna found for this task. The results obtained in the Finite Element Work Unit have also been used to evaluate the scattered fields from typical anti-personnel mines. We are now seeking techniques to be used to identify these mines.

One of the prime target identification candidates is the Complex Natural Resonances (CNR's) which was also funded by JSEP a decade or so ago. Such CNR's have proven useful in identifying UneXploded Ordnance (UXO's) in the past year. A demonstration was held at Tyndal Air Force Base over a series of UXO's buried in sand. They were easily detected by the Ground Penetrating Radar and their lengths were correctly deduced by the CNR identification techniques.

The UTD solutions which have been developed for analyzing the phenomena of EM radiation/scattering within paraxial regions of smooth elongated convex bodies, and also those UTD solutions which are currently under development for extending these paraxial solutions to include end caps in otherwise smooth elongated convex bodies, are of significant importance in predicting the effects of the shadowing of a jet engine inlet by the fuselage of an aircraft, when it is illuminated near nose on by a radar. It appears from our preliminary analysis that even though a significant part of an inlet is in the shadow of the fuselage to

which it is attached, the indirect illumination of the shadowed part of the inlet opening that can result from the diffraction within paraxial region of the fuselage is almost as strong as the field that would have directly illuminated the inlet cavity opening if the fuselage was absent. This work is presently being conducted for the Air Force.

Work is still continuing on the development of naval shipboard antenna models based on the generalized ray expansion (GRE) concept for the Navy. Also OSU is involved with assisting the NAVY by incorporating UTD concepts into a ray based code in order to improve its capabilities and efficiency for predicting the effects the topside environment on shipboard antenna performance.

The UTD and hybrid developments leading to systematic approaches for controlling undesired edge effects in the radiation by antennas, via material treatment, is continuing to be utilized. In particular, different types of new materials are being systematically incorporated into the design for controlling the seriously detrimental edge diffraction effects of platforms for microstrip antenna elements in GPS applications. This work is being performed for Trimble. Resistive cards are also being incorporated in a novel fashion into the design of reflector antennas for controlling edge diffraction effects without modifying the feed illumination. This work is being done for Rockwell. In addition, R-cards are being employed for making measurements on test antennas mounted in a small size ground plane such that the edge effects of these finite ground planes can be essentially removed, simulating the behavior of such antennas on large bodies such as an aircraft fuselage.

The method of moments (MM) solution for a wire attached to an arbitrary body is being integrated into the "Helicopter Antenna Radiation Prediction" (HARP) code, currently being developed under NASA support. HARP, which features a sophisticated graphical interface, is a collection of high and low frequency computer codes for analyzing the radiation from antennas on complex bodies such as helicopters, aircraft, autmobiles, etc. HARP's low frequency code is the "Electromagnetic Surface Patch Code" (ESP), which at present cannot treat a wire attached to an arbitrary surface. Thus, when HARP or ESP analyzes a monopole on a helicopter, the monopole must be replced by a dipole "floating" a short distance off the body. While this is a reasonable approximation for far zone patterns, it is impossible to compute such near zone quantities as input impedance and mutual coupling. However,

when the solution for a wire attached to an arbitrary body is integrated into ESP, HARP will be able to better model antennas on complicated support structure, and in particular compute input impedance and mutual coupling.

These programs are also in use in a recently funded Technology Transfer Program by the Ford Motor Company. This program is concerned with the design of hidden automobile antennas.

The Perfectly Matched Absorbing Layer (PML) boundary condition is likely to become the choice for finite element and finite difference codes in the near future because of its ease of implementation and its good performance. For frequency domain finite element methods, the anisotropic PML is probably the most popular choice, because many of the currently available finite element codes already can handle anisotropic materials. There are researchers who have already begun adapting the anisotropic PML to their codes including Professor John Volakis at Michigan and Professor Steve Gedney at Kentucky. At this point, the use of the anisotropic PML in the time domain is uncertain; however if it can be developed, then it offers possible advantages for time domain finite element methods.

The currently available elements for frequency domain finite element methods are not very efficient for electromagnetic modeling. The work on the solenoidal elements under JSEP funding has shown that these elements have great potential for significantly improving the performance and efficiency of finite element codes. The positive initial work will likely lead to funding from Motorola for developing finite element codes for them. The movement toward the development of numerical methods specifically for electromagnetic modeling will lead to a new generation of high performance and high efficiency codes in the near future.

It becomes clear from the above that a major portion of technology transition of JSEP research takes the form of additional supported research from other DoD agencies. Other forms of transition include former graduate students, who upon graduation are employed in DoD related positions, and publication of JSEP research results. Yet another form of such transition is represented by computer codes that incorporate the results of our research. These complex codes are available to DoD related industries for a nominal fee of $300. Last year 125 such codes were issued which approximately doubles the number issued the year before. This indicates a resurgence of interest in Electromagnetics in the DoD community.

Our JSEP research continues to focus on electromagnetics topics. The four work units included in last year's Summary report are each showing significant results.

The Diffraction Work Unit includes several subtopics. The Time Domain Uniform Theory of Diffraction (TD-UTD) concept introduced last year is showing excellent progress. Recall that the standard FD-UTD was developed under JSEP and has been very frequently used by non-OSU researchers. As noted in the Director's Overview, this led to Prof. Kouyoumjian's election to the National Academy of Engineering. This year, the TD-UTD has been extended to include a much more general wedge geometry, the slope diffraction case and the shadow side solution for the creeping wave generated by smooth convex conducting shapes. These are the very terms most used by the FD-UTD and for a long time formed the basis for such FD-UTD solutions. It is anticipated that the TD-UTD will prove as rewarding for transient solutions as the FD-UTD has been for steady state harmonic solutions.

The concept of an asymptotic analysis using Gaussian Beams (GB's) when the use of rays becomes computationally intensive or inaccurate (i.e., at caustics) is continuing. The limitation on special edge orientation has been replaced by one where a curved edge can be arbitrarily located provided it is locally plane. Research in this area is continuing and is expected to be completed soon. This activity should lead to a far more efficient and physically appealing solution when applied to synthesis of antenna feeds and also synthesis of large shaped reflectors for generating multiple, spot or contour beams. The use of GB's for the treatment and design of large planar arrays is to be investigated. They are expected to play a very significant role in the development of antenna synthesis technique for wireless communications systems, and the analysis of radomes used in conjunction with electrically large antennas.

The Integral Equations Work Unit has shifted its focus from the treatment of Artificial Media to a novel time swept approach for scattering from large bodies. The concept is to sweep over the body in finite segments with each segment terminated in a tapered R-card to eliminate edge diffraction terms. This, in essence, breaks the large body problem into a series of small bodies with a substantial reduction of computer time and resources.

The Finite Element Work Unit focussed attention on two topics this past year which should have a substantial impact on these powerful solutions for electromagnetic problems.

The first is the Perfectly Matched Absorbing Layer (PML) which is used to truncate the computation domain in differential based numerical solutions. The adaptation of anisotropic PML is considered for Time Domain Finite Element Solution. This involves a question of dynamic stability which is examined carefully. The second topic being pursued is the solenoidal edge element. It has been specifically designed to minimize errors due to numerical dispersion.

The Hybrid Studies Work Unit continues to demonstrate that it is achieving the same prominence that the original UTD has achieved by being able to treat a number of configurations that would otherwise be untreatable by any single form of analysis. This Hybrid Work Unit, of course, demonstrates the synergistic nature of our JSEP program.

As an example, the design analyses and measurement of the properties of an oscillator incorporated into an antenna has come to fruition in the past year. This incorporates the solid state electron device and antenna technology as a hybrid solution. Other examples include the use of various forms of Green's functions (impedance loaded wedges and UTD solution of coated convex surfaces) with obstacles for both radiation, radome and scattering problems. Another form of Hybrid Solution involves the Fast Multiple Method (FMM) which is gaining increasing interest by the computational community. Modification of the FMM makes use of asymptotic techniques to make this high speed solution even faster. Several interesting computational techniques, are also being examined that may ultimately be included in the Hybrid Library. These are: a) the Finite Volume Time Domain (FVTD) Solver which could prove to be superior to the FDTD Solver in some applications, and b) a more efficient UTD transition function involving Fock type integrals that appear in the UTD special Green's functions which will dramatically speed up computations for radiators mounted on convex material coated conducting surfaces.

III. DIFFRACTION STUDIES

Researchers:

R. G. Kouyoumjian, Professor Emeritus	(Phone: 614/292-7302)
P. H. Pathak, Professor	(Phone: 614/292-6097)
R. G. Rojas, Associate Professor	(Phone: 614/292-2530)
R. J. Burkholder, Senior Research Associate	(Phone: 614/292-4597)
P. R. Rousseau, Graduate Research Associate	(Phone: 614/292-7981)
P. Munk, Graduate Research Associate	(Phone: 614/292-7981)
H-T. Chou, Graduate Research Associate	(Phone: 614/292-7981)

1. Introduction

The frequency domain (FD) based uniform geometrical theory of diffraction (UTD), developed mostly at The Ohio State University and primarily under JSEP support, has proven to be an efficient analytical method for the prediction of EM radiation/scattering from electrically large, relatively complex objects for which exact analytical solutions are virtually impossible to obtain. In addition, the UTD concept is simple and it provides physical insight into the radiation/scattering mechanisms. In contrast, brute force numerical solution methods lack insight into the relevant physics and become rapidly inefficient or intractable as the radiating object becomes large in terms of the electrical wavelength.

Of course, the range of phenomena to which the UTD may be applied as an analysis/design tool depends on the availability of the pertinent canonical UTD solutions from which the UTD model of a complex radiating object can be "built up." While several canonical UTD solutions have been obtained for perfectly-conducting boundaries (e.g., curved wedges; smooth convex surface; etc.) and recently also for non-conducting or material boundaries (e.g., edges in uniform material slabs, and wedges with impedance boundary conditions, etc.), there still remain a host of important canonical UTD configurations which need to be analyzed. Furthermore, a similar basic problem to that in the frequency domain (FD) exists also in the time domain (TD), namely brute force numerical TD solutions cannot provide efficient or even tractable procedures for predicting the transient response of short

pulse excited complex radiating objects. The need for efficient TD analysis based prediction tools is motivated by the development of short pulse or ultra wide band (UWB) radars for target identification, and remote sensing. Also, it is important to predict the effects of natural and manmade electromagnetic pulses (EMP) on EM radiating systems. The FD based approaches are also cumbersome for predicting transient response because the FD solution has to be found at a very large number of discrete frequencies and then inverted numerically into the TD via the IFFT algorithm.

Thus, during the last year, the diffraction studies unit has focused on the two major issues discussed above. In particular, we have made significant progress in the development of a new TD-UTD for analyzing early to intermediate time transient response of some highly useful canonical configurations, and their generalizations, so that realistic and hence complex, pulse excited radiating objects can be handled efficiently and in a physically appealing manner via TD rays. The TD-UTD development is in addition to the important progress made in the development of new and useful FD based asymptotic HF or UTD solutions for non-conducting as well as conducting objects. The increased use of composite materials in aerospace, satellite and other antenna systems motivates the FD-UTD research on material effects on radiating objects. Specifically, in the area of transient EM analysis the TD-UTD solution for an arbitrary curved conducting wedge, whose development was indicated last year in our 1994 JSEP annual report, has been significantly extended to arrive at a TD-UTD slope diffraction solution for the same curved wedge geometry when it is excited by a pulse with a rapid spatial variation near the edge. This rapid spatial variation can occur, for example, when the pulsed antenna illuminating a wedge exhibits a null close to the edge of the wedge. The transient response by the wedge in this case is caused by the large slope (derivative) of the rapid spatial variation of the pulsed incident field, and the ordinary TD-UTD solution reported last year would produce a negligible response in this instance thus requiring the need for the slope TD-UTD curved wedge diffraction solution. In addition, a TD-UTD solution has been developed for the shadow side response of a smooth convex conducting surface illuminated by a pulsed incident field. The analytical development of TD-UTD for convex surfaces is found to be even more involved than that for the wedge, although the analytical TD-UTD solutions obtained for these geometries is still relatively simple to

use. Presently, the TD-UTD for the lit region of the convex surface is being developed. The TD-UTD is being developed separately for the lit and shadow sides of the convex boundary because the corresponding FD-UTD solution which is analytically being inverted to the TD is also obtained separately for the lit and shadow sides for reasons of convenience of analysis, but the TD-UTD lit and shadow representations should be continuous at the shadow boundary just as they are in the FD-UTD. Also, an asymptotic HF (or FD-UTD like) has been developed for an impedance wedge with arbitrary source and observer locations, and also for elongated smooth, convex conducting objects where the source and observer can again be located arbitrarily. The latter two FD solutions are crucial to the development of important hybrid combination of numerical-asymptotic methods for the analysis/design of material treated antenna configurations for optimizing antenna performance, and to the development of radiation/scattering from aerospace configurations, respectively. Some more discussion of this hybrid connection is presented later in the section on Hybrid Studies under JSEP.

Work has also progressed to extend the reflection and diffraction of general, astigmatic Gaussian beams (GB's) by smooth curved boundaries with an edge in which the edge is no longer parallel to the principal planes of the surface where the axis of the incident astigmatic GB strikes the surface or its mathematical extension past the edge beyond which the actual surface ceases to exist. This novel GB technique is expected to be useful especially in predicting EM phenomena for focused fields where even ray methods become cumbersome or inapplicable. In particular, such a GB technique is expected to be highly useful in the analysis/synthesis of large aperture antennas such as general reflectors (which can be shaped or array fed, etc.), planar phased array antennas and lens antennas.

2. Time Domain UTD (TD-UTD)

The TD-UTD concept provides a new way of examining transient electromagnetic (EM) radiation, scattering and diffraction phenomena which has been analyzed in the past for only some special canonical geometries, or for some more complicated but relatively small radiating configurations by brute force numerical methods (which depend on a particular excitation pulse shape). In particular, the TD-UTD extends the ray concept of the frequency

domain (FD) based uniform geometrical theory of diffraction (UTD) to the time domain (TD). Such a TD-UTD, when it is sufficiently developed will become as powerful as the FD based UTD; it would be able to predict the transient response of pulse excited large complex radiating objects in the form of an analytical solution given in a physically appealing manner in terms of TD rays. Since the FD based UTD is an asymptotic high frequency technique, its counterpart in the TD would provide a TD-UTD which is accurate for early to intermediate times with respect to the time of arrival of each of the various wavefronts associated with the different ray contributions. As is well known, the early to intermediate time response is produced largely by the local features of the radiating object, whereas the late time response is largely dominated by the global effects (including resonances). The development of TD-UTD is motivated by the need to analyze transient EM phenomena directly in the TD. Such an analytical prediction tool would be extremely useful for assessing the effects of short pulse radars, lightning or nuclear explosions, etc. on communication systems; it will also be useful in remote sensing and target identification applications.

Significant developments have been made in the TD-UTD area since its initiation on the JSEP program about two years ago. The developments to date in the TD-UTD have been made possible largely due to the novel use of analytic time transforms (ATT), since the TD-UTD is being developed by analytically transforming the corresponding FD based UTD solution into TD. It is important to note that the use of conventional inverse Fourier or Laplace transformations, in which time variable (t)is real, generally leads to difficulties in obtaining a TD-UTD from its FD based UTD; these difficulties are further compounded in the case when the TD-UTD must be found from a FD-UTD in which the incident, reflected or diffracted rays pass through their respective caustics. In the latter case, conventional Fourier/Laplace inversion techniques require one to essentially find the Hilbert transform which is generally extremely difficult to obtain analytically in closed form. By making the time variable (t) complex, it is possible to use the ATT and thereby make the inversion to the TD case resemble the direct Laplace transform in the conventional FD except that the usual roles of the time and frequency variables are now switched. Thus, the present TD-UTD development makes it possible to deal with concave or saddle shaped incident wavefronts (i.e., other than just convex wavefronts) with great ease. Even though the ATT

is used, the actual real time TD-UTD is obtained by taking the real part of the analytic time solution for the TD-UTD. Furthermore, the use of the ATT has also led to another important development in that it allows the TD-UTD response to a time impulsive general astigmatic incident ray field to yield in closed form the TD-UTD response to a finite energy (finite bandwidth) incident pulse via complex t convolution (as opposed to conventional real time convolution) by expanding the incident pulse in a set of generally few special basis functions whose ATT can also be found in closed form; these basis functions are simple exponentials in the "frequency domain" or FD. Many useful transient incident waveforms or pulse shapes can be synthesized by three to ten such basis functions. This result is important because it allows the convolution with a known analytic time impulse response in closed form; the efficiency and advantages gained by obtaining a closed form TD-UTD impulse response would otherwise be lost by a numerical convolution which is now avoided.

During the previous year's effort in which the TD-UTD development was initiated, use of the ATT made it possible to obtain, for the first time, a TD-UTD for an arbitrary curved perfectly conducting wedge excited by an arbitrary astigmatic time impulsive ray field. The results of this work were summarized in the 1994 JSEP annual report for last year's effort. During the present contract period the TD-UTD has been extended to two additional and important situations; namely to include the slope diffraction by an arbitrary curved conducting wedge, and to the diffraction by an arbitrary smooth convex conducting surface in the shadow region, respectively.

The TD-UTD for slope diffraction by a wedge was obtained by inverting two different corresponding FD based UTD solutions by Hwang and Kouyoumjian, and by Verrutipong and Kouyoumjian, respectively, The slope diffracted TD-UTD is required when the incident transient ray field varies rapidly in space near the point of diffraction on the edge; this is important for many antenna applications such as pulsed apertures (or slots) in edge structures, and also cases in which the antenna pattern illuminating an edge exhibits a rapid spatial variation, as for example, near a pattern null. In this instance, the slope of the TD-UTD for the curved wedge will exhibit a discontinuity near the incident/reflected shadow boundaries that can be removed by the addition of the new slope TD-UTD just as in the FD case. The ATT was used again and it was this analytic time signal representation that

made it possible to obtain the slope TD-UTD for an arbitrary wedge. The development of the slope TD-UTD for the arbitrary curved wedge was slightly more involved than the development of the TD-UTD for the arbitrary curved wedge. While the slope TD-UTD is also obtained for a general curved wedge, the numerical results based on this TD-UTD are illustrated in Figures 1 and 2 for a straight wedge because an exact TD analytical solution exists for this special case [1] and hence it can be used as a reference solution to validate the more general TD-UTD result. The field incident on the wedge in these examples is time impulsive spherical wave and it is produced by an electric or magnetic current moment (with a step current moment behavior in time) which is aimed so that the pattern null along its axis is close to the edge to produce a rapid spatial variation of the incident field at the edge. It is seen that the slope TD-UTD development based on Hwang and Kouyoumjian slope FD-UTD (denoted by "Hwa" in the figures) behaves slightly better for intermediate to later times with respect to the arrival of the diffracted wavefront, while the other slope TD-UTD based on the Verrutipong-Kouyoumjian slope FD-UTD (denoted by "Ver" in the figures) is slightly better for early times. Nevertheless, both TD-UTD results are sufficiently accurate in general in the early to intermediate times as they should be.

The diffraction by a smooth convex surface is far more involved to invert into the time domain. At the present time, a significant breakthrough has been made which allows ATT, or analytic time signal based representation to provide for the first time a TD-UTD for describing the fields on the shadow side of an arbitrary smooth convex perfectly conducting boundary. Work is in progress to obtain a similar TD-UTD result for the same configuration on the lit side of the shadow boundary; this lit zone analysis appears to be even more challenging than the shadow side. The excitation is time impulsive arbitrary astigmatic wavefront that is incident on the convex surface. It is found for the shadow side that the TD-UTD version of the FD-UTD transition function can be represented separately for the early times and the intermediate (or later) times with respect to the time of arrival of the diffracted wavefront. Furthermore, these two representations smoothly overlap thereby yielding a useful TD-UTD result. It turns out that the early time TD-UTD representation comes from an asymptotic expansion in the FD requiring a large number of so-called creeping wave mode terms to be summed in the TD; this sum has been converted to a sum on a small

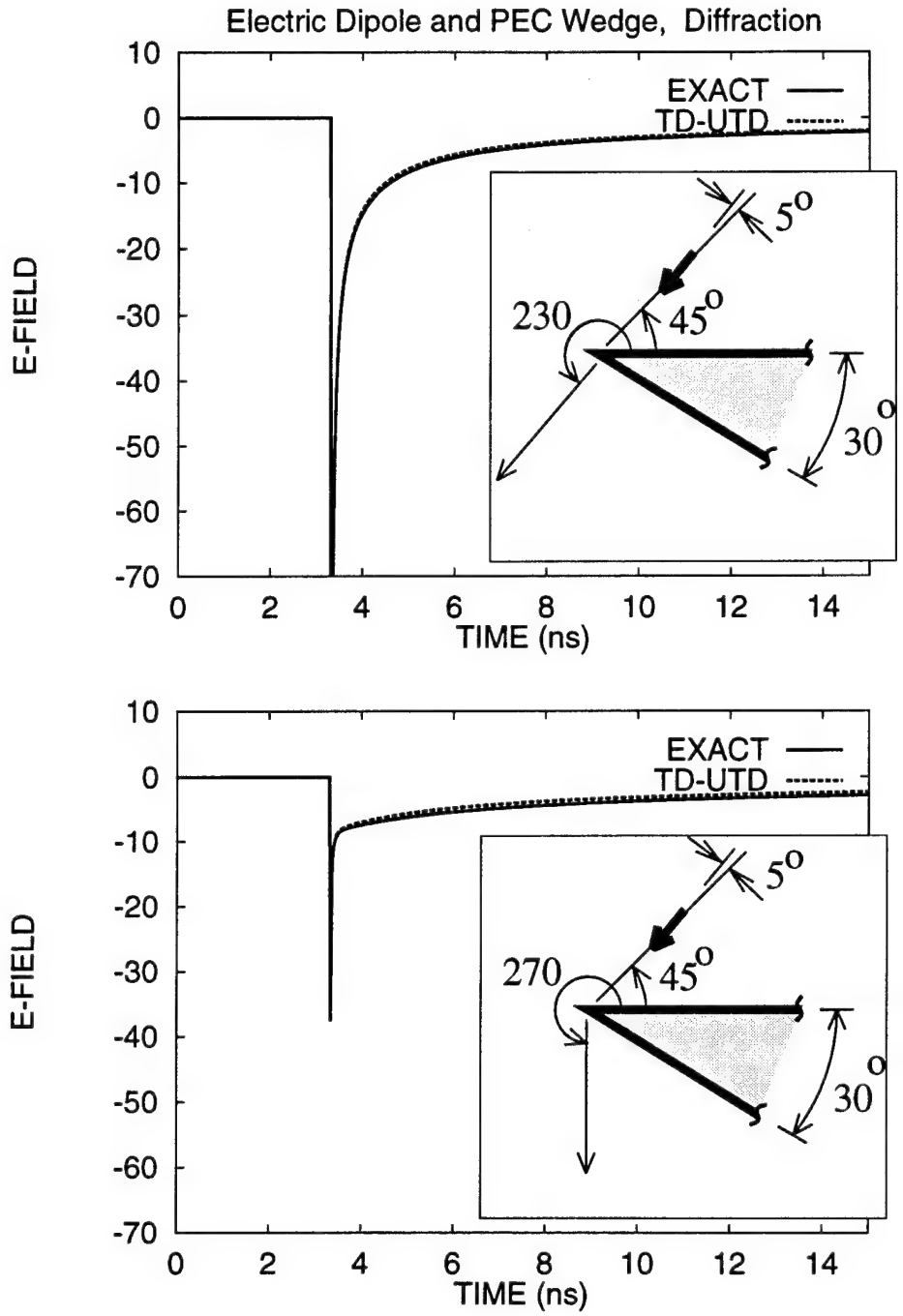

Figure 1: The TD-UTD impulse response is compared with an exact result. The infinitesimal electric current has a unit step time behavior which approximately illuminates the wedge with an impulsive spherical wave.

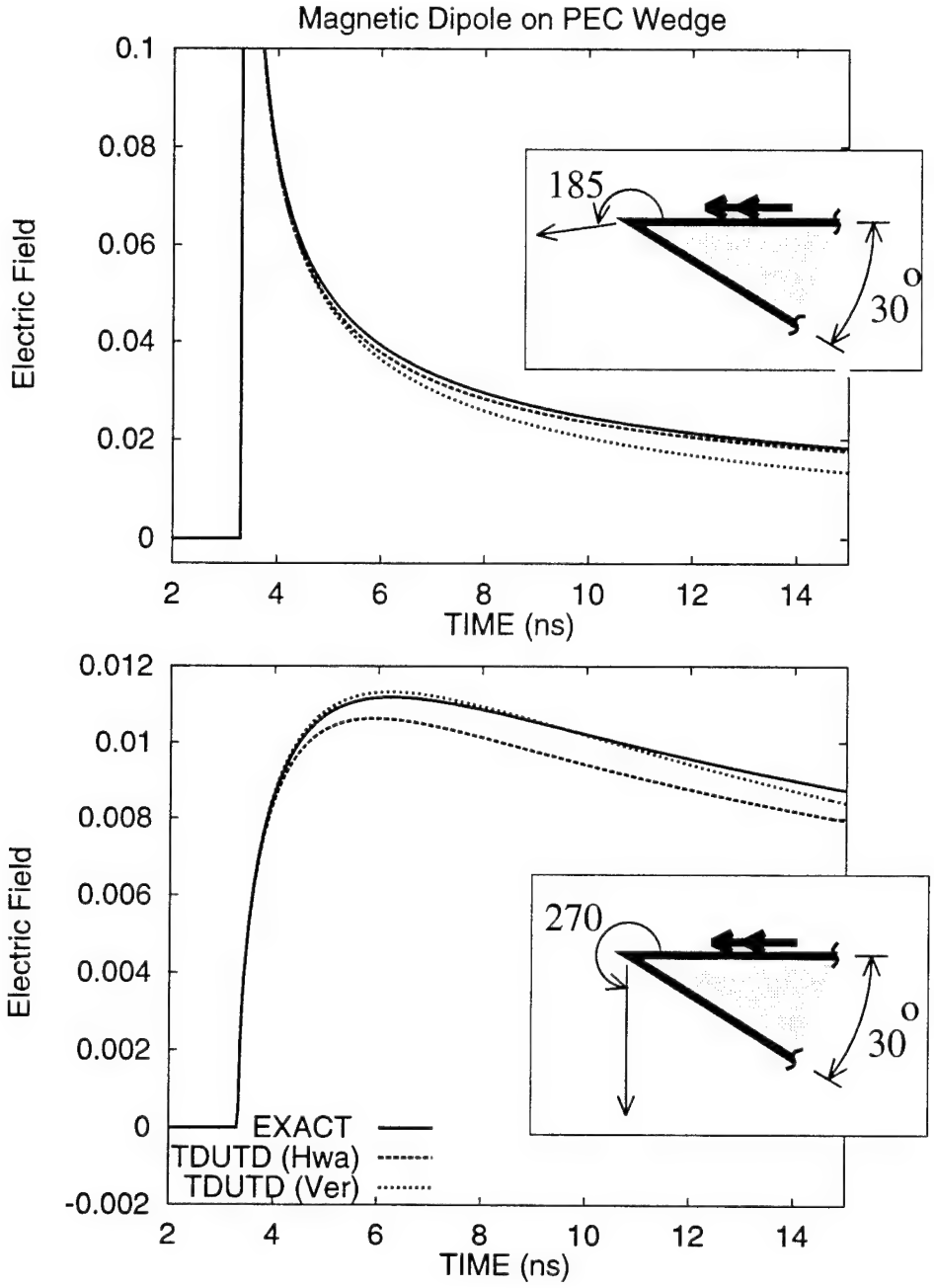

Figure 2: The two versions of the TD-UTD slope diffraction are compared with an exact result. The infinitesimal magnetic current has a unit step time behavior which approximately illuminates the wedge with an impulsive spherical wave.

number of terms with the remainder evaluated in closed form via an integral approximation. For later times, the FD-UTD transition function behaves in powers of frequency yielding a TD-UTD representation in inverse powers of time (or valid for intermediate and later times) which becomes more important near the shadow boundary. Breaking the TD-UTD into the two representations which turn out to smoothly overlap in the shadow region yields a tractable TD-UTD solution; it does not appear possible at this time to obtain a single representation. Figures 3 and 4 illustrate this remarkable overlap of the two representations for the TD-UTD diffraction by a circular cylinder. A non-uniform TD solution has been obtained previously be some researchers for the special case of a circular cylinder; in contrast the present TD-UTD is a uniform solution which is valid for an arbitrary convex surface.

Currently work is in progress, as mentioned earlier, to complete the TD-UTD development for the diffraction by a smooth convex surface by extending it into the lit region. Work has also been initiated to develop a TD version of the equivalent current method (ECM) as well as of the physical theory of diffraction (PTD) for edged bodies to augment the TD-UTD edge diffraction solution in those special cases where there is an overlap of ray caustic and shadow boundary regions in the FD so that the FD-UTD is not directly applicable and neither is the corresponding TD-UTD for that reason.

An additional related study which was undertaken deals with the development of an analytical closed form prediction of early time transient radiation from a parabolic reflector illuminated by a pulsed feed antenna at the focus. The feed antenna generates a pulsed spherical wave in this model. It is seen that if the spherical wave from the feed is taken to exhibit a step function behavior in time, then the early time radiation from the reflector exhibits an impulse like behavior on boresight. Such an impulse like radiation from a parabolic reflector was predicted originally by C. E. Baum and his co-workers [2, 3] when the feed was a TEM four wire transmission line configuration; they were able to predict the behavior of the fields in the two principal planes analytically in closed form. The present analysis proceeds in a fashion which is somewhat different than the one given previously by Baum, et al. [3] and it provides, to within the model chosen, an analytic closed form solution for the fields in any plane (rather than only the principal planes) both near and far from the reflector; furthermore, it is valid for a more general spherical wave feed illumination and it

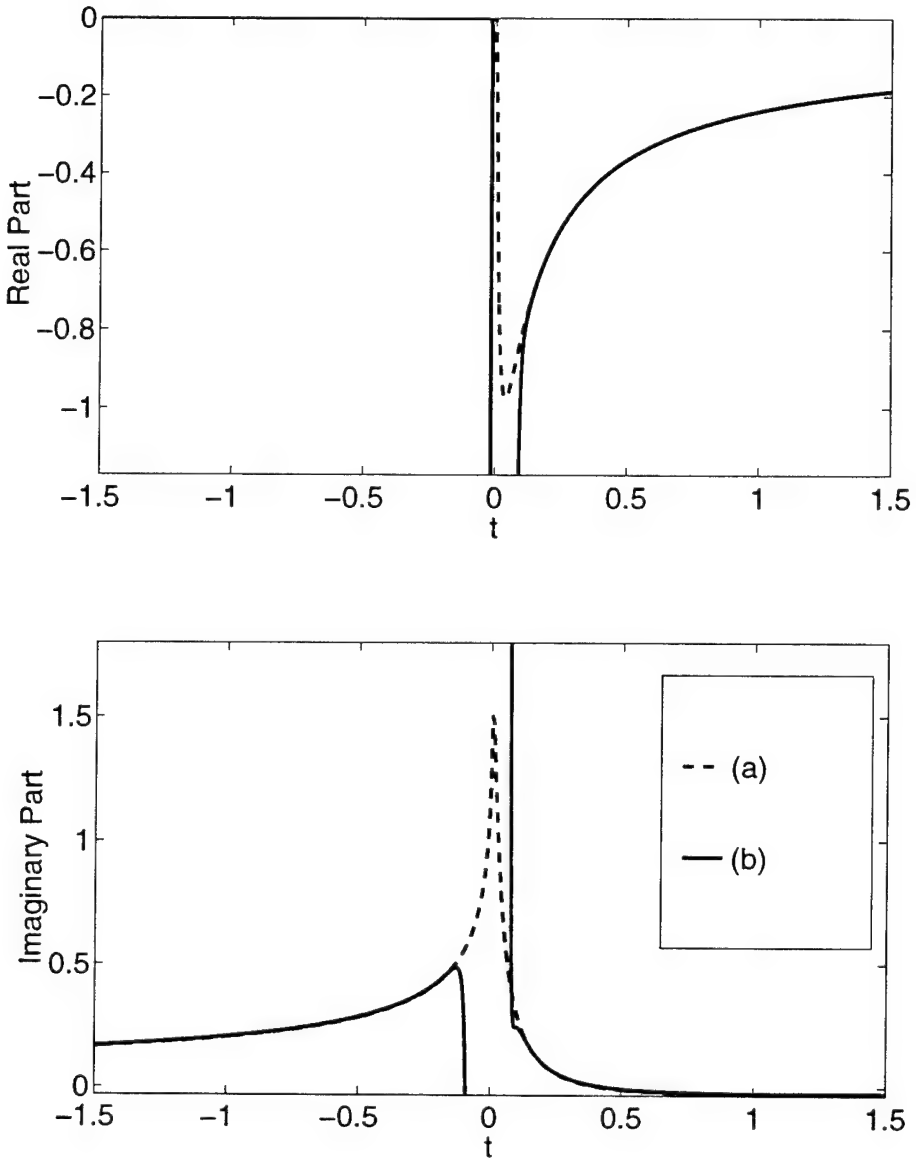

Figure 3: The special function $\overset{+}{F}{}_h^P(\Xi, t)$ when the observer is in the shadow region and $\Xi = 1$. The polarization is hard. Comparison between (a) the "early time" creeping wave mode series and (b) the "late time" representation.

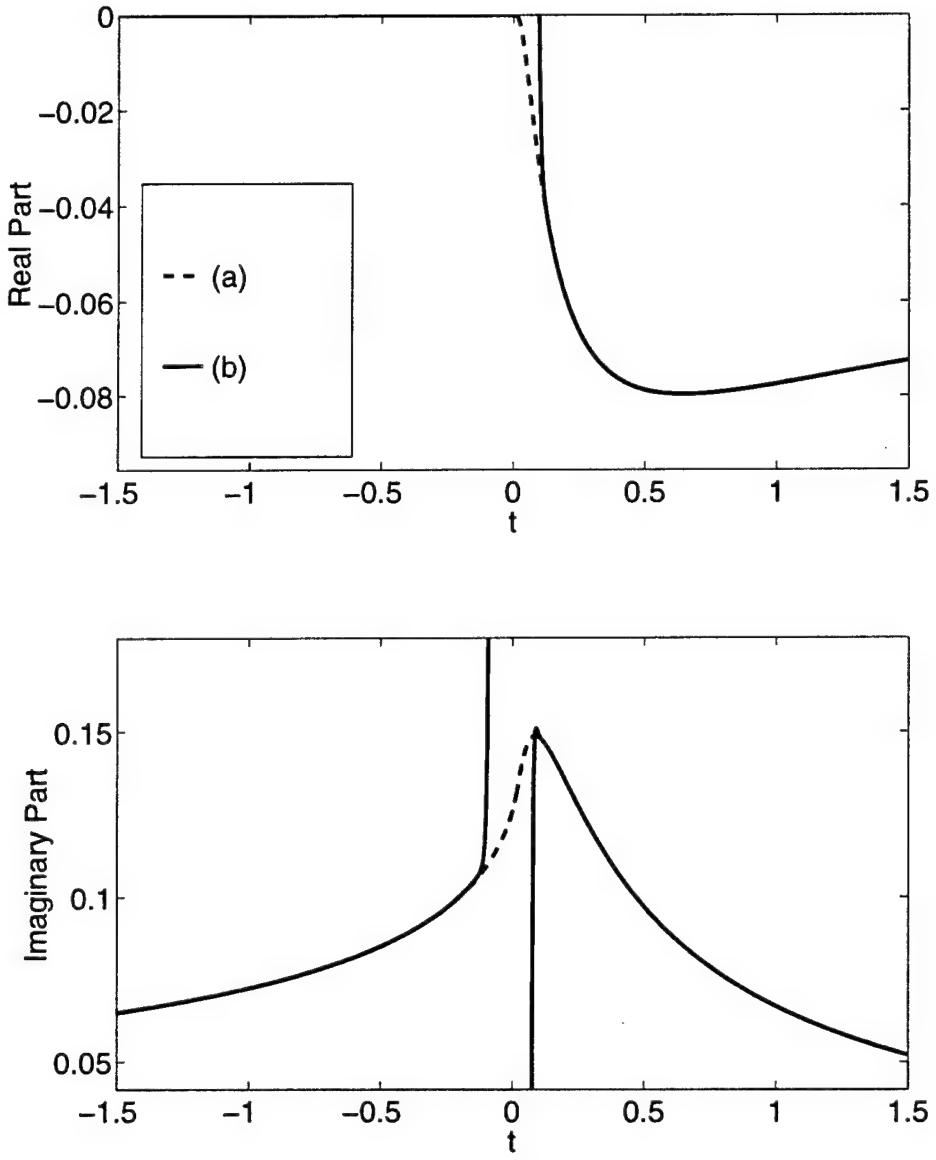

Figure 4: The special function $\overset{+P}{F}_s\ (\Xi, t)$ when the observer is in the shadow region and $\Xi = 1$. The polarization is soft. Comparison between (a) the "early time" creeping wave mode series and (b) the "late time" representation.

can be modified without any additional complications to deal with an offset parabolic reflector. In this sense, the present work extends or generalizes the earlier work on this topic. A motivation for this study is that is would be useful in the design of pulsed reflector antennas which can radiate concentrated energy for use in an impulse like radar or a short pulse radar as might be needed in target identification or remote sensing application. The analytical closed form result for the transient radiation by a parabolic reflector illuminated by a step like transient spherical wave from the feed can be differentiated with respect to time to provide the transient response of the reflector to a time impulsive spherical wave illumination from the feed; in the latter case, the reflector radiates a doublet like field on boresight. In addition, the transient radiation from the reflector when it is illuminated by the feed with a transient spherical wave and a given pulse shape can be synthesized via convolution with the closed form impulse response (i.e., response of the reflector to a time impulsive spherical wave from the feed). An example of the impulse like radiation from the parabolic reflector when it is illuminated by a transient step (function) type spherical wave is shown in the more general $\phi = 45°$ plane (rather than the principal planes at $\phi = 0°; 90°$) in Figures 5 and 6, for two different distances from the reflector, respectively. On boresight, the field behaves more and more like an impulse as one moves farther away from the reflector; it is noted that this impulse like character is evidenced by the fact that the net height of this impulse like field on boresight is independent of the distance away from the reflector! The pulse width of the impulse like transient field (on boresight) decreases with distance but its pulse amplitude increases to maintain the same area under the pulse; however, the additional range effect (or decrease in the field due to an algebraic range factor) exactly nullifies this increase in the pulse height giving a net field amplitude which stays constant with distance from the reflector along its axis (boresight). Figures 5 and 6 also indicate the manner in which the impulse like behavior is lost as one moves off boresight. The level of the field off boresight in the $\phi = 45°$ plane is seen to lie somewhere in between its two different values in the principal $\phi = 0°$ and $\phi = 90°$ planes, respectively. The general trend of the field behavior in the two principal planes ($\phi = 0°; \phi = 90°$ planes) is seen to be similar to that in the $\phi = 45°$ plane (illustrated here in Figures 5 and 6), or for that matter in any arbitrary $\phi =$ constant plane.

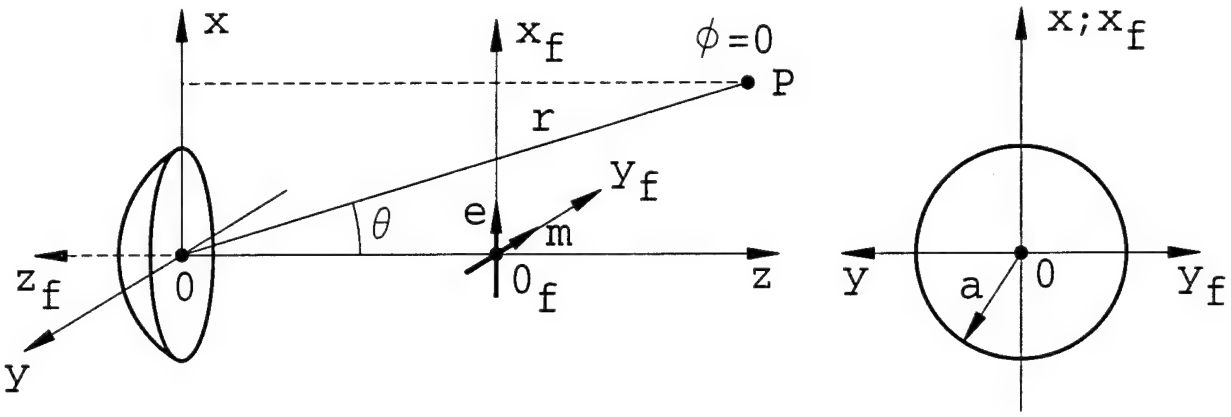

D = 2a = diameter ; F = focal length

r = range

D = 2m ; F = 2D

r = 10m ; ϕ = 45°

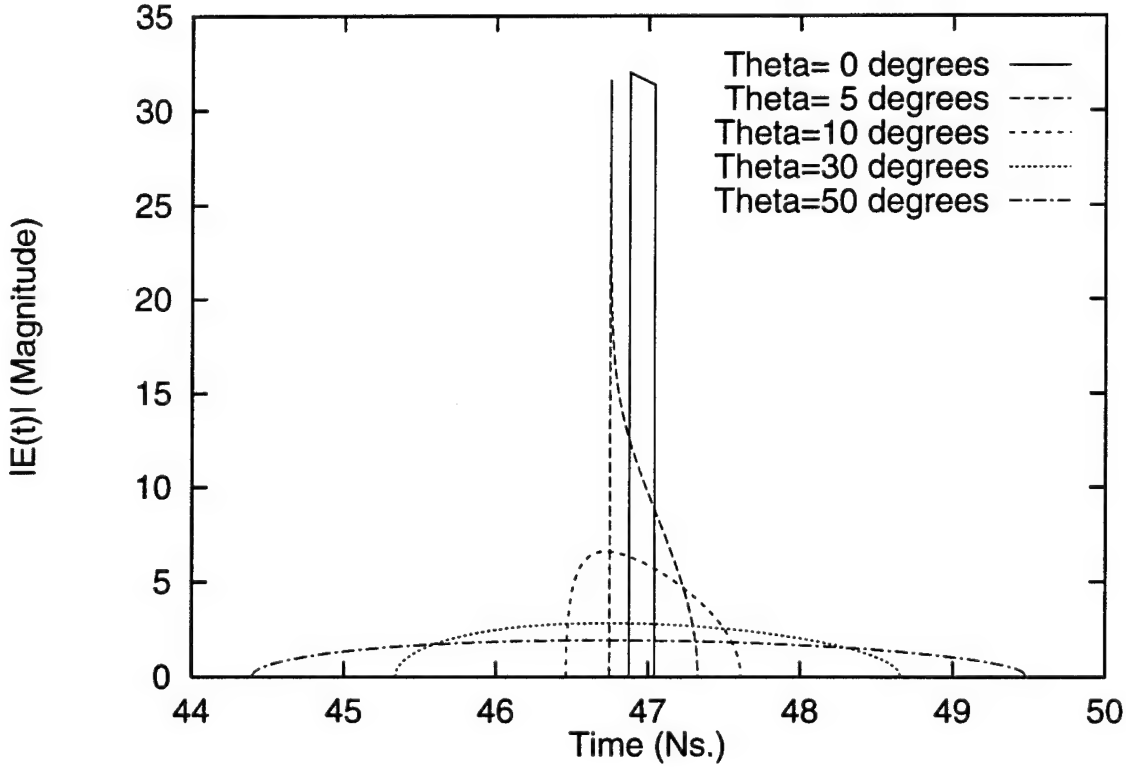

Figure 5: Behavior of impulse like radiation at 10 m from 0 along boresight.

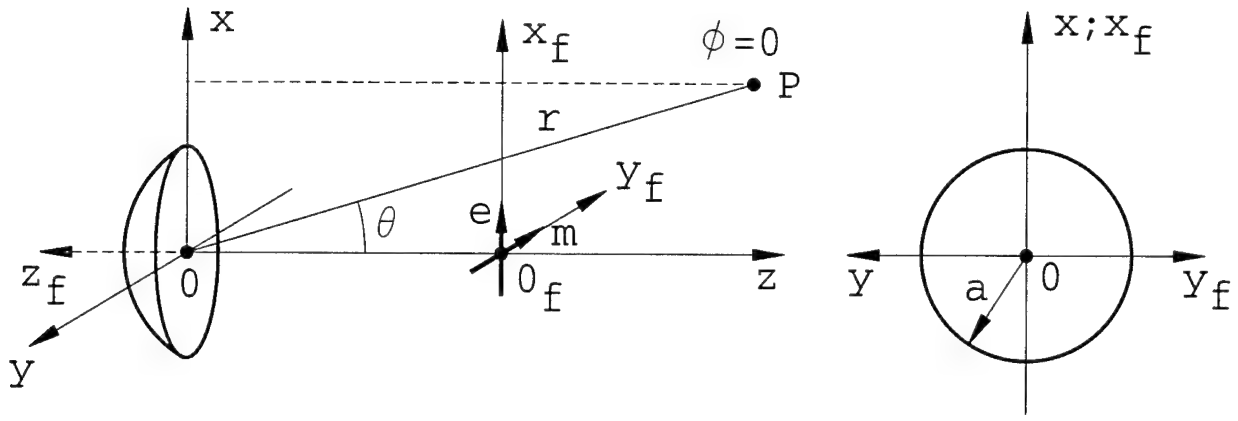

D = 2a = diameter ; F = focal length

r = range

D = 2m ; F = 2D

r = 100m ; ϕ = 45°

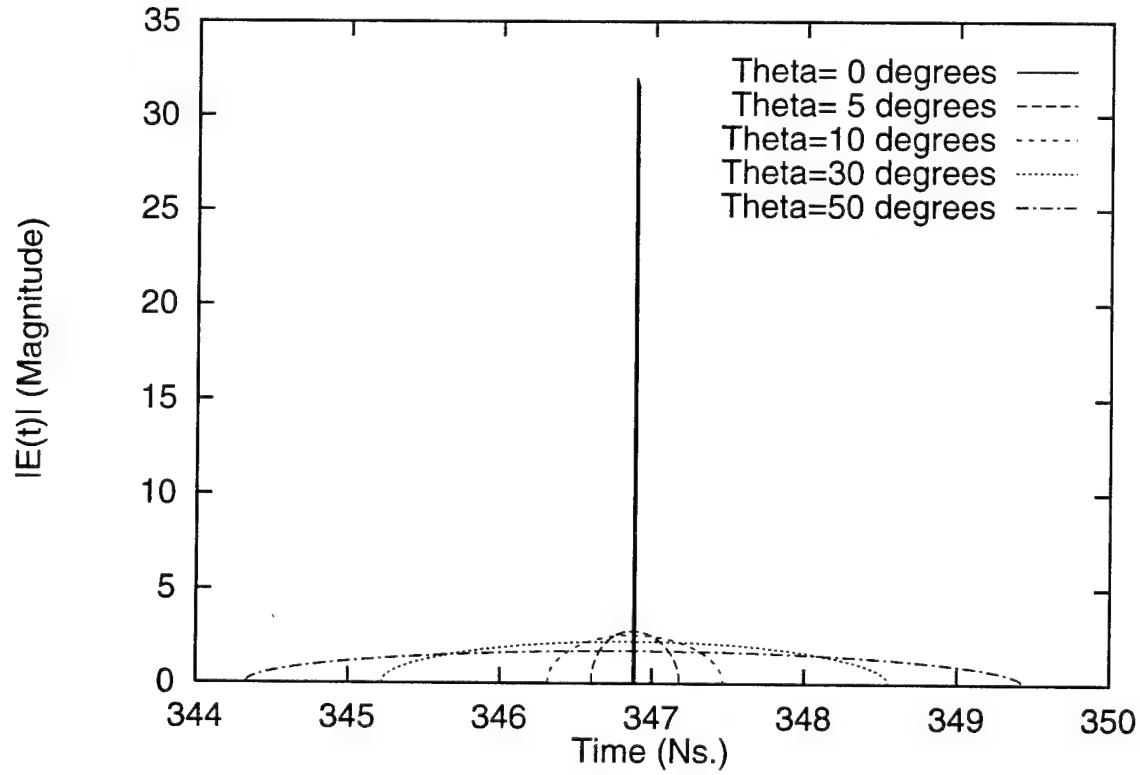

Figure 6: Behavior of impulse like radiation at 100 m from 0 along boresight.

3. Gaussian Beam Methods

Development of Gaussian beam (GB) based methods were initiated on our JSEP for analyzing a class of high frequency radiation/scattering phenomena that cannot be analyzed efficiently, or in a tractable fashion, by other approaches including ray methods. In particular, difficulties often arise due to the presence of caustics in the ray picture when employing ray methods for describing fields in regions of strong focusing, and also in situations where an extremely large number of rays are required to describe the fields; GB's can efficiently handle the above types of situations because they yield bounded and well behaved fields in regions of focusing where ray methods become singular. With this view in mind, a GB based expansion was developed which employs general astigmatic GB's to represent the fields. The coefficients of this expansion can be found approximately but accurately, in closed form in a simple manner, or quite efficiently by a numerical Galerkin procedure if desired. This expansion is more efficient than other GB expansions which employ higher order Gauss-Hermite/Gauss-Laguerre beam modes; also, this is more convenient and efficient to use than a Gabor type GB expansion. Such a GB expansion can be used to represent an incident field, for example, and the radiation or scattering phenomena resulting from an interaction of this incident field with a conducting object containing an edge can be handled by using essentially a beam-optical theory developed here. In particular, such a theory which resembles an extension of ray methods to deal with general astigmatic GB excitation has been developed which provides closed form expressions for reflection and diffraction of general astigmatic GB's by a perfectly conducting edge in an otherwise smooth curved surface. This development was described in the previous 1994 JSEP annual report. However, the edge diffraction of GB's in that previous work was restricted to edges which were parallel to the principal directions of a local paraboloidal approximation to the actual surface (or its analytic extension) at the point of incidence of a GB near the actual edge. That restriction has recently been removed such that the edge can be arbitrarily located but the edge contour must lie locally in a plane; however, it appears that even the restriction to the latter case of a planar edge contour can be removed heuristically and is under investigation. It is noted that most edge contours in practical antenna applications are locally planar. The extension to handle the more arbitrarily located planar edge was developed recently in a tractable fashion by using

asymptotic evaluation of the radiation integral for the scattered field when the illumination is a general astigmatic Gaussian beam. Such an asymptotic evaluation is far more tractable for this more complicated edge geometry than the approach used in the earlier development for the case when the edge was parallel to the local surface principal directions mentioned above; however, the asymptotics results in a complex stationary point which must be found when implementing such a solution in analyzing practical phenomena involving GB diffraction by relatively arbitrary curved edges. It appears at present that the required parameters in the solution related to this complex stationary point can be found approximately but accurately in closed form in which case the implementation of this solution is expected to be quite efficient. Work is continuing to study this situation. Upon the completion of this part of the study, applications of this solution are then planned to be initiated, before the end of this year, to deal in turn with the development of GB synthesis methods for electrically large antennas. In particular, the fast synthesis of reflector antenna feeds and shaped reflectors, respectively, will be investigated to provide multiple, spot or contour beams in a far more efficient and physically appealing manner than is currently possible. The development of GB expansions for large planar phased arrays is also being investigated. Both, the use of planar phased arrays, and the use of large shaped reflectors are expected to play a very significant role in the future for both, military and commercial satellite antenna systems in wireless communication applications. Eventually, it is also proposed to develop GB techniques for dealing with the complex phenomena of radiation/transmission of fields of large antennas through radomes (including frequency selective surfaces (FSS)), and with millimeter wave systems. It is noted that ray techniques are not directly applicable for analyzing many of these antenna phenomena; on the other hand physical optics or integral methods are found to be very cumbersome numerically. The GB techniques being developed here are not expected to suffer these limitations.

4. Diffraction by material edges/junctions

The study of diffraction by material bodies (semi-transparent or opaque) with edges and/or junctions is important due to the rapid development of composite materials. The analytical study of this class of diffraction phenomena is extremely complex and so far only a very

limited number of canonical shapes has been studied rigorously [4]-[9]. This list is by no means complete and only includes few papers related to this topic. In order to further develop this area of research, it is necessary to use some combination of analytical and numerical techniques. This approach allows us to study more general shapes and also it is possible to consider fairly arbitrary material properties. The approach that was used in this study is the Method of Moments/Green's function scheme [10], where the Green's function of a canonical geometry is obtained analytically (if possible) and any perturbation of the canonical geometry is handled by the Method of Moments. The canonical geometry considered in this study is a material cylinder of arbitrary shape and material properties which is located near or attached to a wedge. Note that the faces of the wedge satisfy impedance boundary conditions, which provides the means for studying objects whose surfaces are non-perfectly conducting, such as coated conductors, conductors with surface roughness or corrugations. The very general configuration of a wedge was chosen for its versatility in representing a wide variety of geometries. Most of the details of this work are discussed in the the Hybrid Studies unit. It is important to note that the work that is relevant to this diffraction studies unit has to do with the development of the two-dimensional Green's function for the impedance wedge shown in Figure 7. It turns out that the key step in the present hybrid approach is to obtain a Green's function for the impedance wedge that is numerically efficient. The Green's function thus developed also provides a useful physical insight into the various scattering mechanisms that exist because it allows the individual components of the fields to be isolated; such as field components that diffract from the tip, reflect from the faces, and propagate along the faces, etc.

The Green's function obtained in this study for the geometry in Figure 7 is valid for all source and observation locations. There have been some developments for the wedge Green's function in the past, all of which have had certain restrictions placed on them [8]–[9]. The development of the present Green's function for the impedance wedge depicted in Figure 7 is based on a method originally developed by Clemmow [11]. The keys steps in this analysis are (1) obtain the plane wave response of the impedance wedge, (2) use analytic continuation to extend the results of the plane wave response for complex angles of incidence, (3) expand

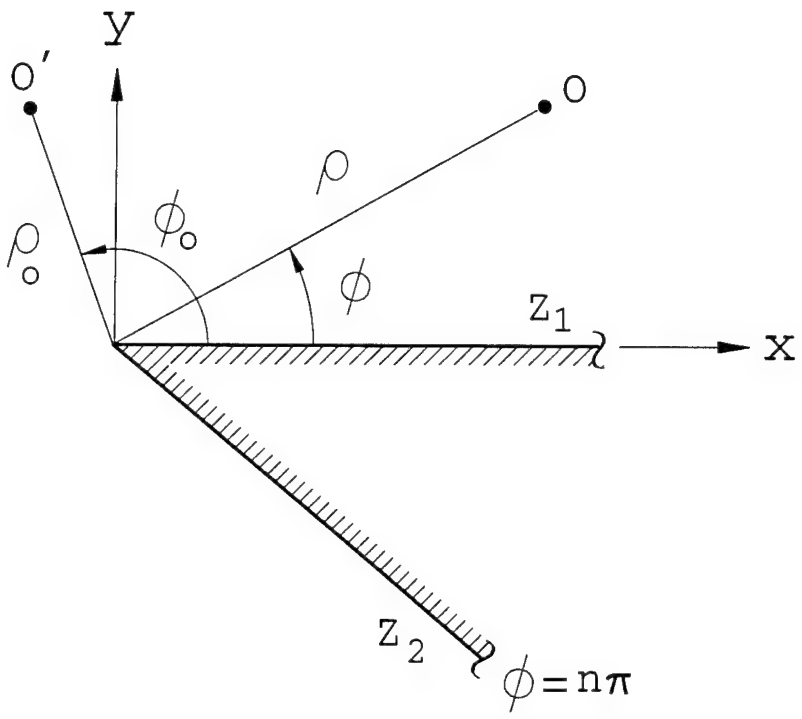

Figure 7: Coordinate system used for analyzing the line source response for a wedge with impedance faces.

the incident field from the line source into a spectrum of plane waves and (4) represent the line source response of the wedge as a spectrum of plane waves.

The line source response for the wedge can be written as

$$U(\vec{\rho},\vec{\rho_o}) = \frac{i}{4\pi}\int\limits_{S(\frac{\pi}{2})} U^p(\phi,\alpha)e^{ik\rho_o\cos(\phi_o-\alpha)}d\alpha. \tag{1}$$

where $S(\pi/2)$ is an Steepest Descent Path (SDP) through $\alpha = \pi/2$.

The total field can be represented as the Sommerfeld integral

$$U^p(\phi,\phi') = \frac{1}{2\pi i}\int_\gamma \hat{U}(\omega + n\pi/2 - \phi)e^{-ik\rho\cos\omega}d\omega, \tag{2}$$

where γ is the twofold Sommerfeld contour. The term $\hat{U}$ is given by

$$\hat{U}(\omega + n\pi/2 - \phi) = \frac{\Psi(\omega + n\pi/2 - \phi)}{n\Psi(n\pi/2 - \phi')}\frac{\sin(\phi'/n)}{\cos(\frac{\omega-\phi}{n}) - \cos(\frac{\phi'}{n})}. \tag{3}$$

where Ψ represents the product of four Maliuzhinets functions ψ with different arguments. The resulting expressions are, in general, extremely complicated and computationally intensive to evaluate. It is therefore important that every effort be made to make them as efficient as possible to evaluate numerically. For certain special cases, such as when the observation or source points are either extremely far or extremely close to the wedge vertex, it will be possible to asymptotically approximate these integrals with a closed form expression. This will, however, not be the case in general and the integrals have to be evaluated numerically. To numerically evaluate such integrals, the contour of integration is deformed to one for which the integrand decays very rapidly as the magnitude of the variable of integration increases. This allows the range of integration to be truncated. One of two types of contours of integration are chosen, either an SDP or a Sommerfeld contour. When the distance parameter is larger than a certain specified value, the SDP is used, otherwise the Sommerfeld contour is used. In addition to deforming the contours of integration, the singularities of the integrands are explicitly separated and evaluated in closed form.

The results for the development of the Green's function were verified numerically by comparing it with a MM reference solution. The reference solution was developed by formulating an integral equation, which utilizes a free-space Green's function, to determine the scattering from an impedance wedge. The integral equation was then solved using a MM

technique that utilized pulse basis functions and point matching. If either the source or observation point is less than 0.25λ from the vertex, the form of the Green's function which was developed for the case when one of the distance parameters is small is used, otherwise the form developed for the case when it is large is used. For the MM solution, 50 pulse basis functions, each of width 0.1 λ, is placed on each of the wedge faces. Since we are modeling an infinite structure, enforcing the impedance boundary condition only along 5 λ long sections of the wedge faces could be a problem because it creates spurious endpoints that could be points of diffraction for any unattenuated surface waves propagating away from the vertex. Therefore, only for the sake of comparison with the results based on the MM solution, we will be considering impedance surfaces that are lossy so that any surface waves that are excited will be sufficiently attenuated when they propagate along the wedge face and there will be a negligible interaction with these endpoints.

First, we will consider the case when the line source is at $\rho_o = 0.2\ \lambda$ and the observation distance is $\rho = 0.75\ \lambda$; therefore we are using the form of the Green's function developed for the small distance parameter. Two different wedge configurations are considered where the exterior wedge angle may be 330° or 210°. The results for the two wedges with the surface impedance values $Z_1 = 37.7 - i566\Omega$ /sq. and $Z_2 = 189 - i377\Omega$ /sq. are shown in Figures 8 and 9 for both TM_z and TE_z polarizations. These are bistatic plots of the total field vs. the observation angle ϕ.

In all of these cases the agreement between the Green's function and MM solution is excellent. When the imaginary part of the surface impedance is negative, that surface can support surface waves for a TE_z field but not for a TM_z field, whereas when the imaginary part of the surface impedance is positive, it is the TM_z field that can excite surface waves and not the TE_z field. The presence of surface waves, when they are present, is clearly seen by the sharp increase of the fields as the observation point approaches the wedge faces, with the stronger surface wave being along face 1. This is to be expected since the magnitude of the imaginary part of Z_1 is larger than that for Z_2 and face 1 has less loss. Also, note that all of the plots for the Green's function are continuous across the many shadow boundaries that exist for these solutions.

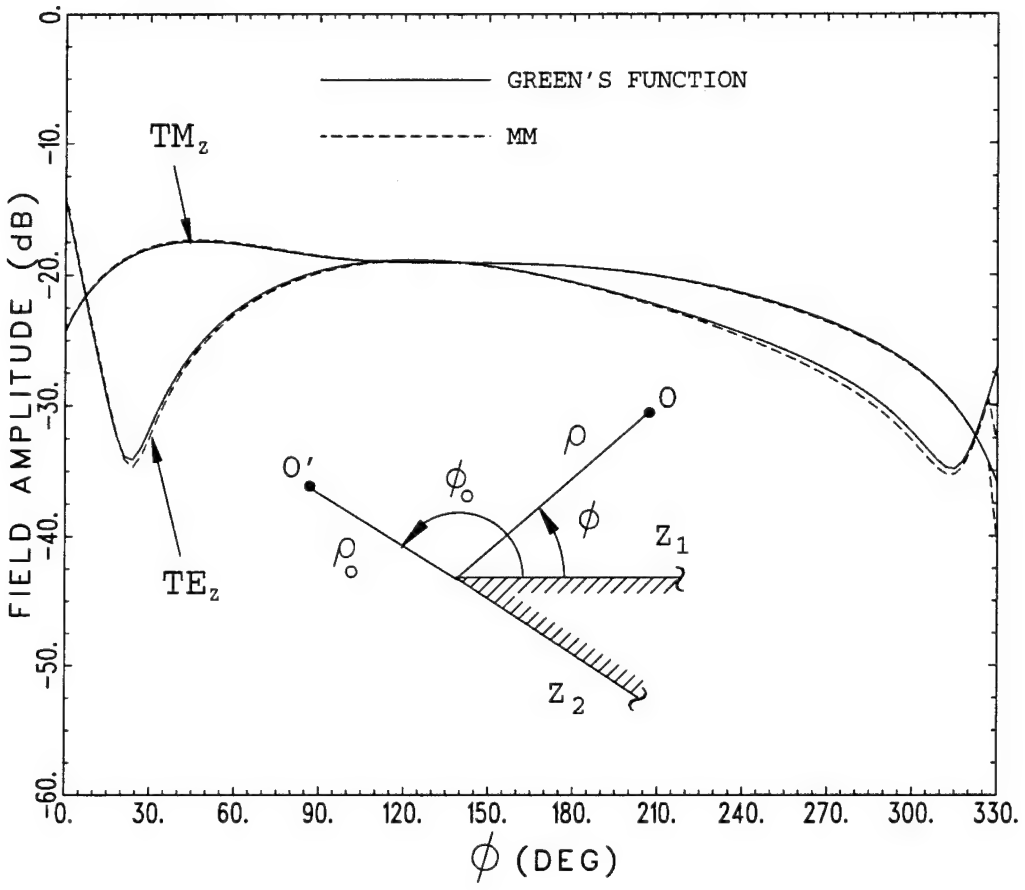

Figure 8: Bistatic plot comparing the Green's function solution to a moment method solution. The parameters are $\rho_o = .2\lambda$, $\rho = .75\lambda$, $\phi_o = 120°$, $Z_1 = 37.7 - i566\ \Omega$/sq., $Z_2 = 189 - i377\ \Omega$/sq., and the exterior wedge angle is 330°.

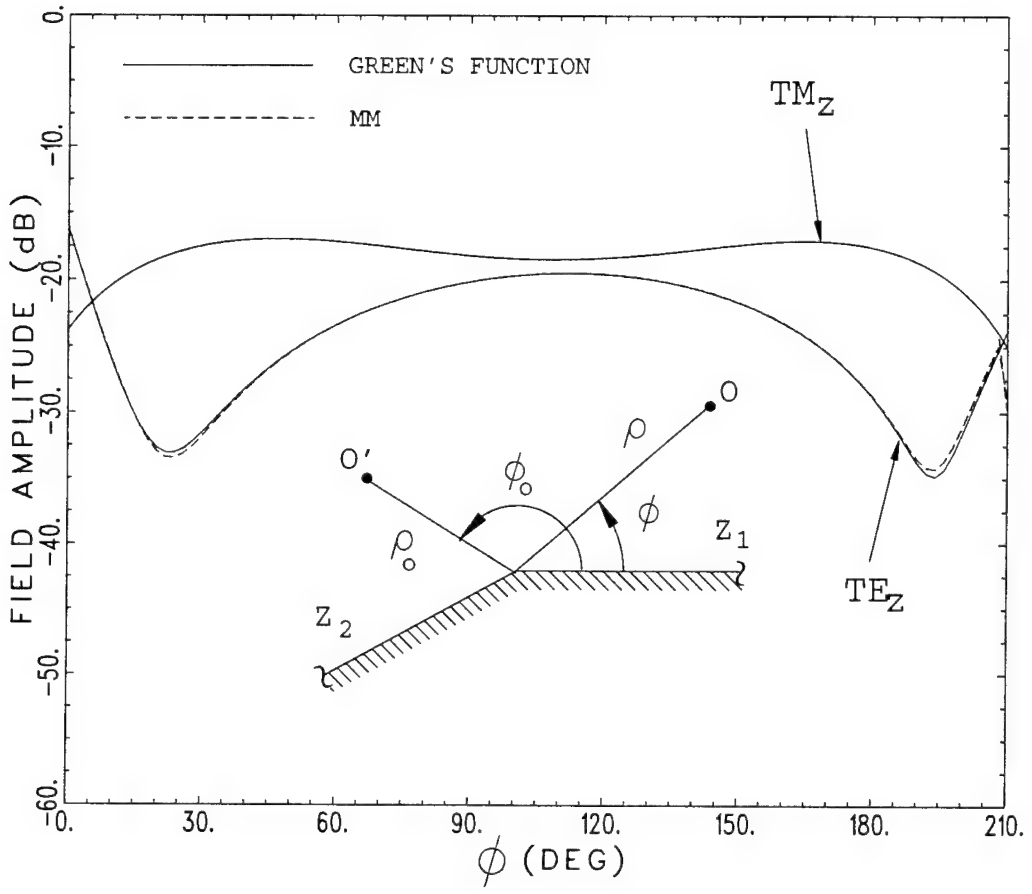

Figure 9: Bistatic plot comparing the Green's function solution to a moment method solution. The parameters are $\rho_o = .2\lambda$, $\rho = .75\lambda$, $\phi_o = 120°$, $Z_1 = 37.7 - i566\ \Omega$/sq., $Z_2 = 189 - i377\ \Omega$/sq., and the exterior wedge angle is 210°.

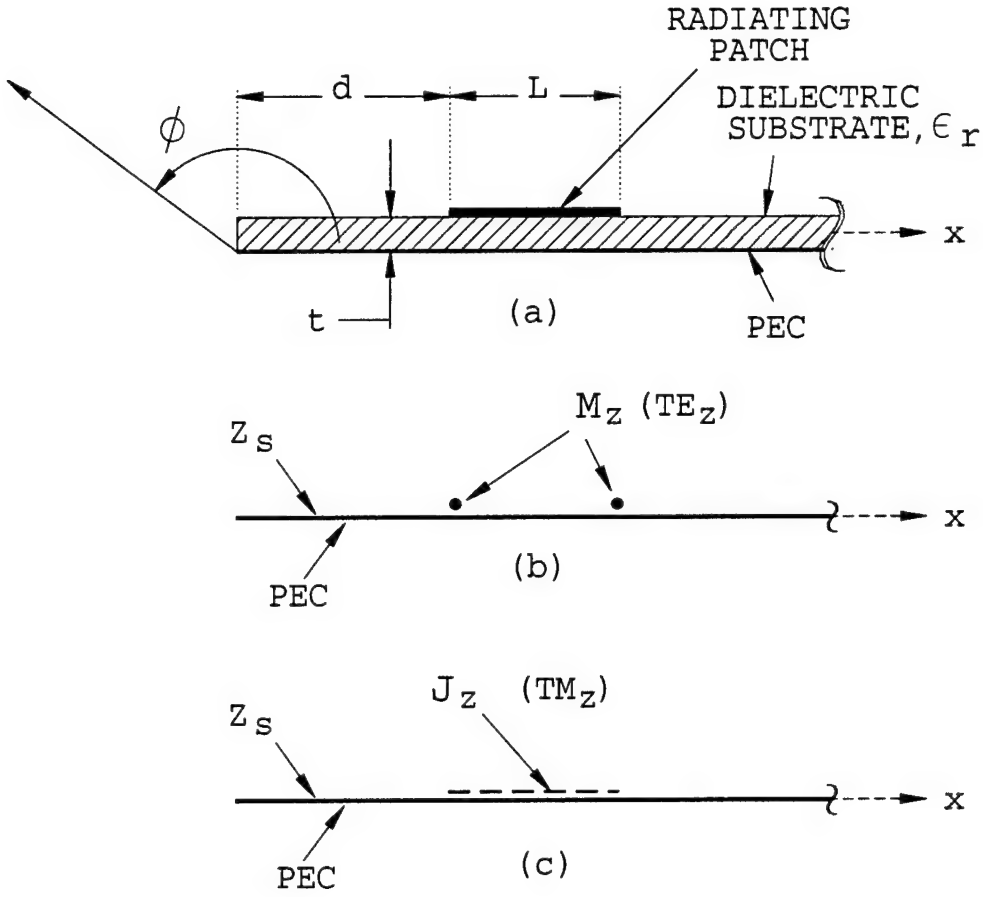

Figure 10: Two-dimensional configuration for a microstrip patch antenna on a semi-infinite, grounded, dielectric substrate (a), and the equivalent models for the TE_z case (b), and the TM_z case (c).

The two-dimensional (2-D) wedge Green's function is also applicable for studying edge effects on the radiation pattern of antennas. One of the types of antennas that can be effectively modelled with this Green's function is a microstrip patch mounted on a grounded dielectric substrate, an example of which is shown in Figure 10(a).

Here, the substrate is terminated at one end leaving an edge that can give rise to a point of diffraction. The fields that diffract from that edge can have a significant impact on the radiation pattern and, hence, degrade the antenna's performance. The wedge Green's function allows us to isolate the effect of a single edge on the radiation pattern and it also provides the means to study how the different field components interact with the edge. Although our model is 2-D, it can be effectively used to analyze a 3-D configuration if we use the TM_z and TE_z polarizations in the 2-D case to analyze the H-plane and E-plane

patterns, respectively, for the 3-D case. The configuration in Figure 10(a) is modelled by an impedance wedge with an exterior wedge angle of 2π, the grounded dielectric substrate is replaced by the equivalent impedance surface Z_s for the top face of the wedge, the bottom face remains a PEC, and the radiating patch is replaced by its equivalent currents; either two magnetic line sources for the TE_z case (Figure 10(b)), or a sheet of electric current for the TM_z case (Figure 10(c)).

One of the advantages of using the wedge Green's function in this analysis is that the different field components can be explicitly separated and studied individually. This can be a valuable tool in providing physical insight into the various mechanisms involved in the radiation and scattering from structures and hence into their control to achieve desired performance. In determining the radiation pattern of the patch antenna in the presence of the edge, there are three field components that should be considered. The direct space wave represents the field that is radiated by the patch and travels directly to the observation point without interacting with the edge, and then there is a component of this space wave that diffracts from the edge. Since there is an impedance surface, surface waves can be excited which travel away from the patch along the surface and the one that travels toward edge can diffract and contribute to the total field seen at the observation point. For the structure shown in Figure 10 with $Z_s = -i34\Omega/\text{sq.}$ and $d = 0.184\lambda$, the E-plane radiation patterns are shown in Figure 11 for the direct, diffracted space wave (DIFF), diffracted surface wave (SW), and total fields. The direct field is the field that exists for the antenna mounted on an infinite substrate, no edge being present. The effect of the edge is to give rise to a point of diffraction that causes a considerable amount of radiation in the back region, $180° < \phi < 360°$. The main contribution to the scattered fields in this region comes from the space wave that diffracts from the edge, whereas the surface wave contribution is almost negligible. However, if the surface impedance were higher, as a result of a thicker dielectric which is modeled by this surface impedance, for example, then the contribution from the surface wave would be more noticeable. Note that the Green's function presented here can be made more general by replacing the Leontovich boundary conditions by Generalized Impedance boundary conditions [12].

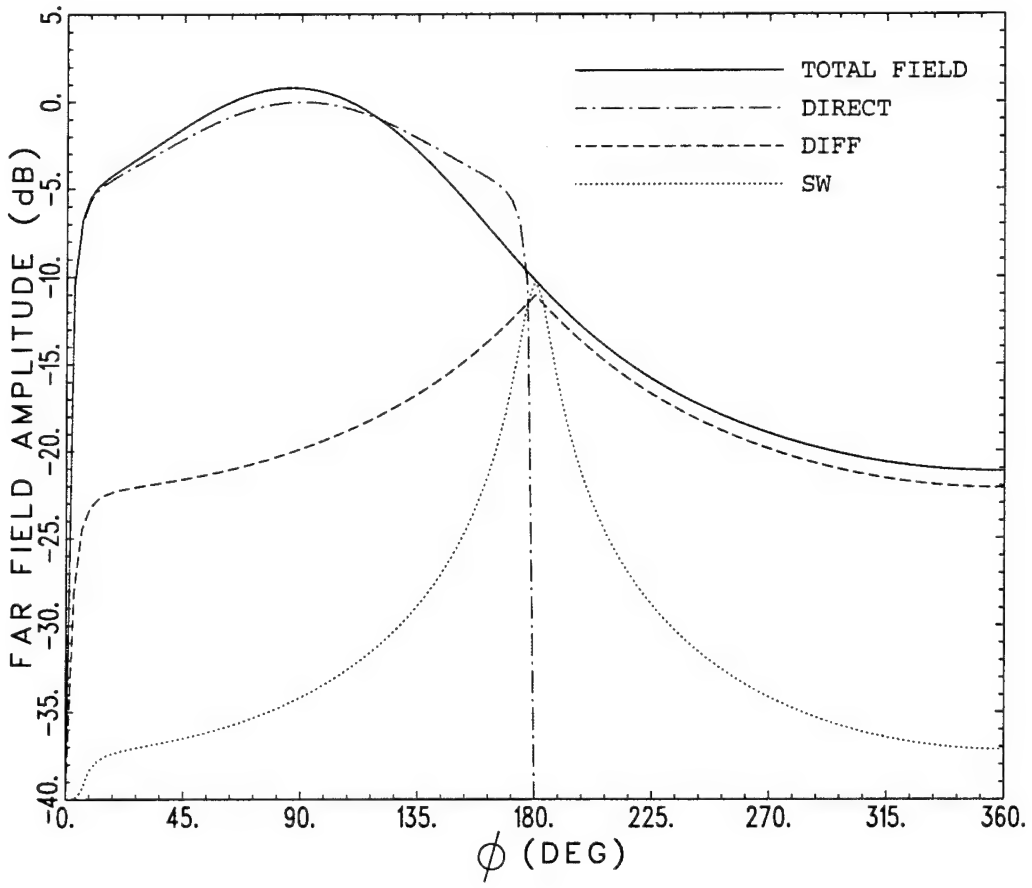

Figure 11: TE_z radiation pattern for the configuration shown in Figure 10 with $Z_s = -i34\Omega/\text{sq.}$, $d = 0.184\lambda$, and $L = 0.3\lambda$. The individual field terms are; the total field in the presence of the edge (TOTAL), direct field term that does not include the edge (DIRECT), diffracted space wave (DIFF), and diffracted surface wave (SW).

5. Extensions of UTD for Conducting Surfaces

A UTD solution has been developed for predicting the near fields (but not extremely near fields) and far fields of antennas that are placed close to a smooth perfectly-conducting convex surface; these results reduce to the ones previously obtained [13] for antennas located directly on the smooth, perfectly-conducting convex surface. Work is also in progress to obtain an extended UTD solution for source (antenna) and observer (field point) which are both close to a smooth perfectly-conducting convex surface; this solution is required for numerically blending into the other solution valid for an antenna close to (but for an observer *not* close to) the smooth convex boundary, which has recently been developed as mentioned above. Also, this extended UTD solution, which is currently under development, is expected to reduce to the UTD solution obtained previously [14] for source and observer that are both directly on a smooth convex boundary. The reason for obtaining these different UTD solutions (or different UTD representations) for different regions of source and observer location is that such different representations can be obtained in terms of UTD transition functions that are dependent only on a single parameter, and which are therefore also well tabulated. On the other hand, a general solution valid for arbitrary source and observer location involves the use of special UTD transition functions which are dependent on several parameters, and therefore cannot be easily tabulated as are universal functions of a single parameter. It is for this reason that a general UTD solution valid for arbitrary source and observer location is not being employed; instead, different representations of such a general solution, which are simpler to use from a numerical computation point of view and which are to remain valid for different range of source and observer locations are sought in this study. It is expected that the extended UTD solution for source and observer both very close to the convex surface will be completed by the end of this year. Also, work has progressed significantly to obtain an asymptotic high frequency solution, for the scattering by an elongated smooth convex surface with an endcap, which remains valid in the paraxial region of the elongated surface, to simulate the scattering from the fuselage of an aircraft/missile in which the end cap models the bulkhead for the nose antenna inside a radome (which is assumed transparent). This asymptotic solution is also expected to be completed by the end of the year. The main reasons for the development of all the UTD, or asymptotic solutions described under this

subtopic are that they will be crucial for not only predicting additional important effects of aircraft/missile structure on the performance of antennas located on such complex realistic structures which cannot be handled presently, but also be crucial for predicting radiation and scattering of EM waves by such structures via a hybrid MM-UTD approach discussed in slightly more detail within the Hybrid Studies unit of JSEP.

6. Development of UTD Solutions for Arbitrary Convex Conducting Surfaces with Uniform Material Coating

Recently, highly useful UTD solutions have been developed to analyze the radiation from, and mutual coupling between antennas located on or in material coated smooth perfectly conducting convex surfaces. Actually, the antenna element chosen in this UTD development is a point electric or magnetic current source; however, the UTD solutions for a point source excitation can be used to directly obtain the corresponding UTD solutions for an arbitrary antenna source distribution via superposition. Thus, UTD Green's functions for exterior radiation and surface fields have been developed for point source excitation of a coated conducting convex surface. It is assumed that the material coating is homogeneous and of uniform thickness; also the coating is assumed to be thick with respect to the radii of curvature of the convex surface which in turn are assumed to be electrically large. These UTD solutions properly reduce to those obtained previously [13, 14] also under JSEP for a perfectly-conducting smooth convex surface, in the limit when the thickness of the coating is allowed to vanish. Presently, the special UTD transition functions, which involve modified Fock functions for this coated case, are being coded so that they can be computed very efficiently making these UTD solutions not only physically appealing but also useful in analyzing the performance of antennas which truly conform to an arbitrary 3-D smooth perfectly conducting convex surface with a uniform material coating. It is expected that the computations of the special UTD transition functions, which occur in these UTD Green's functions for the coated convex surface, will be completed before the end of this year. As such, these UTD solutions would provide for the first time, essentially closed form analytical results for predicting the effects of surface curvature and material coating on the performance of antennas located on such curved coated boundaries. Surface ray torsion explicitly shows in

these UTD solutions how the polarization properties of antennas on or in coated conducting surfaces change with the direction of radiation, and also how that affects antenna mutual coupling. If the antenna source distribution is not known exactly or even approximately, then these UTD Green's functions can be employed as the kernel of an integral equation for the unknown antenna source distribution. The unknowns, because of the special choice of the UTD Green's functions, reside only over the relatively small regions of the antenna source distribution and can thus be found very efficiently via the numerical moment method (MM) thereby leading to a hybrid MM-UTD procedure. Such a hybrid scheme is particularly useful for the analysis/design of large but obviously finite antenna arrays with relatively arbitrary antenna elements that conform to an arbitrarily curved 3-D smooth perfectly conducting surface with a thin, uniform material coating; this aspect is discussed later in the section on Hybrid Studies under JSEP.

References

[1] L.B. Felsen and N. Marcuvitz, *Radiation and Scattering of Waves.* Englewood Cliffs, NJ: Prentice-Hall, 1973.

[2] E.G. Farr and C.E. Baum, "The Radiation Pattern of Reflector Impulse Radiating Antennas, Early-Time Response," Sensor and Simulation Note 358, June 1993.

[3] D.V. Giri and H. Lackner, "A Reflector Antenna for Radiating Impulse-Like Waveforms," Sensor and Simulation Note 382, July 1995.

[4] G.D. Maliuzhinets, "Excitation, Reflection and Emission of Surface Waves from a Wedge with Given Face Impedances," *Sov. Phys. Dokl.*, Vol. 3, pp. 752–755, 1959.

[5] R.G. Rojas and M. Otero, "EM Diffraction by a Resistive Strip Attached to an Impedance Wedge," *J. Electromagnetic Waves and Applications*, Vol. 7, pp. 373–402, 1993.

[6] H.C. Ly and R.G. Rojas, "Analysis of Diffraction by Material Discontinuities in Thin Material Coated Planar Surfaces Based on Maliuzhinets Method," *Radio Science*, Vol. 28, pp. 281–297, May–June 1993.

[7] R. G. Rojas, "Electromagnetic Diffraction of an Obliquely Incident Plane Wave Field by a Wedge with Impedance Faces," *IEEE Trans. Antennas Propagat.*, Vol. AP-36, No. 7, pp. 956–969, July 1988.

[8] R. Tiberio, G. Pelosi, G. Manara and P.H. Pathak, "High-Frequency Scattering from a Wedge with Impedance Faces Illuminated by a Line Source, Part I: Diffraction," *IEEE Trans. Antennas Propagat.*, Vol. AP-37, No. 2, pp. 212–218, Feb. 1989.

[9] G. Pelosi, R. Tiberio, and R. G. Rojas, "Electromagnetic Field Excited by a Line Source Placed at the Edge of an Impedance Wedge," *IEEE Trans. Antennas Propagat.*, Vol. AP-39, No. 7, pp. 1043–1046, July 1991.

[10] E. H. Newman, "An Overview of the Hybrid MM/Green's Function Method in Electromagnetics," *Proceedings of the IEEE*, Vol. 76, No. 3, pp. 270–282, March 1988.

[11] P. C. Clemmow, "A Note on the Diffraction of a Cylindrical Wave by a Perfectly Conducting Half-Plane," *Quart. Journ. Mech. and Applied Math.*, Vol. III, Pt. 3, pp. 377–384, 1950.

[12] R.G. Rojas and Z. Al-hekail, "Generalized Impedance/Resistive Boundary Conditions for Electromagnetic Scattering Problems," *Radio Science*, Vol. 24, Number 1, pp. 1–12, Jan-Feb 1989.

[13] P.H. Pathak, N. Wang, W.D. Burnside and R.G. Kouyoumjian, "A Uniform GTD Solution for the Radiation from Sources on a Convex Surface," *IEEE Trans. Antennas Propagat.*, vol. AP-29, pp. 609–621, July 1981.

[14] P.H. Pathak and N. Wang, "Ray Analysis of Mutual Coupling between Antennas on a Convex Surface," *IEEE Trans. Antennas Propagat.*, vol. AP-29, Nov. 1981.

Refereed publications

1. R.G. Rojas, "Integral Equations for the EM Scattering by Homogeneous/Inhomogeneous Two Dimensional Chiral Bodies," *IEE Proceedings, Microwave, Antennas and Propagation*, vol. 141, pp. 385–392, October 1994.

2. H.T. Anastassiu and P.H. Pathak, "High Frequency Analysis of Gaussian Beam Scattering by a Two-Dimensional Parabolic Contour of Finite Width," *Radio Science*, vol. 30, pp. 493–503, May-June 1995.

3. M.F Otero and R.G. Rojas, "Synthesis of the Frequency Response of an Inhomogeneous Resistive Strip," *Annales des Telecommunications, Special issue on RCS of complex objects*, vol. 50, n. 5-6, pp. 582–589, May-June 1995.

4. A. Altintas, O.M. Büyükdura, and P.H. Pathak, "An Extension of the Physical Theory of Diffraction Concept for Aperture Radiation Problems," *Radio Science*, vol. 29, pp. 1403–1407, November-December 1994.

Papers accepted for publication

1. P. Rousseau and P.H. Pathak, "Time Domain Uniform Geometrical Theory of Diffraction (TD-UTD) for a Curved Wedge," to appear in *IEEE Transactions on Antennas and Propagation*, December 1995.

2. O.M. Buyukdura, S.D. Goad, R.G. Kouyoumjian, "A Spherical Wave Representation of the Dyadic Green's Function for the Wedge," to appear in *IEEE Transactions on Antennas and Propagation*, January 1996.

3. M. C. Liang, C.W. Chuang and P.H. Pathak, "A Generalized Uniform GTD Ray Solution for the Diffraction by a Wedge with Convex Faces," accepted for publication in *Radio Science.*

Papers submitted for publication

1. M.F. Otero and R.G. Rojas, "Two Dimensional Greens' Function for a Wedge with Impedance Faces," *IEEE Transactions on Antennas and Propagation.*

Papers in preparation for publication

1. H.T. Chou, P.H. Pathak and M. Hsu, "Extended UTD Solution for the Radiation by Antennas located close to an Arbitrary Smooth Perfectly Conducting Convex Surface," *Journal of Electromagnetic Wave and Applications.*

2. H.T. Chou, P.H. Pathak and P.R. Rousseau, "Analytical Solution for Early Time Transient Radiation from Pulse Excited Parabolic Reflector Antennas," *IEEE Transactions on Antennas and Propagation.*

3. R.G. Kouyoumjian, G. Manara, P. Nepa and B.J.E. Taute, "Diffraction of an Inhomogeneous Plane Wave by a Wedge," *Radio Science.*

4. R.G. Rojas, "Generalized Impedance/Resistive Boundary Conditions for a Planar Homogeneous Chiral Slab,"

5. Y.M. Hwang, R.G. Kouyoumjian and M. Hsu, "Asymptotic Analysis of the Scattering by a Wedge Illuminated by a Field with a Rapid Spatial Variation."

6. M. Hsu, P.H. Pathak and C.W. Chuang, "Analysis of the Asymptotic HF EM Coupling between Sources Anywhere in the Vicinity of a Circular Cylinder."

7. P.H. Pathak, R.J. Burkholder and P. Rousseau, "On the Question of Causality Associated with the Inversion into Time Domain of Ray Fields that Pass Through Caustics.

8. G. Zogbi, R.J. Burkholder and P.H. Pathak, "An Efficient Planar Antenna Near and Far Field Analysis using Gaussian Aperture Elements."

Conferences/Oral Presentations

1. P. Rousseau and P. Pathak, "Development of TD-UTD and its Modifications for Analyzing the Transient Scattering from Curved Wedge Configurations," 5th Symposium on Mathematical Methods in Electromagnetic Theory (MMET '94), Kharkov, Ukraine, September 1994, invited paper.

2. M.F. Otero and R.G. Rojas, "Analysis and Treatment of Edge Effects on the Radiation Pattern of a Microstrip Patch Antenna," IEEE/APS International Symposium and Radio Science Meeting, Newport Beach, California, June 1995.

3. P. Rousseau and P.H. Pathak, "TD-UTD Slope Diffraction for a Perfectly Conducting Curved Wedge," IEEE/APS International Symposium and Radio Science Meeting, Newport Beach, California, June 1995.

4. P.R. Rousseau and P.H. Pathak, "TD-UTD Analysis of the Scattering from a Perfectly Conducting Finite Cylinder," IEEE/APS International Symposium and Radio Science Meeting, Newport Beach, California, June 1995.

Honors and Awards:

1. R.G. Kouyoumjian was elected to the National Academy of Engineering, September 1994.

IV. INTEGRAL EQUATION STUDIES

Researchers:

E.H. Newman, Professor (Phone: 614/292-4999)
I. Tekin, Graduate Research Associate (Phone: 614/292-7981)
D. Torrungrueng, Graduate Research Associate (Phone: 614/292-7981)

1. Overview

This section will summarize our work in integral equation studies from September 1994 to September 1995. This year represents a change in direction for the Integral Equation Studies area. In particular, over the past few years our research has concentrated on the integral equation and method of moments (MM) analysis of artificial media [1]-[6] and extremely low frequency electromagnetic shielding [7]. This work is now over, and our present research involves two topics:

1. The *Time Division Method of Moments* (TDMM) analysis of the scattering by electrically large bodies.

2. Two important junction problems necessary for the MM analysis of arbitrary bodies.

Our work over the past year on these two topics is briefly summarized below.

2. The TDMM Analysis of Electrically Large Bodies

a. Introduction

In the MM, the current on a body is approximated by an N term expansion of the form

$$\mathbf{J} \approx \mathbf{J}^N = \sum_{n=1}^{N} I_n \mathbf{F}_n \tag{4}$$

where the $\mathbf{F}_n$ are a series of N known basis or expansion functions and the I_n are a series of N unknown coefficients. By defining suitable weighting functions and applying the MM procedure, the I_n are found as a solution of the order N matrix equation

$$[Z]I = V \tag{5}$$

where $[Z]$ is the the order N impedance matrix, V is the length N voltage vector, and I is the length N current vector which holds the unknown coefficients, I_n, from Equation 4.

The number of terms, N, which must be kept in the summation of Equation 4, in order that $\mathbf{J}^N$ be a reasonable approximation to the true current $\mathbf{J}$, is proportional to the electrical size of the body. For large N, the major computational resources necessary to carry out the MM solution are

- the $\mathcal{O}(N^2)$ CPU time to compute the N^2 elements of the $[Z]$ matrix.
- the $\mathcal{O}(N^2)$ (complex) memory locations to store the N^2 elements of the $[Z]$ matrix.
- the $\mathcal{O}(N^3)$ CPU time to solve Equation 5 for I by direct methods such as LU decomposition.

The major obstacle in applying to the MM to electrically large bodies is the $\mathcal{O}(N^3)$ solution time. Over the past few years several different methods have been developed in order to reduce this CPU time including iterative solutions of the matrix equation, the use of the fast multipole method (FMM) to reduce matrix storage and the CPU time per iteration, spatial decomposition techniques in which a large body is split into smaller parts, combining the MM with an asymptotic technique such as the GTD, the use of wavelet and other special basis function to obtain a sparse matrix, and many others [8].

The method presented here is termed the *Time Division Method of Moments* (TDMM). Although it is a frequency domain solution for the time harmonic current on a body, it is helpful to visualize it as the current induced by a time unit step plane wave excitation of the scatterer. The scatterer will be analyzed in a sequence of time intervals which directly correspond to spatial sections on the body. As one proceeds for one time interval to the next, the scatterer current can only change on a single section of the body, thus allowing us to analyze the large order N problem as a sequence of smaller order N/P problems, where P is the number of sections into which the scatterer has been split.

For simplicity the method will be described for the 2D problem of TE to z scattering by a perfect electric conducting (PEC) strip, however, it should be applicable to any smooth convex body. The problem is to find the time harmonic current induced on the strip by the

plane wave

$$H_z^i(x,y,t) = e^{jk_0(x\cos\phi_i + y\sin\phi_i)}e^{j\omega t} \tag{6}$$

incident with angle ϕ_i on a (PEC) strip of width W. Here k_0 is the free space wavenumber and $\omega = 2\pi f$ is the radian frequency.

As illustrated in Figure 12, in the TDMM method it is helpful to think of the strip excited by the unit step plane wave

$$H_z^{iu}(x,y,t) = H_z^i(x,y,t)u[c(x\cos\phi_i + y\sin\phi_i) + t] \tag{7}$$

where c is the speed of light, t is time, and the unit step function

$$u(x) = \begin{cases} 0 & x < 0 \\ 1 & x > 0 \end{cases} . \tag{8}$$

For the purposes of a standard MM solution, the strip is segmented into N sections of width $d = W/N$, corresponding to the N expansion functions of Equation 4. For the purposes of the TDMM solution the MM basis functions are grouped into P sections of width $D = W/P$, and with $N_p = N/P$ basis functions per section. The advantage of the TDMM method it that it is only necessary to solve equations of order N/P, as opposed to N for a standard MM solution.

b. The First Sweep

The TDMM method begins with the $k = 1$ or *first sweep* which computes the current caused by the unit step incident plane wave as it first washes across the strip, i.e., in the time interval

$$0 \le t < \Delta T \qquad \Delta T = W|\cos\phi_i|/c \tag{9}$$

from when the wavefront first hits the left edge of the strip to just before it hits the right edge. The first sweep begins by computing the forced response current caused by the unit step incident plane frozen in time at

$$t = \delta T^- \qquad \delta T = \Delta T/P \tag{10}$$

just before the wavefront hits the right edge of section $p = 1$. At this time there is no current on sections $p = 2, 3, \ldots, P$ of the strip, and thus these sections can be replaced by free space.

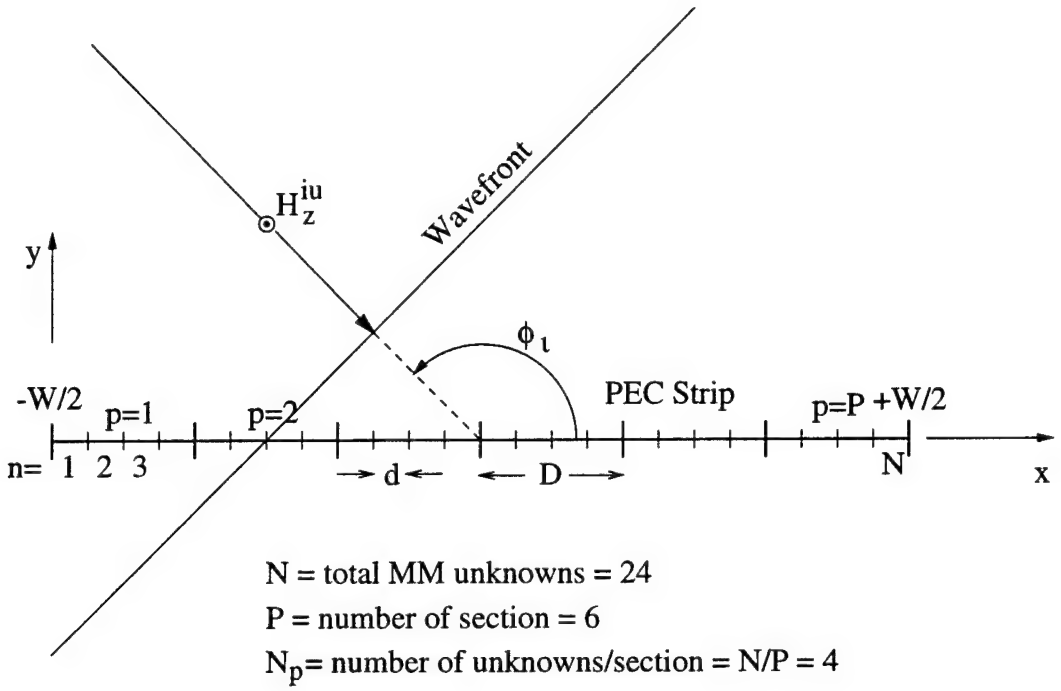

Figure 12: For the TDMM solution the PEC strip is split into P sections of N/P unknowns per section.

As illustrated in Figure 13(a), the current on sweep 1 section 1 is that induced by the *time harmonic* incident plane wave H_z^i, except for the undesired presence of the right edge of section 1. To electromagnetically remove this edge, a tapered resistance or R-card is added to the right edge of section 1. The R-card has a resistance which tapers smoothly from a small resistance at its left edge (junction with PEC section) to a large resistance at its right edge (junction with free space). Typically, the R-card width will be about a wavelength, but for practical reasons, we always choose the R-card to be an integer, P_R, number of sections. In Figure 13 the R-card is shown as $P_R = 2$ sections. Omitting the details, assume that the current, $\mathbf{J}_{p=1}^{k=1}$, on section $p = 1$ for sweep $k = 1$ has been computed.

The next step for sweep 1 is to compute the currents on sections $p = 2, 3, \ldots, P$. As illustrated in Figure 13(b), the sweep 1 currents on section $p > 1$ are produced by the superposition of:

- the time harmonic incident field $H^i(x, y, t)$
- the time harmonic currents, $\mathbf{J}_p^1$, previously computed on sections $1, 2, \ldots, p-1$

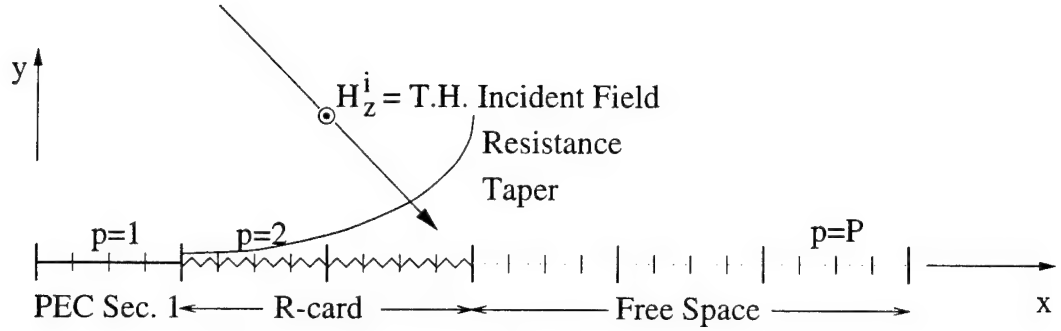

(a) Sweep 1 Current on Section p = 1

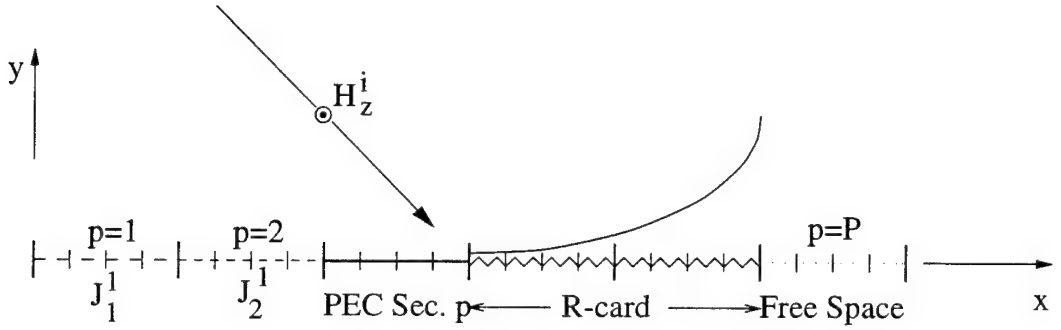

(b) Sweep 1 Current on Section p

Figure 13: Computation of the sweep 1 currents for a PEC strip.

radiating in the presence of PEC section p plus $P_R = 2$ sections of tapered R-card to the right of section p. Note that in the TDMM method, all computations are frequency domain or time harmonic. The concept of time stepping is for conceptual purposes only.

To illustrate the sweep 1 currents, the insert in Figure 14 shows a wave incident from $\phi_i = 135°$ on a strip of width $W = 12\lambda$. The standard MM solution follows that of Richmond [9], and employs a segment size of $d = 0.1\lambda$, thus resulting in $N = 120$ unknowns. For the TDMM solution the basis functions are grouped into $P = 10$ sections of width $D = W/P = 1.2\lambda$, and containing $N_p = N/P = 12$ unknowns each [1]. The R-card occupies $P_R = 2$ sections, and thus is of width $D_R = P_R D = 2.4\lambda$. Its resistance tapers exponentially from 0 to 13,000 $\Omega/\square$. Figure 14(a) compares the standard MM (solid line) and sweep 1 (dashed line) solutions for the magnitude of the MM current vector, $|I_n|$, $n = 1, 2, \ldots, N$. For comparison, the figure also shows the physical optics current (short dashed line). Note that the sweep 1 currents are significantly better than the physical optics current, since they include the effects of diffraction at the leading edge of the strip. The higher frequency oscillations seen in the standard MM solution are not seen in the sweep 1 TDMM solution. This is not an error in the sweep 1 currents, but rather is a result of the fact that the higher frequency oscillations are caused by multiple reflections of the current which occur at later times. Since for sweep 1 the unit step incident wave has not yet hit the right or trailing edge, the sweep 1 currents should be precisely those of a PEC half-plane $x > 0$. Figure 14(a) shows the exact half-plane currents (dotted line) which are virtually identical to the sweep 1 currents.

c. The Second and Subsequent Sweeps

When the wavefront hits the right or trailing edge of the strip, it will produce a reflected current which will modify the current on section P, then section P-1, ..., and finally section 1. To account for this progression, sweep 2 is done in reverse order. As illustrated in Figure 15, the sweep 2 currents on section p, $\mathbf{J}_p^{k=2}$, are produced by the superposition of:

- the time harmonic incident field $H^i(x, y, t)$
- the time harmonic sweep 1 currents, $\mathbf{J}_p^1$, previously computed on sections $1, 2, \ldots, p-1$

[1] Actually due to the use of the overlapping piecewise sinusoidal basis functions, there are $N = 119$ unknowns, with only 11 unknowns in the last section.

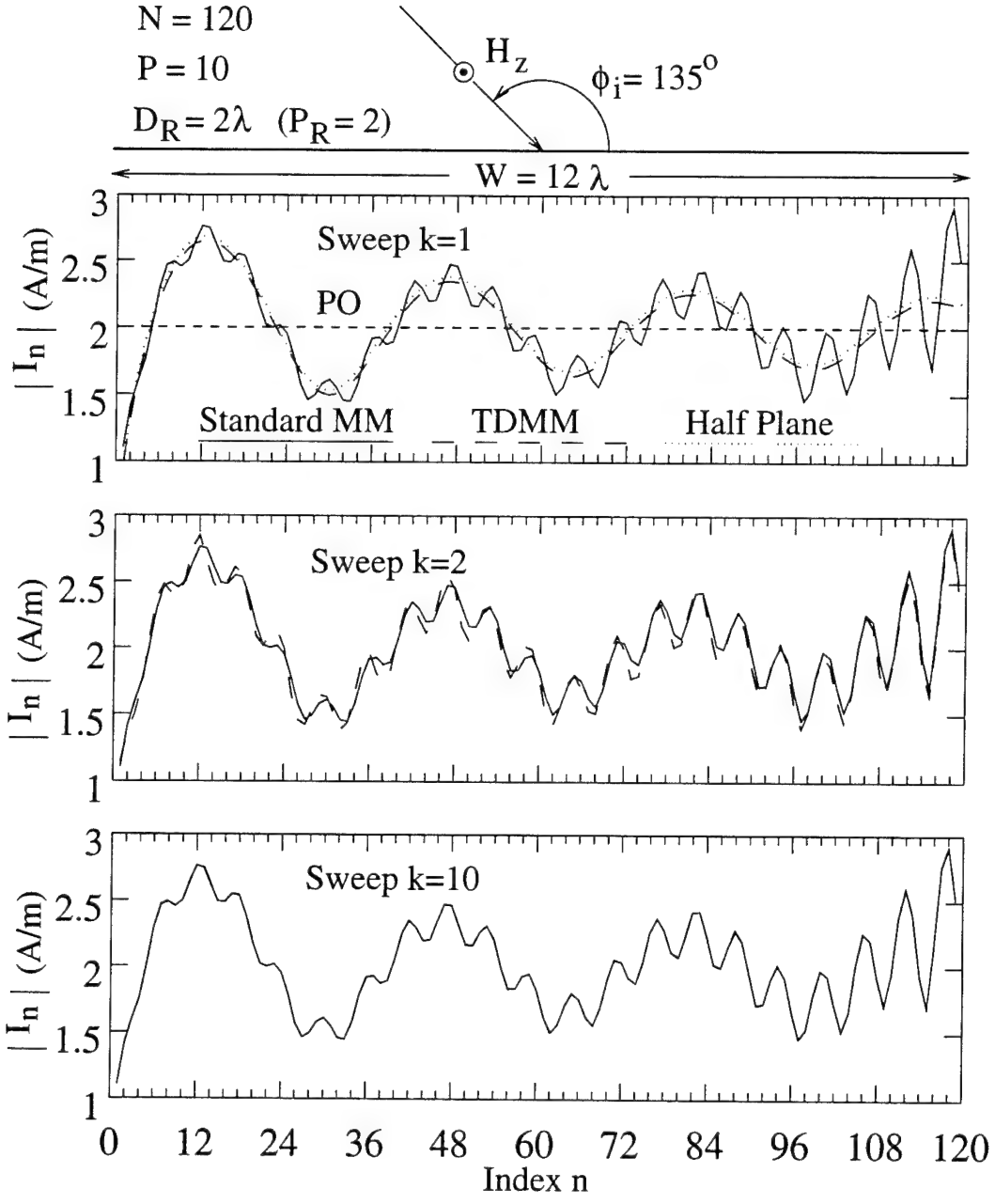

Figure 14: A comparison of the standard MM and the sweep k = 1,2,10 TDMM currents on a PEC strip.

- the time harmonic sweep 2 currents, $\mathbf{J}_p^2$, previously computed on sections $p+1, p+2, \ldots, P$

radiating in the presence of PEC section p. Note that no R-cards are required on the the second or subsequent sweeps since previously computed currents enforce continuity of current at both edges of section p (except for section 1 and P which have a real edge). Figure 14(b) shows a comparison of the standard MM and the sweep 2 currents for the strip. Note that the sweep 2 currents have picked up the higher frequency oscillations caused by the first reflection of the currents from the right or trailing edge of the strip.

Currents for all sweeps $k \geq 2$ are done in precisely the same manner, except that odd numbered sweeps proceed from left to right ($p = 1, 2, \ldots, P$), while even numbered sweeps proceed from from right to left ($p = P, P-1, \ldots, 1$). Figure 14(c) shows that the sweep $k = 10$ TDMM currents are virtually identical to the standard MM currents.

For the above strip, Figure 16 shows the RMS error in the TDMM currents versus the sweep k. Consider the curve for $D_R = 2.4\lambda$ = the width of the R-card for the data of Figure 14. For sweep 1 the RMS error (as compared to the standard MM currents) is about 0.1, and the error drops essentially monotonically to about 0.001 at sweep $k = 16$. For sweeps $k > 16$, the error essentially remains at 0.001. Although this is a very low error, from a theoretical standpoint, one would want to know why the error does not go to zero. To answer this question, Figure 16 also shows the RMS error for R-cards of width $D_R = 1.2\lambda$ and 4.8λ. Note that as D_R increases, the final RMS error decreases. Thus, the use of the R-cards on sweep 1 to electromagnetically remove the right edges of the strips involves an approximation and introduces an error which is not removed by the subsequent sweeps. As the width of the R-card increases, the approximation error decreases, results in a lower limit on the RMS error.

d. Future Work

The initial results for the TDMM method are encouraging. To more fully understand the capabilities and limitations of the method, we intend to study the following:

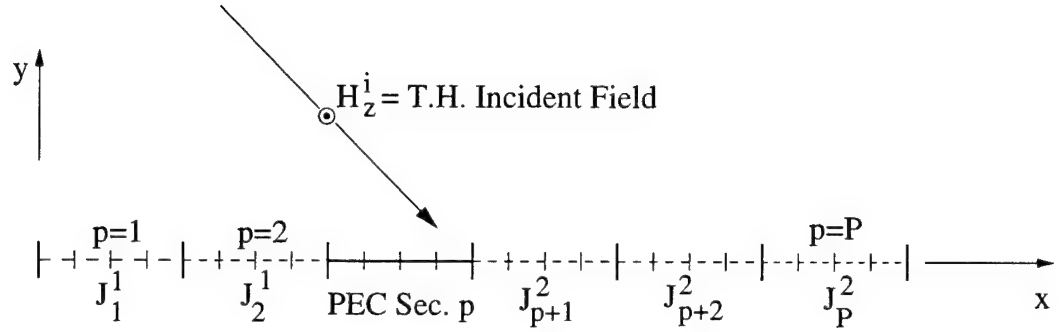

Figure 15: Computation of the sweep 2 currents for a PEC strip.

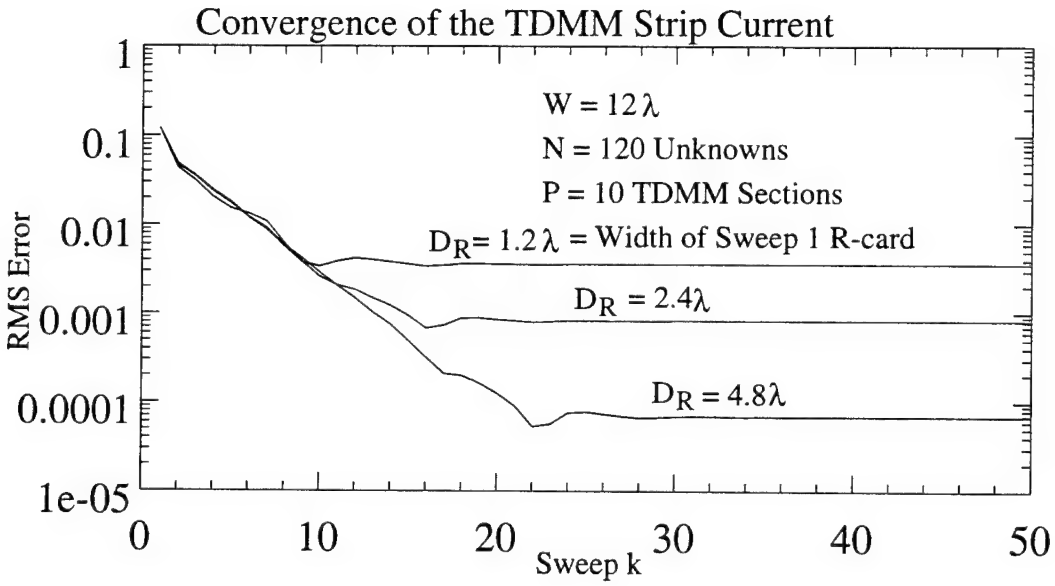

Figure 16: The RMS error for the strip current versus the sweep k, and for various values of the R-card width.

1. Initial results show the TDMM method to be about 10 times faster than the standard MM for a strip with $N = 1000$ unknowns. However, we need to make a more systematic study of the TDMM CPU time, and compare it with the standard MM and other "fast" methods.

2. Apply the method to a scatterer such as a circular cylinder which has a shadow boundary.

3. Apply the method to a non smooth body with a point of diffraction in the interior or the body.

4. Show that, as opposed to most other iterative methods, the currents for a second incident plane wave can be obtained with little additional effort.

5. Show that the fast multipole method (FMM) can be combined with the TDMM to dramatically reduce both the CPU time and storage.

6. Investigate the possibility of combining the TDMM with an asymptotic technique such as the geometrical theory of diffraction (GTD).

3. Junction Problems

a. Wire/Plate Junction Near an Edge

One strategy for modeling a geometrically complex body is to represent it as an *interconnection* of simpler shapes. For example, in "Electromagnetic Surface Patch Code: Version IV" (ESP4) [10] an arbitrary conducting body is modeled as an interconnection of thin wires and polygonal plates. It is not enough to be able to model wires and plates, but one must also be able to treat plate/plate and wire/plate junctions. For example, Figure 17 shows an ESP4 model of a monopole antenna on the underside of a helicopter. The helicopter is modeled as an interconnection of polygonal plates, and a special attachment mode is used to properly treat the wire/plate junction [11],[12]. The attachment mode is valid only when the wire/plate junction is greater than 0.1λ from the edge of the attached plate. In constructing a polygonal plate model of an arbitrary body, such as the helicopter of Figure 17, the plates will typically be of size 0.1λ to 0.2λ. Thus, on a polygonal plate model of an arbitrary body,

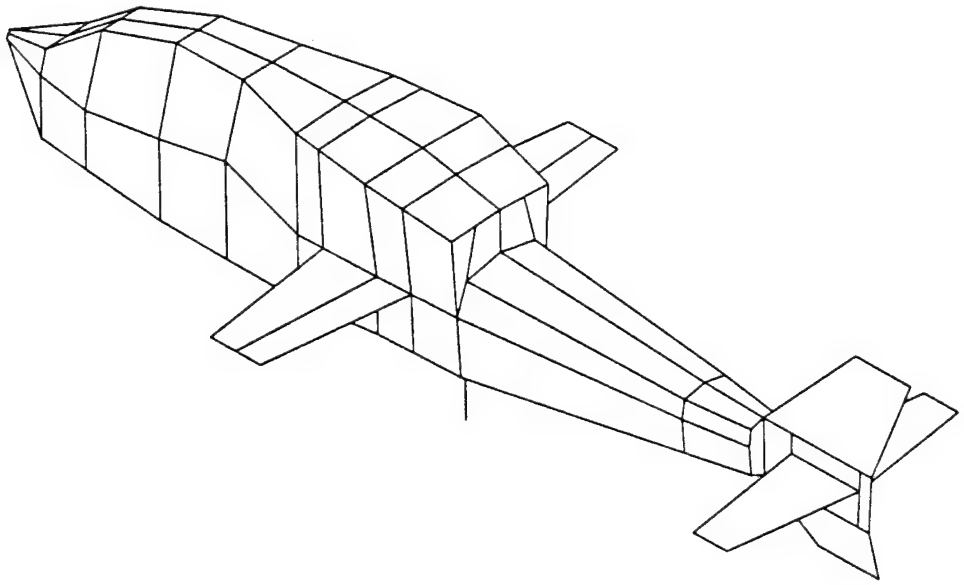

Figure 17: A monopole on a helicopter is modeled as an interconnection of wires and plates.

the wire/plate junction will almost always be less than 0.1λ from an edge, and the simple circular disk attachment mode is practically useless.

Although we worked on the problem of a wire/plate junction near an edge about 15 years ago, the solutions developed were too complicated to be integrated into a general purpose user oriented computer code [13],[14]. Also, they applied only when the attachment point was close to a single edge. Thus, over the past year we developed simper attachment modes which can be integrated into the ESP4 code. Further, they apply when the attachment point is close to a few edges, as would be the case for a wire attached to a polygonal plate model of an arbitrary body.

b. Strip on a Dielectric Substrate

A new Version V of the ESP code is presently under development (not under JSEP support) which will be able to treat dielectrics. In principle, ESP5 should be able to treat printed circuit antennas, with the substrate modeled as a thin dielectric block, and the printed antennas modeled by plates. However, the present code is not applicable to printed circuit antennas since the usual dielectric modes are not capable of representing the large fields at the junction of the metallic strip and the dielectric substrate. To accurately treat this situation, we must develop a strip/dielectric interface mode. This work will begin in the next reporting period.

References

[1] J.L. Blanchard, "Integral Equation Analysis of Artificial Dielectrics", PhD dissertation, Ohio State University, Dept. of Mathematics, 1991.

[2] J.L. Blanchard, E.H. Newman, and M.E. Peters "Integral Equation Analysis of Artificial Media," IEEE Trans. on Antennas and Propagation, Vol. AP-42, May 1994, pp. 727-731.

[3] E.H. Newman and M.E. Peters, "Integral Equation Analysis of Artificial Media," 1993 IEEE Antennas and Propagation Society and Radio Science Meeting, Ann Arbor, Michigan, June 28 - July 2 1993.

[4] M.E. Peters, "Method of Moments Analysis of Artificial Media Composed of Thin Conductive or Dielectric Wire Objects," PhD Dissertation, Ohio State University, Dept. of Electrical Engineering, March 1994.

[5] E.H. Newman and M.E. Peters, "Integral Equation Analysis of Artificial Media," 1993 Workshop on the Electromagnetics of Combat-Induced Atmospheric Obscurants, El Paso, Texas, Nov. 2-4 1993.

[6] M.E. Peters and E.H. Newman, "Method of Moments Analysis of Anisotropic Artificial Media Composed of Dielectric Wire Objects," IEEE Trans. on Microwave Theory and Tech., Vol. MTT-43, Sept. 1995, pp. 2023-2027.

[7] E.H. Newman and M. Kragalott, "Moment Method Analysis of the Electric Shielding Factor of a Conducting Shield at ELF," IEEE Trans. on Electromagnetic Compatibility, Vol. EMC-37, August 1995, pp. 400-408.

[8] E.H. Newman and I. Tekin, "An Overview of the Application of the Method of Moments to Large Bodies in Electromagnetics," Proceeding of the National Research Council Board on Mathematical Sciences Symposium on Large-Scale Structures in Acoustics and Electromagnetics, Sept. 26,27 1994 (proceeding to be published).

[9] J.H. Richmond, "TE Radiation and Scattering from Infinitely-Long Non circular Conducting Cylinders," IEEE Trans. on Antennas and Prop., Vol. AP-22, March 1974, p. 365.

[10] E.H. Newman, "A User's Manual for the Electromagnetic Surface Patch Code: ESP Version IV," Ohio State University, ElectroScience Lab Report 716199-11, prepared under Grant NSG 1498 with the National Aeronautics and Space Administration, Langley Research Center, August 1988.

[11] E.H. Newman and D.M. Pozar, "Electromagnetic Modeling of Composite Wire and Surface Geometries", IEEE Trans. Ant. and Prop., Vol. AP-26, pp. 784-789, Nov. 1978.

[12] E.H. Newman and D.M. Pozar, "Considerations for Efficient Wire/Surface Modeling", IEEE Trans. Ant. and Prop., Vol. AP-28, pp. 121-125, Jan. 1980.

[13] D.M. Pozar and E.H. Newman, "Analysis of a Monopole Mounted at or Near the Edge of a Wedge", IEEE Trans. Ant. and Prop., Vol. AP-29, pp. 488-495, May 1981.

[14] D.M. Pozar and E.H. Newman, "Analysis of a Monopole Mounted Near an Edge or a Vertex", IEEE Trans. Ant. and Prop., Vol. AP-30, pp. 401-408, May 1982.

Refereed Publications

1. E.H. Newman and M. Kragalott, "Moment Method Analysis of the Electric Shielding Factor of a Conducting TM Shield at ELF," *IEEE Trans. on Electromagnetic Compatability*, August 1995.

Papers accepted for publication

1. M.E. Peters and E.H. Newman, "Method of Moments Analysis of Anisotropic Artifical Media Composed of Dielectric Wire Objects," *IEEE Trans. on Microwave Theory and Techniques,* September 1995.

Papers in preparation for publication

1. E.H. Newman and I. Tekin, "Method of Moments Analysis of a Wire Attached to an Arbitrary Surface."

2. E.H. Newman and D. Torrungrueng, "Time Division Method of Moments Analysis of Electrically Large Bodies."

V. FINITE ELEMENT TECHNIQUES

Researchers:

R. Lee, Assistant Professor (Phone: 614/292-1433)
J.O. Jevtic, Graduate Research Associate
J. W. Nehrbass, Graduate Research Associate
J.Y. Wu, Graduate Research Associate

1. Introduction

Over this past year, there have been two significant developments under this work unit, which we believe will have great impact on the development of finite methods for electromagnetic modeling. The first is the development and analysis of a perfectly matched anisotropic absorber for the finite element method (FEM). It is perfectly matched in the sense that a plane wave produces no reflections at the air/absorber interface for all frequencies and incidence angles. These type of absorbers are used to truncate the computation domain in differential-based numerical methods and are commonly called perfectly matched layer (PML).

The first PML has been developed by Berenger [1] for the finite difference time domain (FDTD) method. Chew and Weedon [2] provide a systematic analysis of the PML in terms of the concept of "coordinate stretching". They demonstrate that Berenger's modifications to Maxwell's equations can be derived from a more generalized form of Maxwell's equations. Recently, it has also been discovered by Sacks et. al. [3] that the reflectionless properties of a material can be achieved if the material is assumed to be anisotropic. Unlike Berenger's approach, this one does not require a modification of Maxwell's equations, making it easier to analyze in the general framework of electromagnetics. In this report, we plan to review the analysis for the anisotropic PML and demonstrate its application to FEM. A comparison of the two PML formulations as well as a more detailed discussion of the anisotropic PML's implementation into the FEM formulation is provided in [4].

Another important step is the adaptation of the anisotropic PML to the time domain. In order for any method to be implemented in the time domain, the method must be dynamically stable and formulated with a numerically stable scheme [5]. A dynamically stable system is a system that possesses the property of remaining finitely bounded over all time when excited by a finitely bounded source. Numeric stability is concerned with the behavior of how a system responds to a particular numerical implementation of the system. Very few studies have been performed on numerical stability in the electromagnetics community. Among these are Taflove [6] for the FDTD method and Lee and Sacks [7] for the Whitney elements time domain method.

Currently, we are not able to come up with a formulation of the anisotropic PML that is dynamically stable. To provide some insight into our problem, we have begun to study the behavior of Berenger's equations in the time domain. Although these equations have gained widespread use within the FDTD community, no mathematical analysis has been done to determine the stability associated with the equations. We have done such an analysis, and it is presented in [8]. A review of the numerical stability analysis is provided here for the reader.

The last topic considers the development of finite elements which are specifically tailored for electromagnetics. Both nodal [9] and edge elements [10], [11] produce solutions which have significant numerical dispersion error [12] because they are based on polynomial approximations for the field behavior. This means that to maintain a given accuracy, the mesh density relative to a wavelength must increase as the electrical size of the computation domain increases. This increase may significantly limit the usefulness of FEM for electrically large three-dimensional geometries. In this report, we consider a recently introduced element which we call the solenoidal edge element [13]. As its name implies, it is edge based and divergenceless within the element, and when the order of the element is high enough, the numerical dispersion is negligible.

At present, the solenoidal elements have been developed for the two-dimensional (2-D) case in which we formulate the problem as a vector one rather than a scalar one. We begin with the mathematical analysis of the solenoidal elements. The incorporation of higher order absorbing boundary conditions is especially easy with this formulation. We then analytically

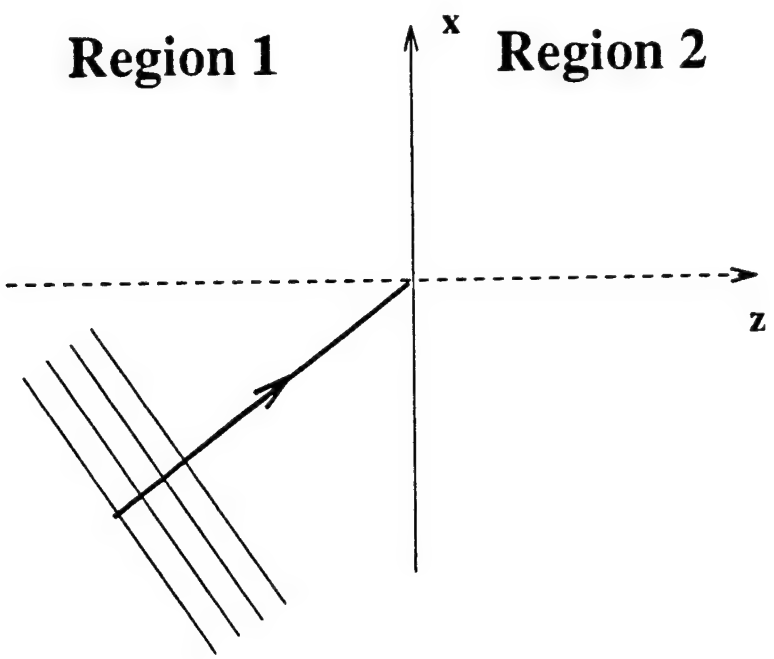

Figure 18: Plane wave incident on an interface separating two halfspaces.

as well as numerically show that these elements produce very little numerical dispersion. Finally, we demonstrate the effectiveness of these elements for scattering problems.

2. Anisotropic PML for Frequency Domain FEM

a. Review of anisotropic PML

Referring to Figure 18, the time-harmonic form of Maxwell's equations in Region 2 can be written as

$$\begin{aligned} \vec{\nabla} \cdot [\overline{\epsilon}]\vec{E} &= 0 \\ \vec{\nabla} \cdot [\overline{\mu}]\vec{H} &= 0 \\ \vec{\nabla} \times \vec{E} &= -j\omega[\overline{\mu}]\vec{H} \\ \vec{\nabla} \times \vec{H} &= j\omega[\overline{\epsilon}]\vec{E} \end{aligned} \tag{11}$$

where $[\overline{\mu}]$ and $[\overline{\epsilon}]$ are the effective permeability and permittivity of Region 2, respectively. In this paper, we concentrate on materials with $[\overline{\mu}]$ and $[\overline{\epsilon}]$ diagonal in the same coordinate system.

$$
\begin{aligned}
[\overline{\mu}] &= \begin{pmatrix} \mu_x + \frac{\sigma_M^x}{j\omega} & 0 & 0 \\ 0 & \mu_y + \frac{\sigma_M^y}{j\omega} & 0 \\ 0 & 0 & \mu_z + \frac{\sigma_M^z}{j\omega} \end{pmatrix} \\
[\overline{\epsilon}] &= \begin{pmatrix} \epsilon_x + \frac{\sigma_E^x}{j\omega} & 0 & 0 \\ 0 & \epsilon_y + \frac{\sigma_E^y}{j\omega} & 0 \\ 0 & 0 & \epsilon_z + \frac{\sigma_E^z}{j\omega} \end{pmatrix}
\end{aligned} \tag{12}
$$

Furthermore, we select $[\overline{\epsilon}]$ and $[\overline{\mu}]$ such that

$$
\frac{[\overline{\epsilon}]}{\epsilon} = \frac{[\overline{\mu}]}{\mu}
$$

to match Region 2 to Region 1. Thus, we can write,

$$
\begin{aligned}
[\overline{\mu}] = \mu[\Lambda] &= \mu \begin{pmatrix} a & 0 & 0 \\ 0 & b & 0 \\ 0 & 0 & c \end{pmatrix} \\
[\overline{\epsilon}] = \epsilon[\Lambda] &= \epsilon \begin{pmatrix} a & 0 & 0 \\ 0 & b & 0 \\ 0 & 0 & c \end{pmatrix}
\end{aligned} \tag{13}
$$

where a, b, c are in general complex. Consequently, Eq. (11) reduces to

$$
\begin{aligned}
\vec{\nabla} \cdot \epsilon[\Lambda]\vec{E} &= 0 \\
\vec{\nabla} \cdot \mu[\Lambda]\vec{H} &= 0 \\
\vec{\nabla} \times \vec{E} &= -j\omega\mu[\Lambda]\vec{H} \\
\vec{\nabla} \times \vec{H} &= j\omega\epsilon[\Lambda]\vec{E}
\end{aligned} \tag{14}
$$

The two curl equations in (14) can be combined to form

$$
[\Lambda]^{-1}\vec{\nabla} \times [\Lambda]^{-1}\vec{\nabla} \times \vec{E} - k^2\vec{E} = 0 \tag{15}
$$

As in Berenger's PML, we must specify a further condition to the PML material to make it reflectionless to a plane wave. For the coordinate system defined in Figure 18, we must specify $a = b = 1/c$. For a propagating wave to decay exponentially, we must specify that the $\mathrm{Im}(a) < 0$. Also, the $\mathrm{Re}(a)$ can be specified for the desired absorption of evanescent waves.

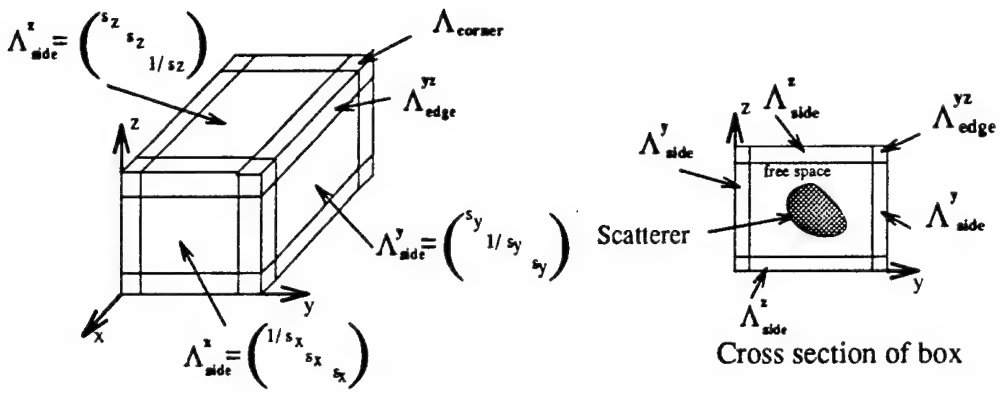

Figure 19: Geometry of the PML region surrounding the scatterer, regular view and cross sectional view.

b. Modeling of Edge and Corner Regions of the PML

The theory for the anisotropic PML is based on the assumption that a plane wave is propagating through a planar media interface of infinite extent. However, the main interest for the PML in our case is to use it to absorb the scattered field from an object in free space. Thus, the PML material must totally surround the scatterer, and the outer surface of the PML must also be terminated in some way. For this work, we terminate the PML with a perfect electric conductor. The PML material is placed in the shape of a box (Figure 19) in order to best approximate the reflectionless properties of the PML.

The choice for the material properties of the side regions of the box ($\Lambda^i_{side}, i = x, y, z$) is straightforward and is shown in the figure, where s_x, s_y, s_z are arbitrary complex numbers. However, the method for determining material properties at the edge and corner regions of the box is not so clear. From electromagnetic theory, one expects that any choice would cause some diffracted field from the edges and corners. One approximate approach for the edge region is to choose the edge properties such that they are perfectly matched to the adjacent side regions when the edge/side interface is of infinite extent. We can use a similar approach for the corner region by matching the corner properties to the adjacent edges. If

Table 1: Parameters for the four test cases used in rectangular plate example.

	$d_1(\lambda)$	$d_2(\lambda)$	α	β	meshsize (λ)	no. of unknowns
Case 1	0.2	0.2	1.5	1.5	0.05	212976
Case 2	0.1	0.2	1.5	1.5	0.05	129396
Case 3	0.1	0.2	2.0	2.0	0.05	129396
Case 4	0.2	0.2	4.0	4.0	0.05	212976

we go through the corresponding analysis of a plane wave propagating through an infinite media interface for the edges and corners, we arrive at the interesting relationship that Λ_{edge} is equal to the matrix multiplication of Λ_{side} of the two adjacent sides and Λ_{corner} is equal to the matrix multiplication of Λ_{side} of the three adjacent sides. As an example, let us consider the edge in Figure 19 with material properties Λ_{edge}^{yz}. The matching condition is,

$$\Lambda_{edge}^{yz} = \begin{pmatrix} s_y s_z & 0 & 0 \\ 0 & s_z/s_y & 0 \\ 0 & 0 & s_y/s_z \end{pmatrix} \tag{16}$$

c. Numerical results for anisotropic PML

In order to test the capabilities of the anisotropic PML, we consider its use in the edge-based finite element method [10]. The implementation of the anisotropic media into the finite element formulation is simple and straightforward [14] and therefore is not discussed here. A bi-conjugate gradient solver (BiCG) with diagonal preconditioning is used to solve the matrix equation. The material properties for all the numerical results are given by $s_x = s_y = s_z = \alpha - j\beta$, where s_x, s_y, s_z are as shown in Figure 19, and α and β are some real numbers.

For the first example, we consider the scattering of plane waves by a larger rectangular plate in Figure 20. The size of the plate is $2\lambda \times 1\lambda$, and the mesh is uniform. Our purpose is to try different values of d_1, d_2, α, and β, and see how they affect the patterns for this plate.

Figure 21 shows the RCS patterns for the four different cases listed in Table 1 as compared to the method of moments (MOM) results. As seen in Table 1, Cases 1 and 2 have the same material property but different d_1; Cases 2 and 3 have the same mesh but different material properties; Cases 1 and 4 also have the same mesh but different material properties. As seen

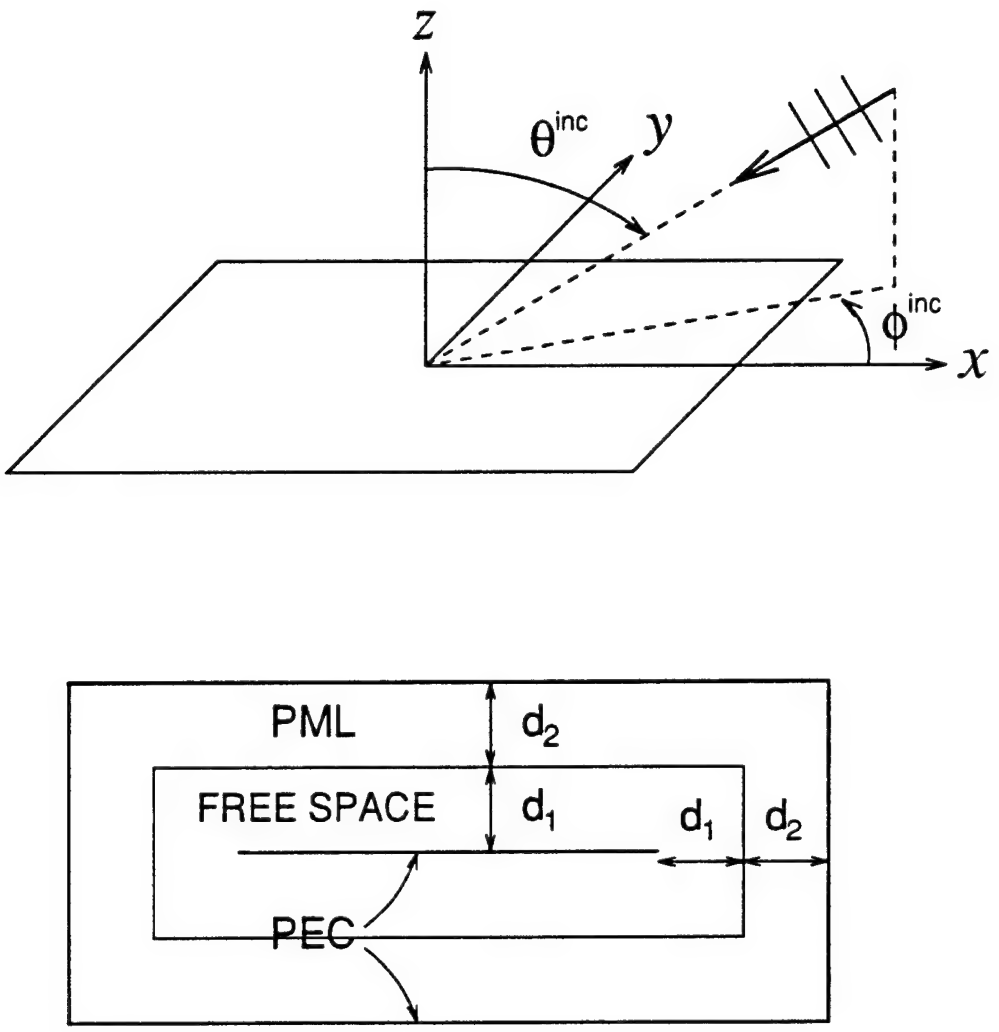

Figure 20: Geometry of rectangular plate and PML configuration.

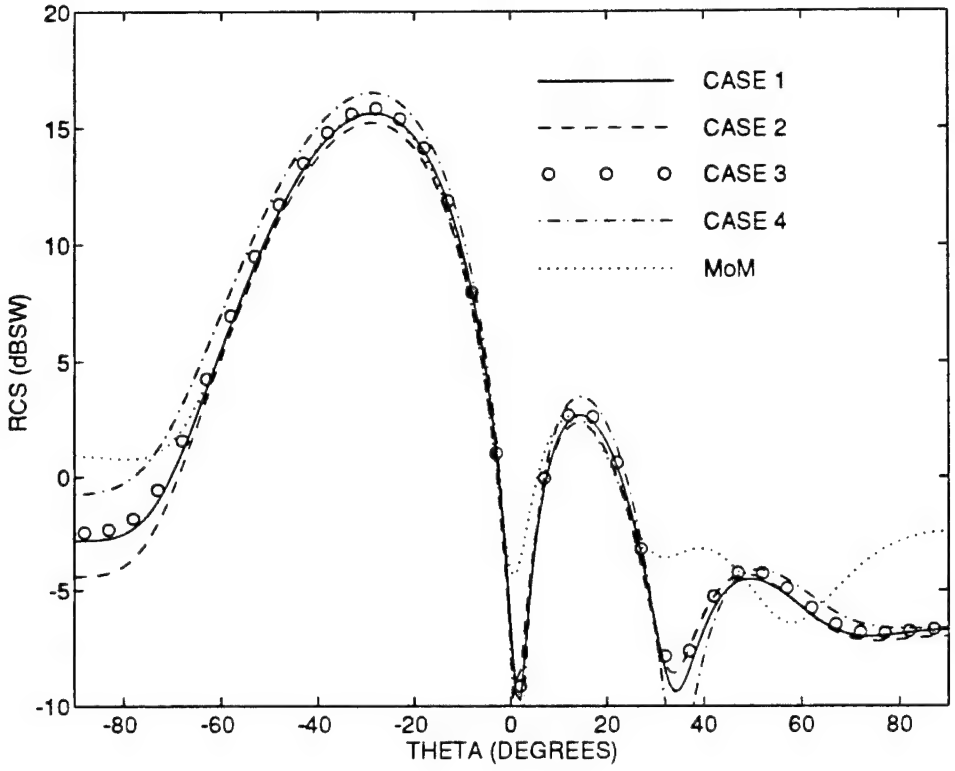

Figure 21: Bistatic patterns for the $2\lambda \times 1\lambda$ rectangular plate. Patterns are in the x-z plane for the $\hat{\phi}$ polarization. The incident plane wave has $\hat{y}$-polarized electric field with $\theta^{inc} = 30°$, $\phi^{inc} = 0°$.

in Figure 21, Case 1 provides better absorption than Case 2; however, when larger material property than those for Case 2 is used, such as in Case 3, the absorption is compensated, and very similar pattern as that of Case 1 is obtained. Finally, Case 4 shows the pattern calculated by using a very large material property ($\alpha = \beta = 4$). It is clear that the pattern for Case 4 is much worse than that for Case 1. This is caused by the increases in the discretization errors and possibly the diffractions by the material interfaces.

For the second example, we consider the scattering of a plane wave by a wedge-cylinder plate. The problem geometry is shown in Figure 22. The plate is composed of a half circle of radius 1λ and an equilateral triangle of side length 2λ. The PML material is placed as close as 0.1λ to the plate in the $\hat{x}$ and $\hat{y}$ directions, and 0.2λ in the $\hat{z}$ direction.

It should be mentioned that a non-uniform mesh is used for this example. The mesh is generated in such a way that it is denser inside the PML material, in the directions normal to the free-space/PML interfaces, where the fields would change the most rapidly. It is hoped that by so doing the number of unknowns can be reduced without too much increase in the discretization errors. The resulting number of unknowns is 48242, in a problem domain of volume $6.968\lambda^3$, as compared to 129396 out of a volume of $2.496\lambda^3$ for Case 2 of the previous example. So the average mesh size is much larger than the previous example.

Figures 23 and 24 show the bistatic RCS patterns (x-z plane; $\hat{\phi}$ polarization) for two incident waves $\theta^{inc} = \phi^{inc} = 0°$ and $\theta^{inc} = 30°, \phi^{inc} = 0°$, respectively, both having $\hat{y}$-polarized electric field. The material property $\alpha = \beta = 1.5$ is used for both cases. It is seen that excellent agreement with the MoM patterns are obtained for both cases.

3. Numerical Stability Analysis for Berenger's PML

Assuming for the moment that Berenger's equations are dynamically stable, the numeric stability of a set of time domain equations is examined. Berenger's time domain equations are given as

$$\mu\frac{\partial \vec{H}_{sx}}{\partial t} + \frac{\sigma_x \mu}{\epsilon}\vec{H}_{sx} = -\frac{\partial}{\partial x}\hat{x} \times \vec{E} \qquad \epsilon\frac{\partial \vec{E}_{sx}}{\partial t} + \sigma_x \vec{E}_{sx} = \frac{\partial}{\partial x}\hat{x} \times \vec{H}$$

$$\mu\frac{\partial \vec{H}_{sy}}{\partial t} + \frac{\sigma_y \mu}{\epsilon}\vec{H}_{sy} = -\frac{\partial}{\partial y}\hat{y} \times \vec{E} \qquad \epsilon\frac{\partial \vec{E}_{sy}}{\partial t} + \sigma_y \vec{E}_{sy} = \frac{\partial}{\partial y}\hat{y} \times \vec{H}$$

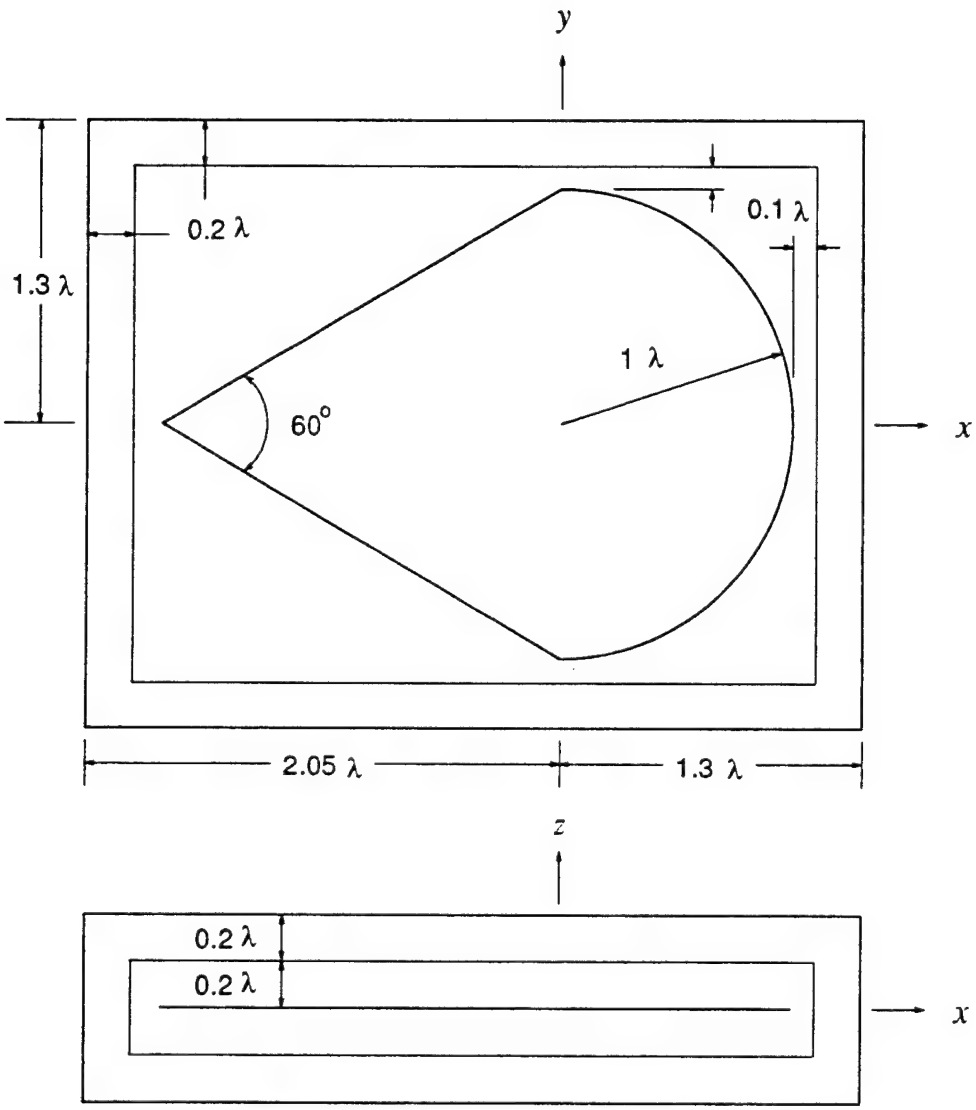

Figure 22: Geometry of the wedge-cylinder plate.

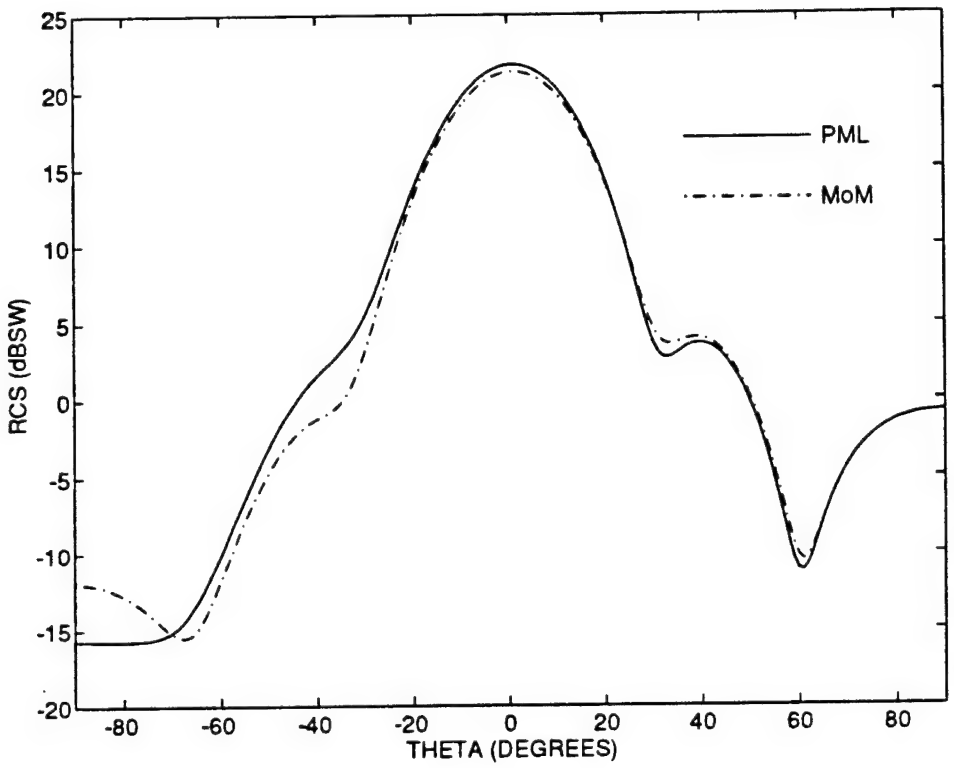

Figure 23: Bistatic patterns for the wedge-cylinder plate. Patterns are in the x-z plane for the $\hat{\phi}$ polarization. The incident plane wave has $\hat{y}$-polarized electric field with $\theta^{inc} = \phi^{inc} = 0°$.

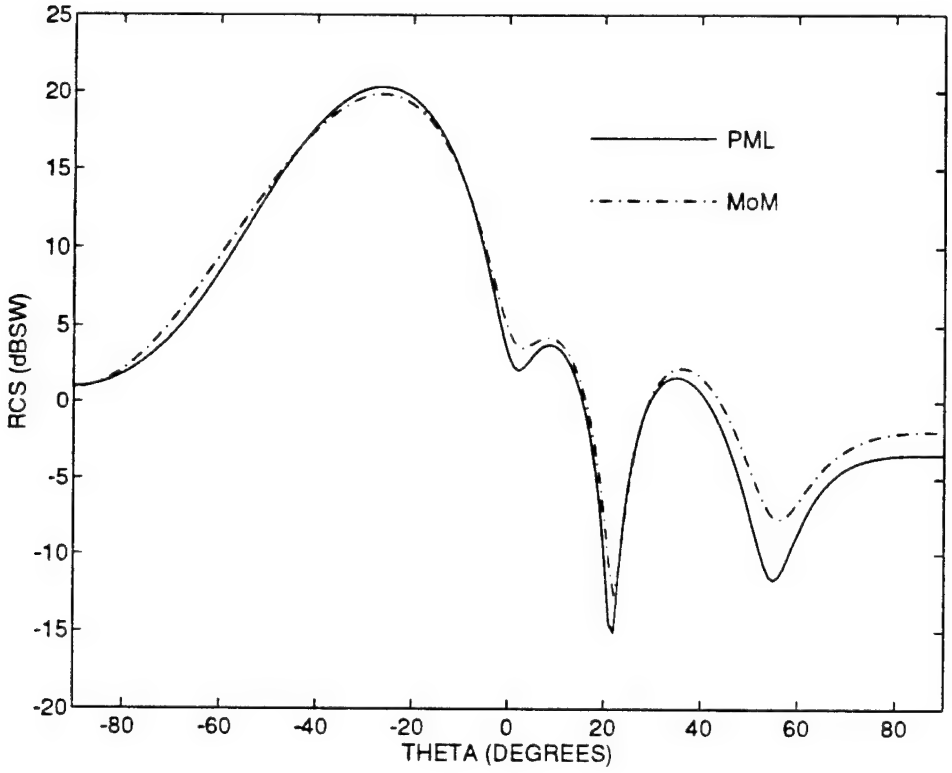

Figure 24: Bistatic patterns for the wedge-cylinder plate. Patterns are in the x-z plane for the $\hat{\phi}$ polarization. The incident plane wave has $\hat{y}$-polarized electric field with $\phi^{inc} = 0°$ and $\theta^{inc} = 30°$.

$$\mu\frac{\partial\vec{H}_{sz}}{\partial t}+\frac{\sigma_z\mu}{\epsilon}\vec{H}_{sz}=-\frac{\partial}{\partial z}\hat{z}\times\vec{E}\qquad\epsilon\frac{\partial\vec{E}_{sz}}{\partial t}+\sigma_z\vec{E}_{sz}=\frac{\partial}{\partial z}\hat{z}\times\vec{H}\tag{17}$$

Both the electric and magnetic total fields ($\vec{E}$, $\vec{H}$) are formed as the sum of the respective coordinate stretched vector fields. These are expressed as

$$\vec{E}=\vec{E}_{sx}+\vec{E}_{sy}+\vec{E}_{sz}\qquad\vec{H}=\vec{H}_{sx}+\vec{H}_{sy}+\vec{H}_{sz}\tag{18}$$

while the cartesian total field components are found as

$$\begin{aligned}E_x&=\left(\vec{E}_{sy}+\vec{E}_{sz}\right)\cdot\hat{x}\quad H_x=\left(\vec{H}_{sy}+\vec{H}_{sz}\right)\cdot\hat{x}\\E_y&=\left(\vec{E}_{sx}+\vec{E}_{sz}\right)\cdot\hat{y}\quad H_y=\left(\vec{H}_{sx}+\vec{H}_{sz}\right)\cdot\hat{y}\\E_z&=\left(\vec{E}_{sx}+\vec{E}_{sy}\right)\cdot\hat{z}\quad H_z=\left(\vec{H}_{sx}+\vec{H}_{sy}\right)\cdot\hat{z}\end{aligned}\tag{19}$$

For convenience, the cartesian components of the coordinate stretched vectors are expressed as

$$\Upsilon_{s\alpha\beta}=\vec{\Upsilon}_{s\beta}\cdot\hat{\alpha}\tag{20}$$

where Υ may be either the $\vec{E}$ or $\vec{H}$ field and α, β, and ζ are each uniquely assigned to one of the cartesian directions x, y, or z.

We form twelve FDTD equations using average discrete time values where appropriate and applying the central difference approximation to (17). By using a leapfrog scheme in time and the standard Yee cells spatial distribution, we obtain a general formula for the $\vec{E}$ and $\vec{H}$ field components as follows,

$$\begin{aligned}E^{n+1}_{s\alpha\beta}(i,j,k)&=f_\beta E^n_{s\alpha\beta}(i,j,k)+sgn(\alpha\times\beta)\tfrac{2\Delta t}{\Delta\beta\gamma_\beta}\\&\quad\left[H^{n+\frac{1}{2}}_\zeta(i+\delta_{x\beta},j+\delta_{y\beta},k+\delta_{z\beta})-H^{n+\frac{1}{2}}_\zeta(i,j,k)\right]\\H^{n+\frac{1}{2}}_{s\alpha\beta}(i,j,k)&=f_\beta H^{n-\frac{1}{2}}_{s\alpha\beta}(i,j,k)+sgn(\alpha\times\beta)\tfrac{2\epsilon\Delta t}{\Delta\beta\mu\gamma_\beta}\\&\quad\left[E^n_\zeta(i-\delta_{x\beta},j-\delta_{y\beta},k-\delta_{z\beta})+E^n_\zeta(i,j,k)\right]\end{aligned}\tag{21}$$

where f_α and γ_α are defined as

$$\gamma_\alpha=2\epsilon+\sigma_\alpha\Delta t\qquad f_\alpha=\tfrac{2\epsilon-\sigma_\alpha\Delta t}{\gamma_\alpha}\tag{22}$$

and $\delta_{\alpha\beta}$ is defined as

$$\delta_{\alpha\beta} = \begin{cases} 1 & \text{if } \alpha \text{ and } \beta \text{ are the same} \\ & \text{cartesian components} \\ 0 & \text{otherwise} \end{cases} \tag{23}$$

Note that as the range of σ_α is varied from 0 to ∞, f_α spans from 1 to -1. Next, the $\vec{E}$ field components of (21) are expanded so that they are only a function of the n and $n-\frac{1}{2}$ time steps. In this way both field components have the same forms. Combining Equations (19) through (21) yields

$$\begin{aligned} E_{s\alpha\beta}^{n+1}(i,j,k) &= f_\beta E_{s\alpha\beta}^{n}(i,j,k) + sgn(\alpha\times\beta)\frac{2\Delta t}{\Delta\beta\gamma_\beta} \\ &\quad [f_\alpha\left(H_{s\zeta\alpha}^{n-\frac{1}{2}}(i+\delta_{x\beta},j+\delta_{y\beta},k+\delta_{z\beta}) - H_{s\zeta\alpha}^{n-\frac{1}{2}}(i,j,k)\right) + \\ &\quad f_\beta\left(H_{s\zeta\beta}^{n-\frac{1}{2}}(i+\delta_{x\beta},j+\delta_{y\beta},k+\delta_{z\beta}) - H_{s\zeta\beta}^{n-\frac{1}{2}}(i,j,k)\right)] + \frac{\epsilon 4\Delta t^2}{\mu\Delta\alpha\Delta\beta\gamma_\alpha\gamma_\beta} \\ &\quad [E_{s\beta}^{n}(i+\delta_{x\beta}-\delta_{x\alpha},j+\delta_{y\beta}-\delta_{y\alpha},k+\delta_{z\beta}-\delta_{z\alpha}) + E_{s\beta}^{n}(i,j,k) \\ &\quad -E_{s\beta}^{n}(i-\delta_{x\alpha},j-\delta_{y\alpha},k-\delta_{z\alpha}) - E_{s\beta}^{n}(i+\delta_{x\beta},j+\delta_{y\beta},k+\delta_{z\beta})] \\ &\quad -\frac{\epsilon}{\mu}\left(\frac{2\Delta t}{\Delta\beta\gamma_\beta}\right)^2 [2E_{s\alpha}^{n}(i,j,k) - E_{s\alpha}^{n}(i+\delta_{x\beta},j+\delta_{y\beta},k+\delta_{z\beta}) \\ &\quad -E_{s\alpha}^{n}(i-\delta_{x\beta},j-\delta_{y\beta},k-\delta_{z\beta})] \end{aligned} \tag{24}$$

As an example, the E_{syx} component of these modified equations is worked out explicitly. For this component the $\vec{E}$ field equations are used while $\alpha = y$, $\beta = x$, and ζ is selected as the z cartesian component.

$$\begin{aligned} E_{syx}^{n+1}(i,j,k) &= f_x E_{syx}^{n}(i,j,k) - \frac{2\Delta t}{\Delta x\gamma_x} \\ &\quad [f_y\left(H_{szy}^{n-\frac{1}{2}}(i+1,j,k) - H_{szy}^{n-\frac{1}{2}}(i,j,k)\right) + \\ &\quad f_x\left(H_{szx}^{n-\frac{1}{2}}(i+1,j,k) - H_{szx}^{n-\frac{1}{2}}(i,j,k)\right)] + \frac{\epsilon 4\Delta t^2}{\mu\Delta y\Delta x\gamma_y\gamma_x} \\ &\quad [E_{sx}^{n}(i+1,j-1,k) + E_{sx}^{n}(i,j,k) \\ &\quad -E_{sx}^{n}(i,j-1,k) - E_{sx}^{n}(i+1,j,k)] \\ &\quad -\frac{\epsilon}{\mu}\left(\frac{2\Delta t}{\Delta x\gamma_x}\right)^2 [2E_{sy}^{n}(i,j,k) - E_{sy}^{n}(i+1,j,k) \\ &\quad -E_{sy}^{n}(i-1,j,k)] \end{aligned} \tag{25}$$

Following the Von Neumann analysis the electric and magnetic fields are separated into time varying modal series,

$$E^n(i,j,k) = \sum_m \sum_n \sum_p \hat{e}^n(t) e^{\mathbf{j}(\mathrm{mi}\Delta\mathrm{x}+\mathrm{nj}\Delta\mathrm{y}+\mathrm{pk}\Delta\mathrm{z})} \tag{26}$$

$$H^{n+\frac{1}{2}}(i,j,k) = \sum_m \sum_n \sum_p \hat{h}^{n+\frac{1}{2}}(t) e^{\mathbf{j}(\mathrm{mi}\Delta\mathrm{x}+\mathrm{nj}\Delta\mathrm{y}+\mathrm{pk}\Delta\mathrm{z})} \tag{27}$$

where $\mathbf{j} = \sqrt{-1}$ and $\hat{e}(t)$ and $\hat{h}(t)$ are complex functions of time. Substituting these series into (25), we obtain a matrix equation in terms of the matrix [G],

$$\vec{U^{n+1}} = [G]\vec{U^n} \tag{28}$$

where

$$\vec{U^{n+1}} = [\hat{e}^{n+\frac{1}{2}}_{syx}, \hat{e}^{n+\frac{1}{2}}_{szx}, \hat{e}^{n+\frac{1}{2}}_{sxy}, \hat{e}^{n+\frac{1}{2}}_{szy}, \hat{e}^{n+\frac{1}{2}}_{sxz}, \hat{e}^{n+\frac{1}{2}}_{syz}, \hat{h}^{n}_{syx}, \hat{h}^{n}_{szx}, \hat{h}^{n}_{sxy}, \hat{h}^{n}_{szy}, \hat{h}^{n}_{sxz}, \hat{h}^{n}_{syz}]^T \tag{29}$$

$$[G] = \begin{bmatrix} [G_{11}] & [G_{12}] \\ [G_{21}] & [G_{22}] \end{bmatrix} \tag{30}$$

$$[G_{11}] = \begin{bmatrix} f_x + C_x k_x^2 & 0 & -C_y k_x k_y & 0 & -C_y k_x k_y & 0 \\ 0 & f_x + C_x k_x^2 & -C_z k_x k_z & -C_x k_x^2 & -C_z k_x k_z & 0 \\ -C_x k_x k_y & 0 & f_y + C_y k_y^2 & 0 & C_y k_y^2 & -C_x k_x k_y \\ -C_z k_y k_z & C_y k y^2 & 0 & f_y + C_y k_y^2 & 0 & -C_z k_y k_z \\ 0 & -C_x k_x k_z & C_z k_z^2 & -C_x k_x k_z & f_z + C_z k_z^2 & 0 \\ C_z k_z^2 & -C_y k y k_z & 0 & -C_y k_y k_z & 0 & f_z + C_z k_z^2 \end{bmatrix} \tag{31}$$

$$[G_{12}] = \begin{bmatrix} 0 & -f_x k_x & 0 & -f_y k_x & 0 & 0 \\ f_x k_x & 0 & 0 & 0 & 0 & f_z k_z \\ 0 & f_x k_y & 0 & f_y k_y & 0 & 0 \\ 0 & 0 & -f_y k_y & 0 & -f_z k_y & 0 \\ -f_x k_z & 0 & 0 & 0 & 0 & -f_z k_z \\ 0 & 0 & f_y k_z & 0 & f_z k_z & 0 \end{bmatrix} \tag{32}$$

$$[G_{21}] = \begin{bmatrix} 0 & C_x k_x & 0 & C_x k x & 0 & 0 \\ -C_x k_x & 0 & 0 & 0 & 0 & -C_x k x \\ 0 & -C_y k_y & 0 & -C_y k y & 0 & 0 \\ 0 & 0 & C_y k_y & 0 & C_y k y & 0 \\ C_z k_z & 0 & 0 & 0 & 0 & C_z k z \\ 0 & 0 & -C_z k_z & 0 & -C_z k z & 0 \end{bmatrix} \tag{33}$$

$$[G_{22}] = \begin{bmatrix} f_x & 0 & 0 & 0 & 0 & 0 \\ 0 & f_x & 0 & 0 & 0 & 0 \\ 0 & 0 & f_y & 0 & 0 & 0 \\ 0 & 0 & 0 & f_y & 0 & 0 \\ 0 & 0 & 0 & 0 & f_z & 0 \\ 0 & 0 & 0 & 0 & 0 & f_z \end{bmatrix} \tag{34}$$

where

$$C_x = \frac{\epsilon}{\mu} e^{-\mathbf{j}\mathrm{i}\Delta\mathrm{x}} \quad C_y = \frac{\epsilon}{\mu} e^{-\mathbf{j}\mathrm{j}\Delta\mathrm{y}} \quad C_z = \frac{\epsilon}{\mu} e^{-\mathbf{j}\mathrm{k}\Delta\mathrm{z}} \tag{35}$$

$$k_x = \frac{2\Delta t}{\Delta x \gamma x}(e^{\mathbf{j}\mathrm{i}\Delta\mathrm{x}} - 1) \quad k_y = \frac{2\Delta t}{\Delta y \gamma y}(e^{\mathbf{j}\mathrm{j}\Delta\mathrm{y}} - 1) \quad k_z = \frac{2\Delta t}{\Delta z \gamma z}(e^{\mathbf{j}\mathrm{k}\Delta\mathrm{z}} - 1) \tag{36}$$

Stability is now reduced to finding the eigenvalues of $[G]$ and showing the conditions under which the modulus of these eigenvalues are bounded by one. The eigenvalues of $[G]$ are found from the solution of the characteristics equation. This characteristic equation decomposes into a repeated sixth order polynomial equation. This implies that all eigenvalues λ are repeated. Finding the six unique eigenvalues reduces to finding the zeroes of the following sixth order equation $Q(\lambda)$,

$$Q(\lambda) = \lambda^6 + a_5\lambda^5 + a_4\lambda^4 + a_3\lambda^3 + a_2\lambda^2 + a_1\lambda + a_0 \tag{37}$$

where

$$a_5 = -(X + Y + Z + 2[f_x + f_y + f_z]) \tag{38}$$

$$a_4 = 2(X[f_y + f_z] + Y[f_x + f_z] + Z[f_x + f_y]) + 4(f_x f_y + f_x f_z + f_y f_z) + f_x^2 + f_y^2 + f_z^2 \tag{39}$$

$$a_3 = -(X(f_y^2 + f_z^2) + Y(f_x^2 + f_z^2) + Z(f_x^2 + f_y^2) + 2(f_x^2[f_y + fz] + f_y^2[f_x + fz] + f_z^2[f_x + fy]) + 4(X f_y f_z + Y f_x f_z + Z f_x f_y) + 8(f_x f_y f_z)) \tag{40}$$

$$a_2 = 2(X[f_y^2 f_z + f_z^2 f_y] + Y[f_x^2 f_z + f_z^2 f_x] + Z[f_x^2 f_y + f_y^2 f_x]) +$$

$$4(f_x^2 f_y f_z + f_x f_y^2 f_z + f_x f_y f_z^2) + f_x^2 f_y^2 + f_x^2 f_z^2 + f_y^2 f_z^2 \tag{41}$$

$$a_1 = -(X f_y^2 f_z^2 + Y f_x^2 f_z^2 + Z f_x^2 f_y^2 + 2(f_x f_y^2 f_z^2 + f_x^2 f_y f_z^2 + f_x^2 f_y^2 f_z)) \tag{42}$$

$$a_0 = f_x^2 f_y^2 f_z^2 \tag{43}$$

and

$$X = C_x k_x^2 = -4\frac{\epsilon}{\mu}\left(\frac{2\Delta t}{\Delta x \gamma x}\right)^2 \sin^2 \frac{i\Delta x}{2} \tag{44}$$

$$Y = C_y k_y^2 = -4\frac{\epsilon}{\mu}\left(\frac{2\Delta t}{\Delta y \gamma y}\right)^2 \sin^2 \frac{j\Delta y}{2} \tag{45}$$

$$Z = C_z k_z^2 = -4\frac{\epsilon}{\mu}\left(\frac{2\Delta t}{\Delta z \gamma z}\right)^2 \sin^2 \frac{k\Delta z^2}{2} \tag{46}$$

Note that because X, Y, and Z are purely real, the coefficients of (37) are also purely real.

Next a simple case is studied and a generalized stability criteria follows. In this example case the wave is absorbed in only one direction (say the z-direction) which implies that $(\sigma_x = \sigma_y = 0)$ and $(\sigma_z \neq 0)$. Further, let the spatial resolution be the same in all directions $(\Delta x = \Delta y = \Delta z)$. This implies that $(f_x = f_y = 1)$ while $(f_z \neq 1)$.

For stability, the values of X, Y, and Z are chosen so as to produce the eigenvalues with the largest moduli. The stability is therefore satisfied for all other choices of indexes i, j, and k.

Putting this information into (37), it is obvious that $(\lambda - 1)^2$ and $P(\lambda)$ both divide $Q(\lambda)$, where $P(\lambda)$ is the fourth order polynomial

$$P(\lambda) = a_4\lambda^4 + a_3\lambda^3 + a_2\lambda^2 + a_1\lambda + a_0 \tag{47}$$

with coefficients

$$a_4 = 1 \tag{48}$$

$$a_3 = 2(2\rho^2(2 + \left(\tfrac{f_z+1}{2}\right)^2) - (f_z + 1)) \tag{49}$$

$$a_2 = -(8\rho^2(2f_z + \left(\tfrac{f_z+1}{2}\right)^2) - (f_z^2 + 4f_z + 1)) \tag{50}$$

$$a_1 = \quad 2(2\rho^2(2f_z^2 + \left(\tfrac{f_z+1}{2}\right)^2) - f_z(f_z+1)) \tag{51}$$

$$a_0 = \quad f_z^2 \tag{52}$$

where

$$\rho^2 = \frac{\Delta t}{\mu\epsilon\Delta x} \tag{53}$$

Using the Jury test [15], the modulus of the roots are forced less than one if the following 5 conditions are met: $P(1) > 0$, $P(-1) > 0$, $|a_0| < a_4$, $|b_0| > |b_3|$, and $|c_0| > |c_2|$ where b_k and c_k are defined as

$$b_k = \begin{vmatrix} a_0 & a_{4-k} \\ a_4 & a_k \end{vmatrix} \qquad c_k = \begin{vmatrix} b_0 & b_{3-k} \\ b_3 & b_k \end{vmatrix} \tag{54}$$

The above five conditions are all satisfied when

$$\rho^2 < 1 \tag{55}$$

Note that the numerical stability of Berenger's formulation is not dependent on the choice of $\sigma_z \geq 0$. For the general case, the values of $\sigma_x \geq 0$, $\sigma_y \geq 0$, and $\sigma_z \geq 0$ can be chosen without effecting the numerical stability. Even in the limit as all three of these values approach infinity, Equation (37) reduces to

$$Q(\lambda) = (\lambda + 1)^6 \tag{56}$$

and the roots remain bounded by 1.

4. Solenodial Edge Elements

a. Analysis

The solenoidal edge elements have been developed specifically to minimize error due to numerical dispersion. These elements must satisfy two criteria other than those imposed by good mesh generation practices. Namely, all elements must be triangular, and the material must be homogeneous within each element. A short review of the solenoidal edge elements is presented in this section.

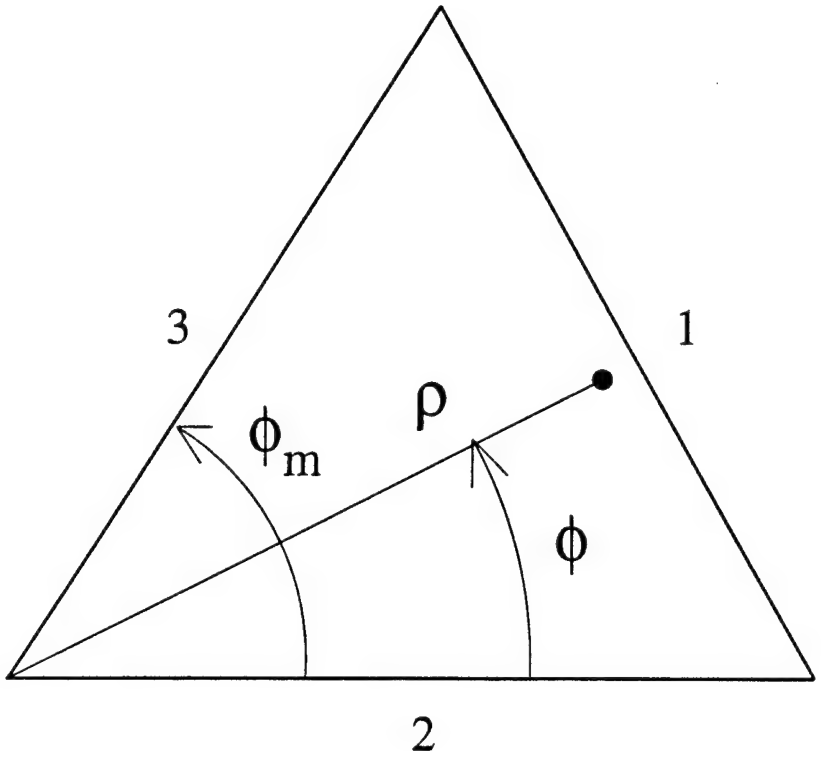

Figure 25: Cylindrical coordinate system for definition of the basis functions associated with the edge number 1.

The unknown field is expanded in terms of basis functions, separately within each element. These are vector basis functions, and as its name implies, they are edge based and divergence free within the element. We require that each basis function within an element be associated with only one of the edges. This can be easily achieved by forcing tangential components of the vector basis to zero along all of the remaining edges.

To be more specific, let us analyze the basis function associated with edge number 1 of an isolated triangular element as shown in Figure 25. We us assume that the polarization is TE_z although the derivation for the TM_z case follows similarly. According to the above discussion, the vector basis must have zero tangential components along edges 2 and 3, and since the transversal field that we are presently analyzing is an electric field, it is immediately seen that the same result is obtained if the edges 2 and 3 are made of perfectly conducting material.

We can now visualize these perfectly conducting edges as forming the tip of an infinitely long wedge with perfectly conducting walls, as in Figure 26. An analysis of the fields satisfying the wave equation inside such an infinite wedge shows that the wedge supports infinitely many standing wave modes. It is important to note that the order of the mode is determined by an integer n and that the higher order modes exhibit faster spatial variation than the lower order modes. These characteristics of the modes are identical to those that we require of an edge based solenoidal vector basis. The solenoidal edge basis for edge number 1 in Figure 25 is defined as:

$$\begin{aligned} w_{\rho_n}(\rho,\phi) &= \nu_n \frac{J_{\nu_n}(k\rho)}{k\rho} sin(\nu_n\phi) \\ w_{\phi_n}(\rho,\phi) &= J'_{\nu_n}(k\rho)cos(\nu_n\phi) \\ h_n(\rho,\phi) &= \frac{1}{k} curl(\vec{w}_n)\cdot\hat{z} = -J_{\nu_n}(k\rho)cos(\nu_n\phi) \\ &\text{where:} \quad \nu_n = n\frac{\pi}{\phi_m}, \quad n = 0,1,2,... \end{aligned} \tag{57}$$

and k and Z are the wavenumber and the characteristic impedance for the homogeneous material inside the element. The h_n basis is used for the H_z field expansion and relates directly to the curl of the $\vec{w}_n$ basis for the transversal $\vec{E}$ field. A different cylindrical coordinate system must be used for each edge; the center of the coordinate system is always at the node opposing the edge in question.

Let us consider some notation for the next equation. We use index e to denote the element number, index i for the edge number, and index n for the order of the basis function. We assume that the highest order of the basis for the i^{th} edge is given by N_i. The electric and magnetic field of a TE_z polarized wave can now be approximated by:

$$\begin{aligned} \vec{E}(\vec{r}) &= \sum_e \sum_i \sum_{n=0}^{N_i-1} A_n^{e,i}\vec{w}_n^{e,i}(\vec{r}) \\ H_z(\vec{r}) &= \frac{1}{Z_e}\sum_e \sum_i \sum_{n=0}^{N_i-1} A_n^{e,i} h_n^{e,i}(\vec{r}) \end{aligned} \tag{58}$$

where the first summation is over all elements, the second summation is over all three edges belonging to the element, and the third summation is over N_i orders of the basis function. Basis function $\vec{w}_n^{e,i}$ is the n^{th} order basis associated with the e^{th} element and edge i which belongs to that element. The coefficients $A_n^{e,i}$ are the amplitudes of the basis functions in the expansion for the field, and they are therefore the unknowns in our model.

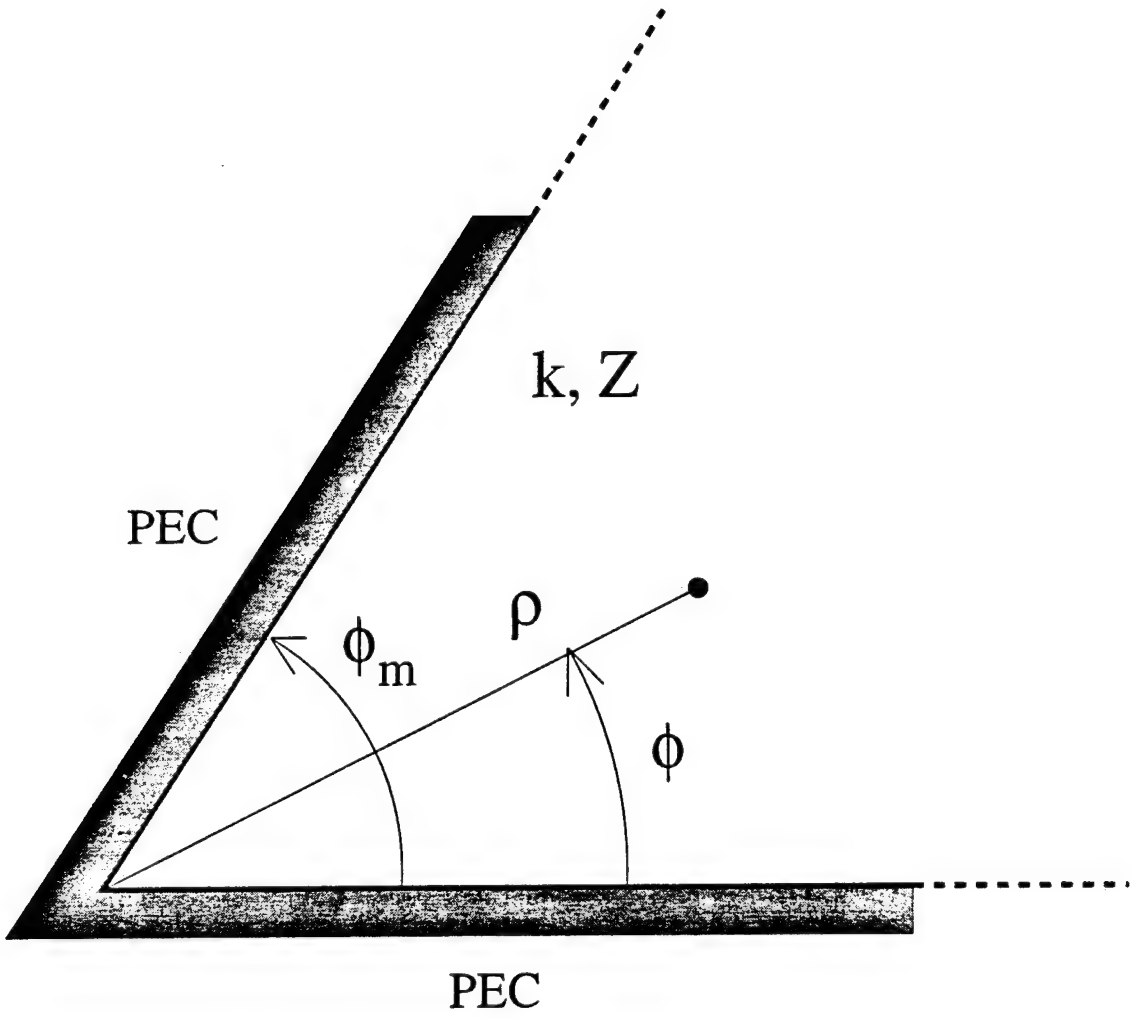

Figure 26: Infinite corner with perfectly conducting walls and filled with a homogeneous material of characteristic impedance Z and wavenumber k.

We see from (58) that the wave equation is exactly satisfied within each element even before we proceed with the computation of the unknown coefficients $A_n^{e,i}$. This is the reason that very little numerical dispersion is present in the numerical solution. To find the unknown coefficients, we apply continuity of the tangential electric and magnetic fields across the interelement boundaries. Let us focus our attention to the problem of field matching at the interelement boundaries, which is indeed the key step in the implementation of the solenoidal edge elements. First, we should realize that each edge in the interior of the mesh belongs to two elements, both of which have separate basis functions associated with this edge. We require that the number of these bases on both sides of the edge be equal. Let this number of basis functions associated with the edge i be equal to N_i. For each interior edge i there are two elements e_1 and e_2 which share the edge. The number of unknowns associated with the edge is simply twice the number of bases on each side, that is $2N_i$. Thus, the matching condition for edge i must be expressed in terms of $2N_i$ equations. We form N_i equations by matching the tangential electric field and the other N_i equations by matching the magnetic field along the i^{th} edge.

The field matching is performed in an integral sense. The matching equations for the electric field defined by the edge common to elements e_1 and e_2 can be put down in the following form:

$$\int_0^1 [\sum_{n=0}^{N_i-1} A_n^{e_1,i} \vec{w}_n^{e_1,i}(\xi_i)]\ \hat{t}_i \Psi_p^i(\xi_i) d\xi_i = \int_0^1 [\sum_{n=0}^{N_i-1} A_n^{e_2,i} \vec{w}_n^{e_2,i}(\xi_i)]\ \hat{t}_i \Psi_p^i(\xi_i) d\xi_i \quad \text{for:} \quad p = 0, ..., N_i - 1 \tag{59}$$

where $\hat{t}_i$ is the unit vector of the i^{th} edge. The weighting function $\Psi_n^i(\xi_i)$ is given by

$$\Psi_n^i(\xi_i) = cos(n\pi\xi_i), \qquad 0 < \xi_i < 1, \qquad n = 0, ..., N_i - 1 \tag{60}$$

where ξ_i is the normalized linear coordinate along the i^{th} edge. Matching of the magnetic field can be done in the same manner, with an important difference that the tangential magnetic field along the edge i, depends not only on basis functions associated with this edge, but also on all other basis functions defined within the elements e_1 and e_2. It should

be noted that ABC's are easily implemented into the solenoidal element formulation because the derivatives of the basis functions can be evaluated analytically.

b. Numerical results for solenoidal elements

For the scattering case, our main interest is in the interaction of the ABC with the solenoidal elements. However, before we do that, let us consider the issue of numerical dispersion. To validate the claims of low numerical dispersion, we consider the problem of plane wave (TM_z polarization) scattering from a homogeneous dielectric circular cylinder of radius $R_1 = 0.8\lambda_0$ (λ_0 is the free space wavelength) with $\epsilon_{rd} = 4$. Since the exact solution is known, we can quantify the error by defining the % RMS error as

$$\% \text{ RMS Error} = \sqrt{\frac{\int_{\Gamma_d} |E_z^{ABC} - E_z^{ex}|^2 \, d\ell}{\int_{\Gamma_d} |E_z^{ex}|^2 \, d\ell}} \times 100 \tag{61}$$

where E_z^{ex} is electric field produced by the exact eigenfunction solution with the radiation boundary condition and E_z^{ABC} is the electric field calculated with a first order BGT ABC as the outer boundary condition. The term E_z^{ABC} represents the solution due to either bilinear quadrilateral nodal elements, the solenoidal elements, or the analytical solution with the ABC [16]. The integration path Γ_d is chosen to be the along the surface of the cylinder.

The % RMS error is shown in Figure 27 as R_2, which represents the location of the outer boundary, is varied from $0.9\lambda_0$ to $2\lambda_0$ for the analytical, solenoidal elements (mesh spacing of $\lambda_0/15$ with third order elements), and nodal elements (mesh spacings of approximately $\lambda_0/20$ and $\lambda_0/40$). The error in the analytical solution is due solely to the ABC. The curve of the error in the solenoidal element follows very closely to the error curve for the analytical case, which indicates that the solenoidal elements produce very little numerical dispersion. The slight differences are most likely caused by the piecewise linear approximation of the circular shape of the cylinder which is used by the mesh for the solenoidal elements. On the other hand, the deviation of the nodal element errors from the analytical case is due almost entirely to numerical dispersion.

To study the accuracy of the solenoidal elements with the ABC, we consider the problem of a TE_z polarized plane wave incident on a dielectric circular cylinder. The geometry is shown in Figure 28, and the associated mesh is given in Figure 29 with 282 elements and

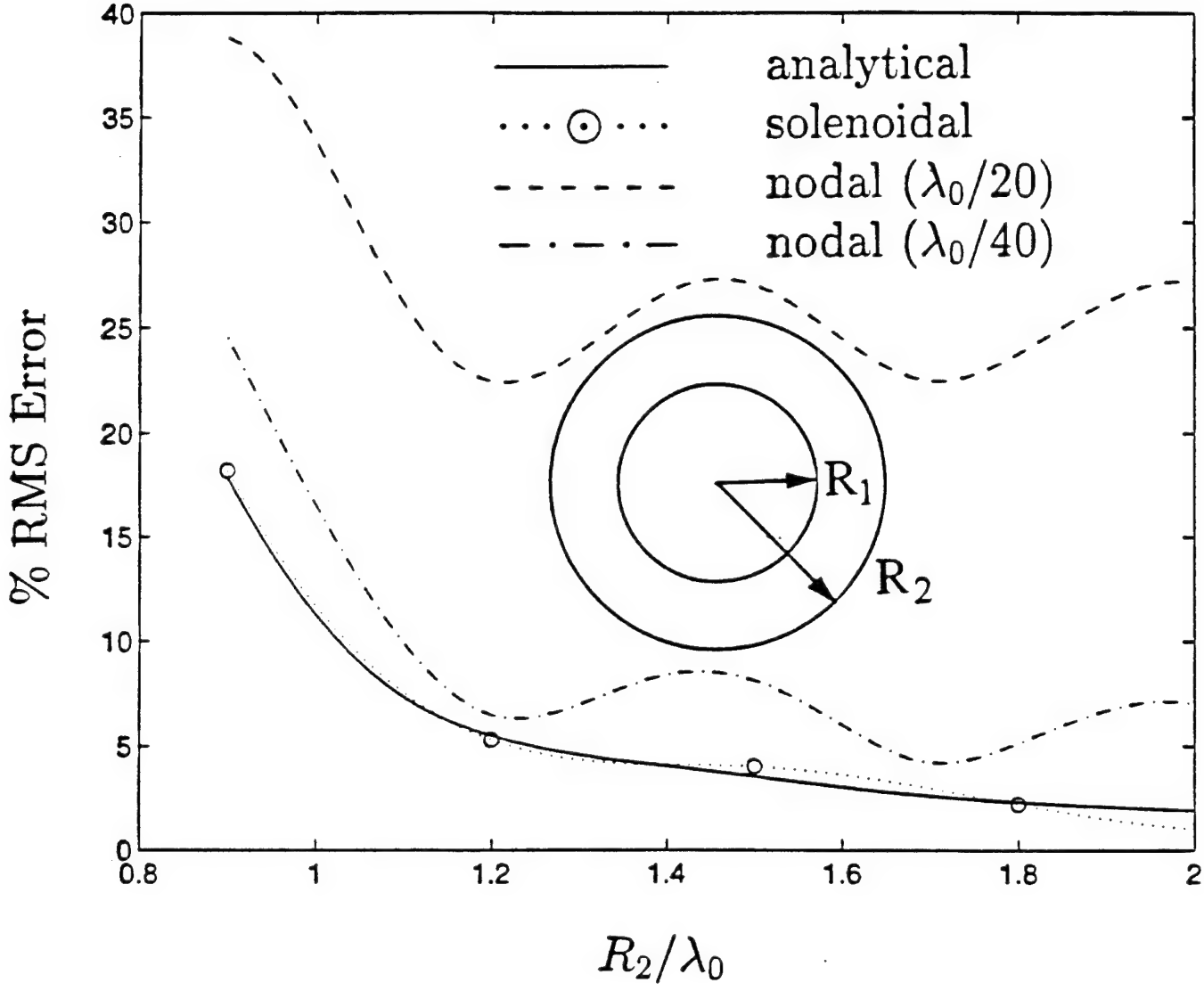

Figure 27: Plot of % RMS error on the dielectric circular cylinder boundary as function of R_2/λ_0 for the analytical, solenoidal solution, and nodal ($\lambda_0/20$ and $\lambda_0/40$ mesh spacing) cases. $R_1 = 0.8\lambda_0$, $\epsilon_{rd} = 4$.

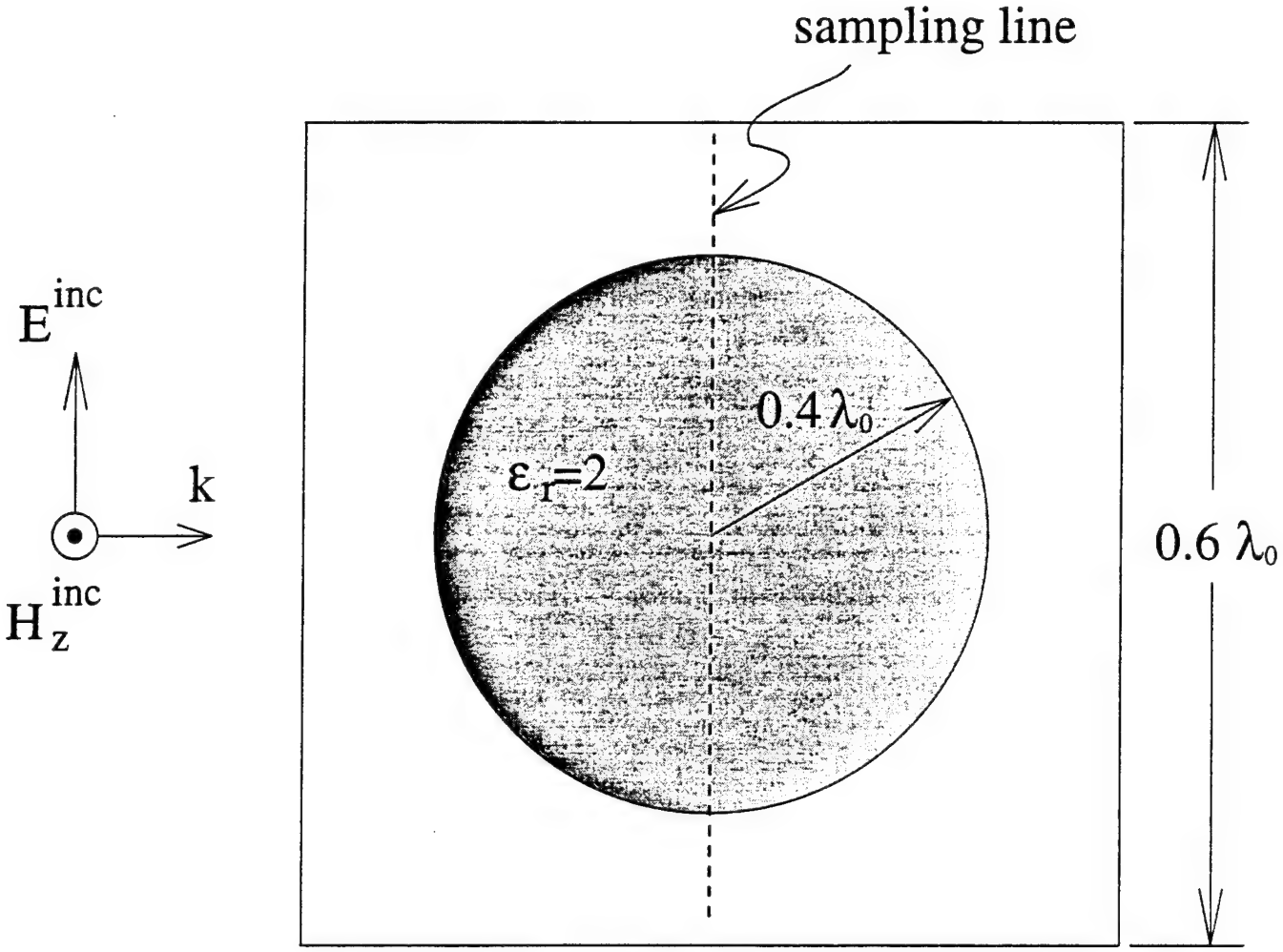

Figure 28: Geometry for a radiation type test problem. Dielectric cylinder with $\epsilon_r = 2$ and radius 0.4λ is illuminated by a TE polarized plane wave. Fields will be compared along the sampling line.

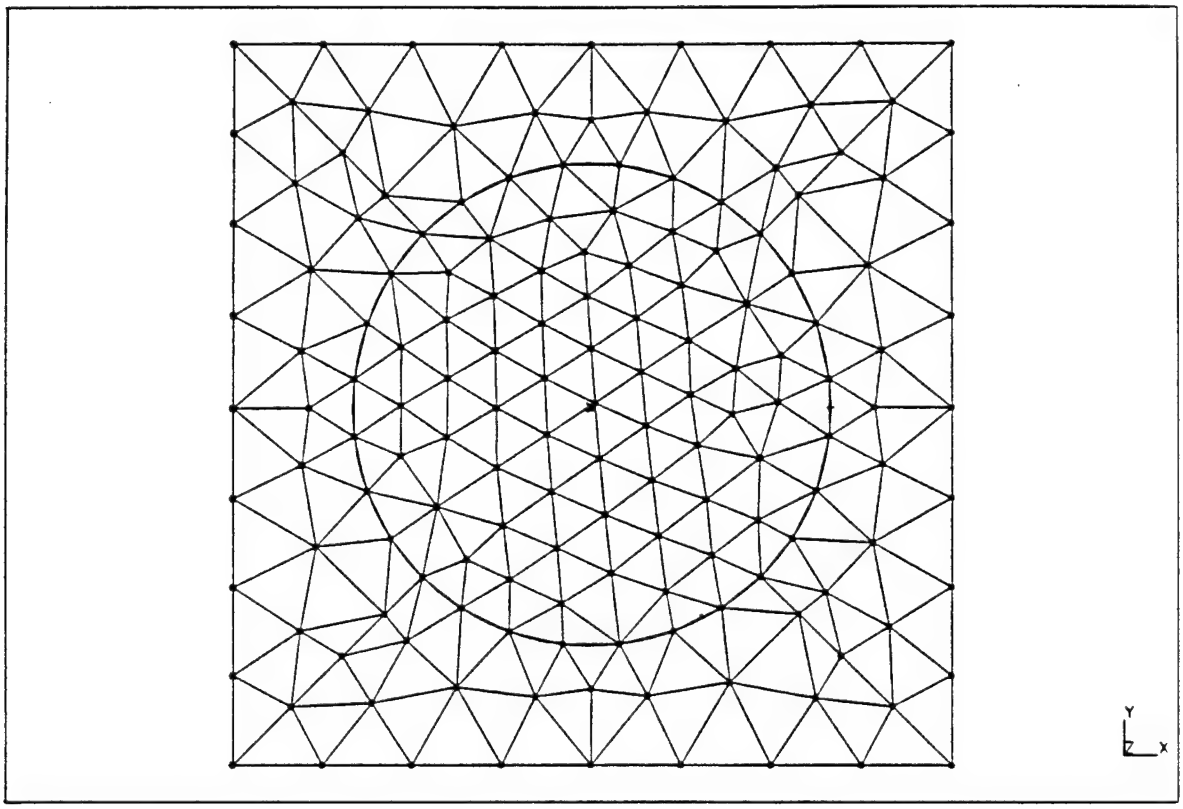

Figure 29: Mesh for a radiation test problem shown in Fig. 26. An absorbing boundary condition is applied on the square boundary of the mesh.

439 edges. In the following plots, we look at the electric field along the sampling line shown in Figure 28. For the first case, we use first order elements with a first order ABC. The magnitude of the x and y components of the electric field is plotted in Figure 30 for the solenoidal element and compared to the series solution. The two components in the FEM solution behave differently because the mesh is oriented such that E_y is tangential to the edges while E_x is normal to the edges. The first order basis function produces an almost constant tangential field along the edge and a linear behavior for a field normal to the edge. We next consider the case where first order elements are used, but a second order ABC is placed at the boundary. In Figure 31, we plot the magnitude of the differences between the numerical and series solution electric field for first order solenoidal elements with either a first or second order ABC. Interestingly enough, the accuracy of the solution is worse for the higher order ABC. It is likely that much of the error is due to poor discretization. Also, the failure of the second order ABC to outperform the first order one may very likely be due to the inaccuracies in the first order solenoidal elements. In order to test this hypothesis, we use third order solenoidal elements with a first order ABC on the same geometry as Figure 28 with the same mesh. The electric field components are plotted in Figure 32. Note that the solution is much smoother and much more accurate than for the first order elements. If we now use a second order ABC, we obtain much more accurate results (Figure 33) than for the first order ABC. These results demonstrate that in order to gain the advantages of a higher order ABC, we must choose the element order to be high enough.

To demonstrate the accuracy of these elements for an electrically larger case, we increase the electrical size of the geometry in Figure 28 by a factor of five. Thus the radius of the dielectric circular cylinder is $2\lambda_0$. Using the same mesh as in Figure 29 (1.6 elements/wavelength), we can produce a very accurate solution (Figure 34) with third order elements and a second order ABC.

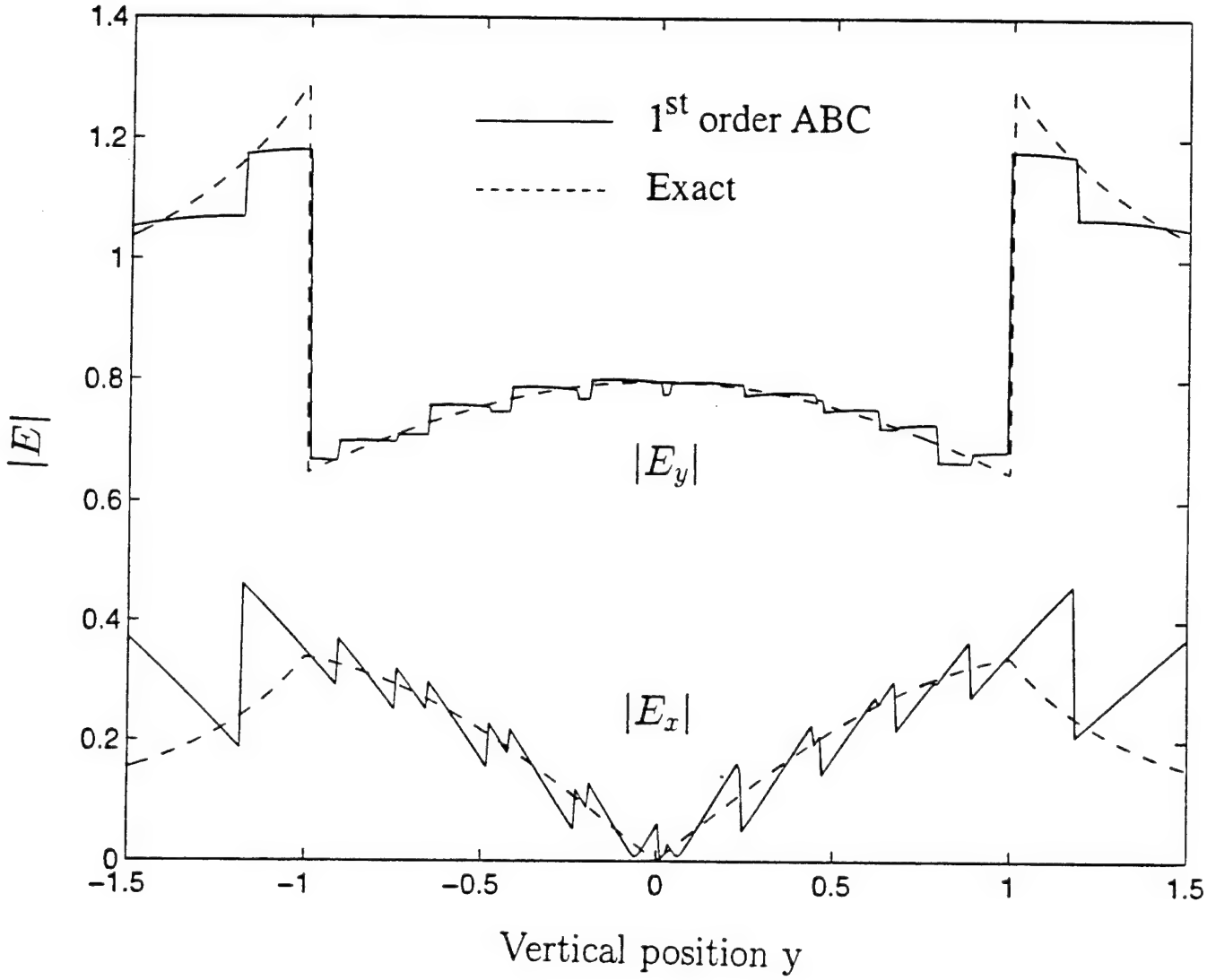

Figure 30: Plot of the magnitude of the vertical and horizontal electric field components for the case in Figs. 27 and 28. Solenoidal edge element solution with 1^{st} order elements and 1^{st} order ABC is compared to the exact solution.

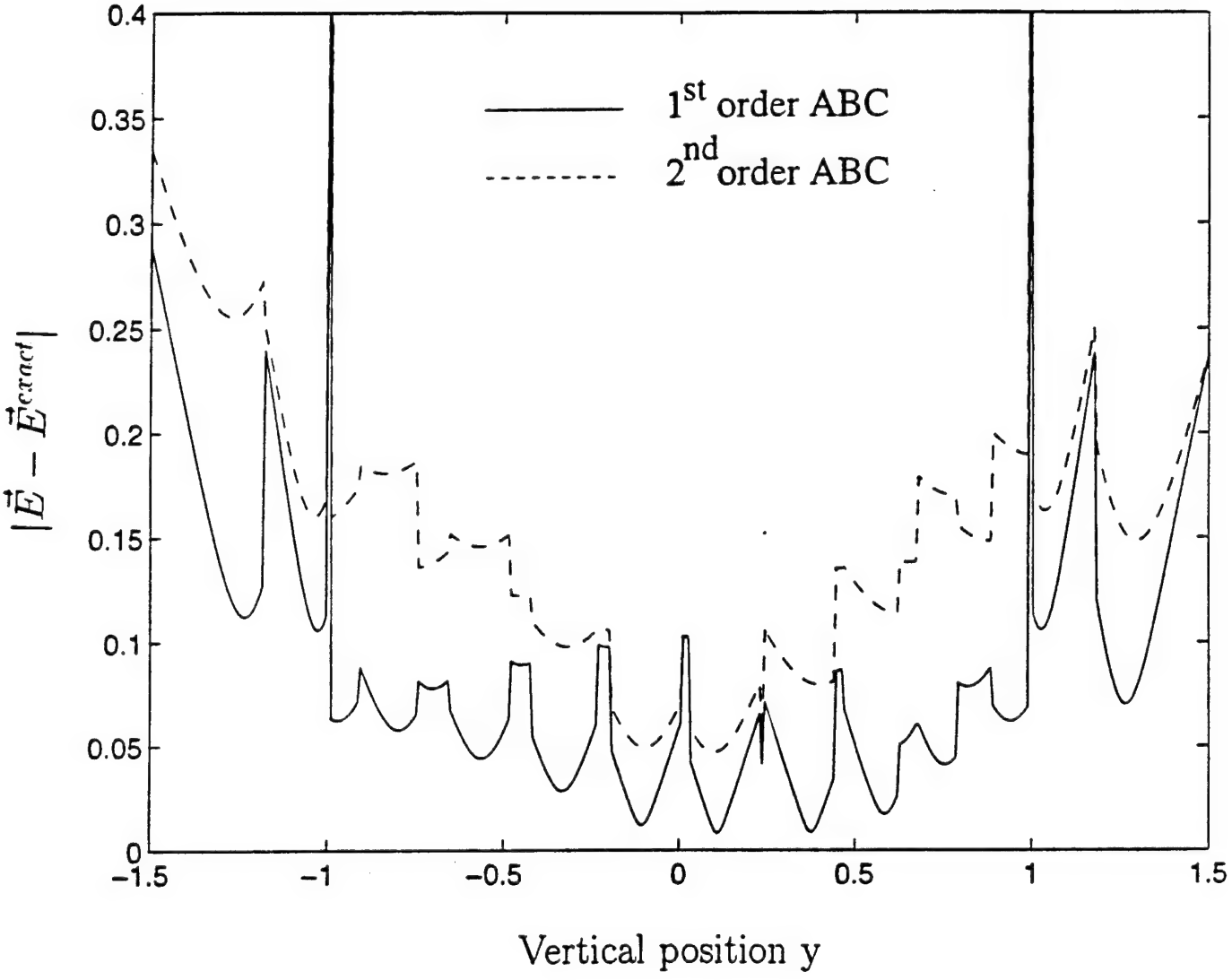

Figure 31: Plot of the magnitude of the error for the transversal electric field for the case in Figs. 27 and 28. Errors are compared for the solenoidal edge elements that use 1^{st} and 2^{nd} order ABC. 1^{st} order elements are used in both cases.

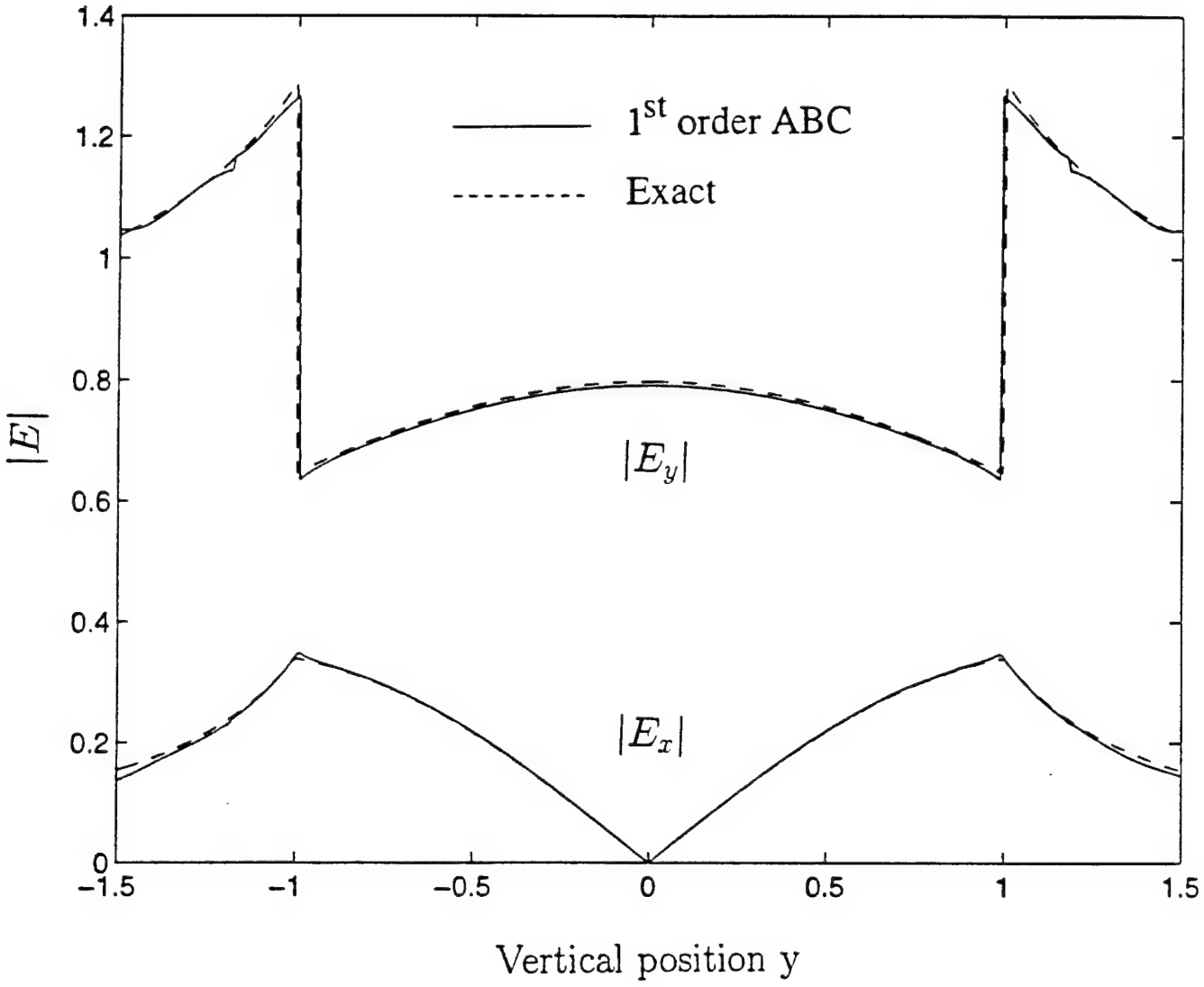

Figure 32: Plot of the magnitude of the vertical and horizontal electric field components for the case in Figs. 27 and 28. 3^{rd} order solenoidal edge element solution with 1^{st} order ABC is compared to the exact solution.

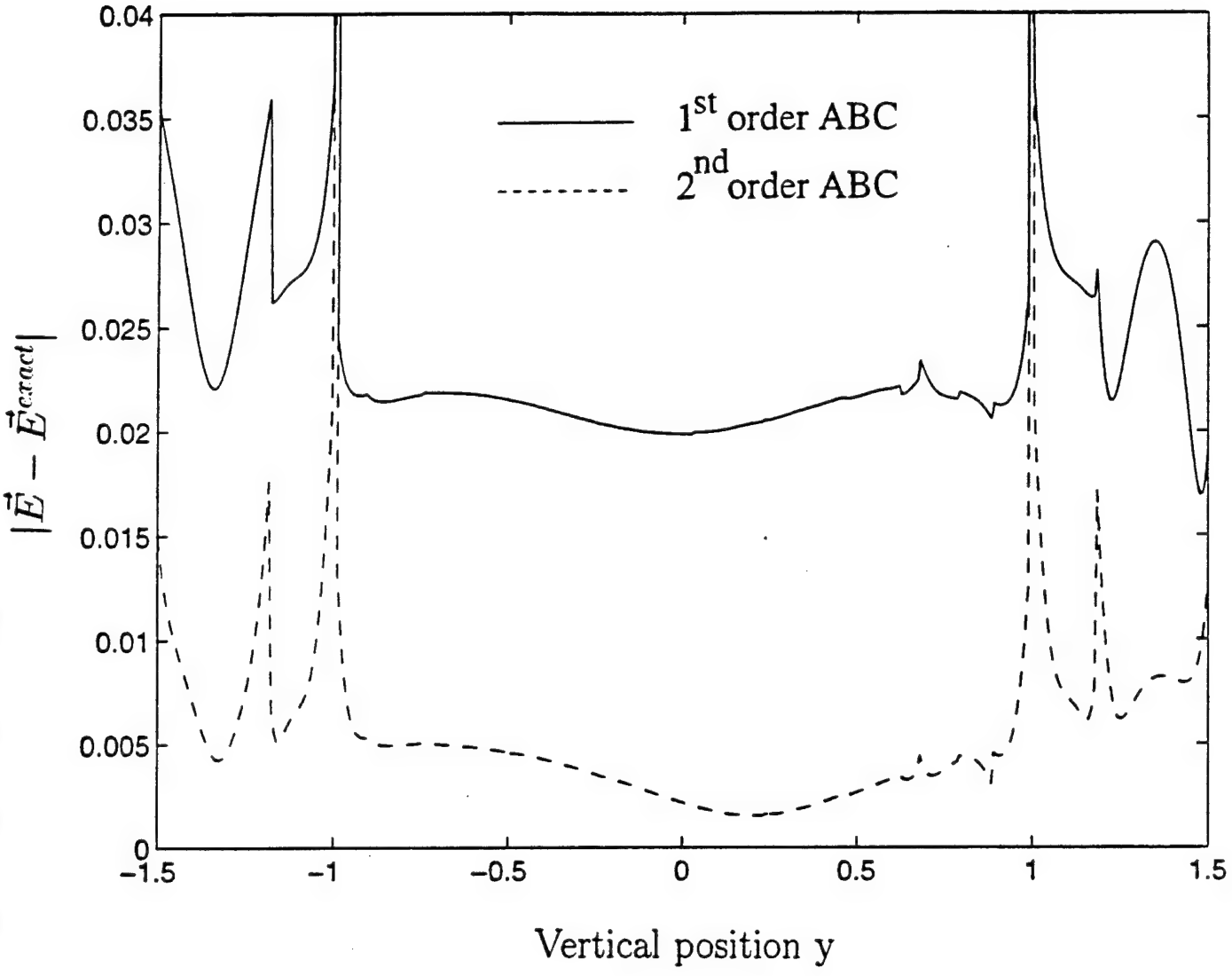

Figure 33: Plot of the magnitude of the error for the transversal electric field for the case in Figs. 27 and 28. Errors are compared for the solenoidal edge elements that use 1^{st} and 2^{nd} order ABC. 3^{rd} order elements are used in both cases.

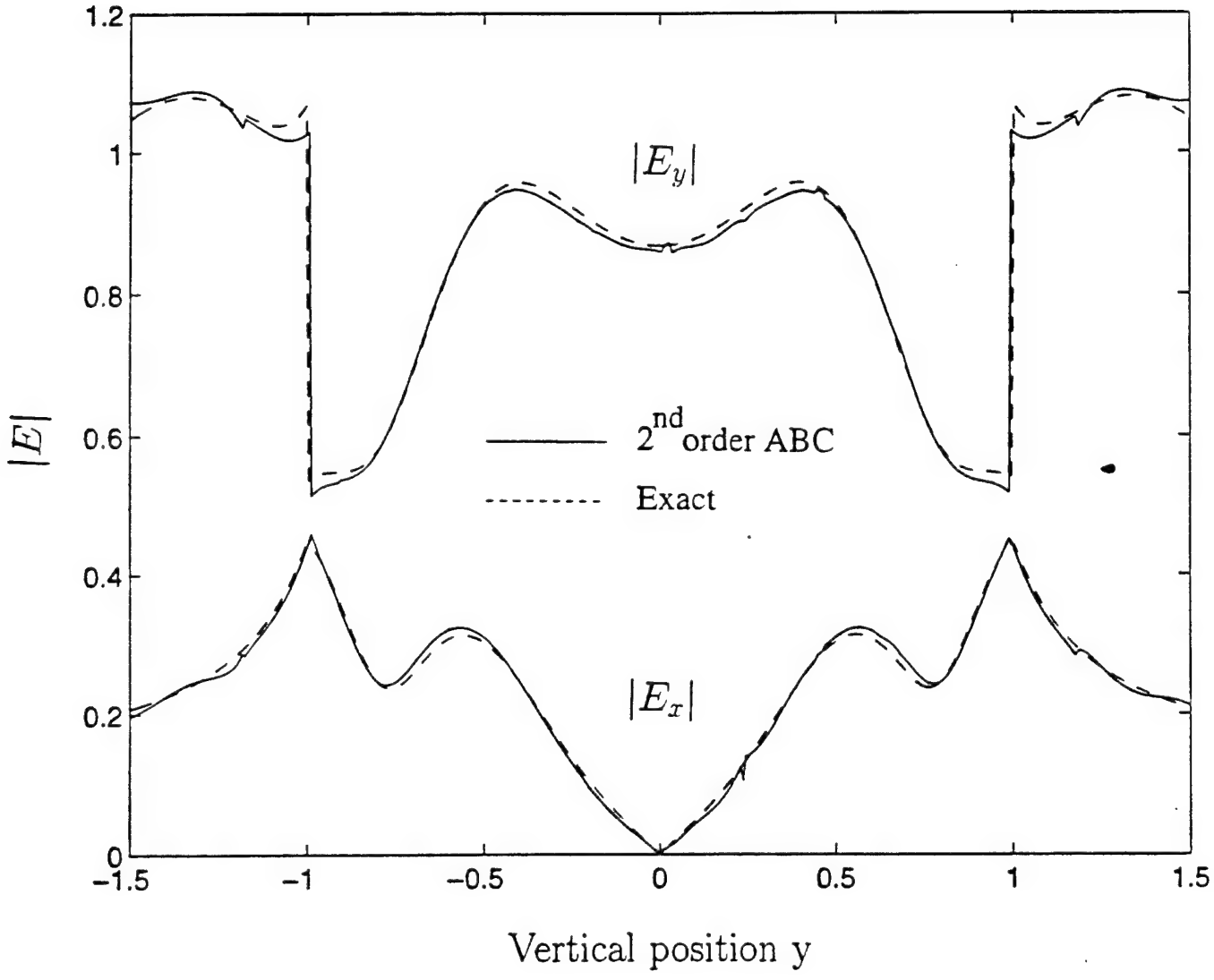

Figure 34: Plot of the magnitude of the vertical and horizontal electric field components for the case in Figs. 27 and 28, but for 5 times electrically larger problem. 3^{rd} order solenoidal edge element solution with 2^{nd} order ABC is compared to the exact solution.

References

[1] J. P. Berenger, "A perfectly matched layer for the absorption of electromagnetic waves," *J. Comp. Physics*, Vol. 114, pp. 185-200, October, 1994.

[2] W. C. Chew and W. H. Weedon, "A 3D perfectly matched medium from modified Maxwell's equations with stretched coordinates," *Microwave and Optical Technology Letters*, pp. 599-604, September, 1994.

[3] Z. S. Sacks, D. M. Kingsland, R. Lee, and J. F. Lee, "A perfectly matched anisotropic absorber for use as an absorbing boundary condition," accepted to *IEEE Trans. Antennas Propagat.*

[4] J. Y. Wu, D. M. Kingsland, J. F. Lee, and R. Lee, "A comparison of anisotropic PML to Berenger's PML and its application to the finite element method for EM scattering," submitted to *IEEE Trans. Antennas and Propagat.*

[5] J. C. Strikwerda, *Finite Difference Schemes and Partial Differential Equations.* California: Wadsworth and Brooks, 1989.

[6] A. Taflove and M. E. Brodwin, "Numerical Solution of Steady-State Electromagnetic Scattering Problems Using the Time-Dependent Maxwell's Equations," *IEEE Trans. on Microwave Theory and Techniques.*, vol. MTT-23, pp. 623–630, August 1975.

[7] J. F. Lee and Z. S. Sacks, "Whitney elements time domain method," *IEEE Transactions on Magnetics*, vol. 31, pp. 1325–1329, May 1995.

[8] J. Nehrbass, J. F. Lee, and R. Lee, "Stability analysis for perfectly matched layer absorber," submitted to *Electromagnetics.*

[9] O. C. Zienkiewicz and R. L. Taylor, *The Finite Element Method* (4th Edition), Vol. 1: *Basic Formulation and Linear Problems.* New York: McGraw-Hill, 1989.

[10] J. C. Nedelec, "Mixed finite elements in R^3," *Numer. Meth.*, vol. 35, pp. 315-341, 1980.

[11] J. F. Lee, D. K. Sun, and Z. J. Cendes, "Tangential vector finite elements for electromagnetic field computations," *IEEE Trans. Magnetics*, MAG-27, pp. 4032-4035, Sept. 1991.

[12] R. Lee and A. C. Cangellaris, "A study of discretization error in the finite element approximation of wave solutions," *IEEE Trans. Antennas and Propagat.*, AP-40, pp. 542-549, May 1992.

[13] J. Jevtic and R. Lee, "Solenoidal edge elements," submitted to *Radio Science.*

[14] W. Sun and C. A. Balanis, "Edge-based FEM solution of scattering from inhomogeneous and anisotropic objects," *IEEE Trans. Antennas and Propagat.*, Vol. AP-42, pp. 627-632, May, 1994.

[15] J.J DiStefano, A.R. Stubbeerud, and I.J. Williams, *Schaum's Outline Series on Theory and Problems of Feedback and Control Systems.* New York: McGraw Hill, 1990.

[16] R. Lee, Z. Chen, J. Jevtic, and J. F. Lee, "Important considerations in the evaluation of absorbing boundary conditions," submitted to *Electromagnetics.*

Refereed Publications

1. W. P. Pinello, R. Lee, and A. C. Cangellaris, "Finite element modeling of electromagnetic wave interactions with periodic structures," *IEEE Trans. Microwave Theory and Techniques*, MTT-42, pp. 2294-2301, December 1994.

2. U. Pekel and R. Lee, "An a posteriori error reduction scheme for the three dimensional finite element solution of Maxwell's equations," *IEEE Trans. Microwave Theory and Techniques*, MTT-43, pp. 421-427, February 1995.

3. J. O. Jevtic and R. Lee, "How invariant is the measured equation of invariance?," *IEEE Microwave and Guided Wave Letters*, Vol. 5, pp. 45-47, February 1995.

4. A. Bataineh, R. Lee, and F. Ozguner, "Electrical characterization of high-speed interconnects with a parallel three-dimensional finite difference time-domain algorithm," *SIMULATION*, Vol. 64, pp. 289-295, May 1995.

5. T. L. Barkdoll and R. Lee, "Finite element analysis of bodies of revolution using the measured equation of invariance," *Radio Science*, Vol. 30, No. 4, July/August 1995.

6. U. Pekel and R. Lee, "A 3-D application of the bymoment method for electromagnetic scattering," *Journal of Electromagnetic Waves and Application*, Vol. 9, pp. 973-992, July/August 1995.

Papers Accepted for Publication

1. J. O. Jevtic and R. Lee, "An analytic characterization of the error in the measured equation of invariance," *IEEE Trans. Antennas and Propagat.*, AP-43, pp. 1109-1115, October 1995.

2. Y. S. Choi-Grogan, K. Eswar, P. Sadayappan, and R. Lee, "Sequential and parallel implementations of a partitioning finite element method," accepted to *IEEE Trans. Antennas and Propagat.*

Papers Submitted for Publication

1. J. Y. Wu, D. M. Kingsland, J. F. Lee, and R. Lee, "A comparison of anisotropic PML to Berenger's PML and its application to the finite element method for EM scattering," submitted to *IEEE Trans. Antennas and Propagat.*

2. J. Nehrbass, J. F. Lee, and R. Lee, "Stability analysis for perfectly matched layer absorber," **Invited paper**, submitted to *Electromagnetics.*

3. R. Lee, Z. Chen, J. Jevtic, and J. F. Lee, "Important considerations in the evaluation of absorbing boundary conditions," **Invited paper**, submitted to *Electromagnetics.*

4. J. Jevtic and R. Lee, "Solenoidal edge elements," **Invited paper**, submitted to *Radio Science.*

Papers in Preparation

1. L. Hamandi, R. Lee, and F. Ozguner, "A fast decomposition technique for the parallel solution of the quasi-minimal residual method on 2D mesh architectures," in preparation.

2. L. Hamandi, F. Ozguner, and R. Lee, "Implementation of QMR on 2D meshes for the parallel finite element solution of 3D electromagnetic problems," in preparation.

Conference Presentations

1. R. Lee, "An overview of computational electromagnetics," **Invited paper**, SICAN Technology Conference, Hanover, Germany, November 1994

2. L. Hamandi, R. Lee, and F. Ozguner, "A domain decomposition technique for the parallel solution of linear systems of equations resulting from finite element discretization," International Conference on Electronic Circuits and Systems, Cairo, Egypt, December, 1994.

3. J. Jevtic and R. Lee, "An investigation of the convergence properties of the measured equation of invariance," URSI Radio Science Meeting, Boulder, CO, January 1995.

4. L. Hamandi, F. Ozguner, and R. Lee, "The performance of the parallel solution of the Quasi-Minimal Residual (QMR) method for 2D mesh architectures," **Invited paper**, 11th Annual Review of Progress in Applied Computational Electromagnetics, Monterey, CA, March, 1995

5. D. Kingsland, R. Dyczij-Edlinger, J. F. Lee, and R. Lee, "Performance characterization of a perfectly matched anisotropic absorber for frequency domain FEM applications," **Invited paper**, Joint AP-S Symposium and URSI Radio Science Meeting, Newport Beach, CA, June, 1995.

6. R. Lee, J. Jevtic, and Z. Chen, "The effect of numerical dispersion on boundary conditions for wave problems," **Invited paper**, Progress in Electromagnetic Research Symposium, Seattle, WA, July, 1995.

7. J. F. Lee, J. Y. Wu, and R. Lee, "Application of an anisotropic PML and its relationship to Beringer's PML," **Invited paper**, Progress in Electromagnetic Research Symposium, Seattle, WA, July, 1995.

8. J. Jevtic and R. Lee, "Further insights into high order solenoidal edge elements," **Invited paper**, Progress in Electromagnetic Research Symposium, Seattle, WA, July, 1995.

Awards

1. J. O. Jevtic, Second Place, 1995 URSI Student Paper Contest, "An investigation of the convergence properties of the measured equation of invariance," URSI Radio Science Meeting, Boulder, CO, January 1995.

2. J. O. Jevtic, 1994 ESL Best Masters Thesis Award, "An Analysis of the Measured Equation of Invariance."

3. Prof. Lee received the 1995 Lumley Research Award from the College of Engineering at The Ohio State University. This award is based on the previous four years of work.

Ph.D. Dissertation

1. "Parallel Algorithms for the Finite Element Method on the Mesh Architecture," Lama Hamandi, May, 1995.

M.Sc. Thesis

1. "A Parallel Automatic Grid Generator for the Finite Difference Time Domain Method," Roger Prenger, July, 1995.

VI. HYBRID STUDIES

Researchers:

P.H. Pathak, Professor	(Phone: 614/292-6097)
R. Rojas, Associate Professor	(Phone: 614/292-2530)
P. Roblin, Associate Professor	(Phone: 614/292-0998)
R.J. Burkholder, Senior Research Associate	(Phone: 614/292-4597)
M. Hsu, (graduated recently)	
M. Otero, Graduate Research Associate	(Phone: 614/292-7981)
D. Kwon, Graduate Research Associate	(Phone: 614/292-7981)
V. Erturk, Graduate Research Associate	(Phone: 614/292-7981)
K.P. Hwang, Graduate Research Associate	(Phone: 614/292-7981)

1. Introduction

EM phenomena associated with radiating objects can be classified according to different scales in terms of the radiated EM wavelength. For example, at one extreme, for the high frequency regimes of interest, a complex radiating object such as an aircraft can exhibit both electrically very large as well as electrically small portions; at the other extreme, radiating antenna elements and their feed components can, either due to need for miniaturization or due to use of very high frequencies, become extremely small physically (as, for example, in some modern wireless systems, or as in millimeter wave antenna array elements, etc.) requiring one to consider integrating a small radiating element directly with its source which is a far smaller active solid state device. Both types of the above situations, depicting extremes of scales, are expected to occur even more frequently in the future. However, there is no single approach or technique which can be used as a prediction or analysis/design tool for dealing with such EM phenomena in a tractable fashion. For example, neither asymptotic high frequency techniques, nor numerical or the low frequency techniques alone can predict the radiation or scattering from an object containing large and small parts; also full wave techniques which can analyze an antenna element cannot really easily deal with an active solid state device which may be used as a source for the antenna. It thus becomes extremely important to develop systematic hybrid combinations of different (two or more) techniques

in which each technique is respectively chosen so that it is best suited for efficiently handling a different part of the complete radiating object, and these techniques when systematically combined in a given hybrid combination can then handle the entire or complete radiating object in a tractable fashion. Clearly, the development of such hybrid tools would be of significant interest, and also of use to present and future EM technology. With this view in mind, this hybrid section of JSEP has focused on the development of hybrid prediction or analysis/design tools.

During the past period, substantial progress was made in the development of a hybrid method for analysis/design of an active integrated microstrip patch antenna using a combination of circuit solvers and nonlinear device analysis to deal with an active bipolar junction transistor (BJT) operating as an oscillator, with a full wave analysis for the microstrip patch type antenna radiating element whose parameters were integrated into the design of the active device operation. This active integrated antenna is an example where it is not possible to design the passive radiating patch with some idealized feed as is often done in microstrip patch antenna full wave analysis; indeed, it is important to know the actual active device parameters as closely as possible so that the passive resonant load provided by the patch can be truly integrated into the active device analysis so that the active device can provide stable oscillations at the desired frequency of operation. A careful large signal analysis of the BJT as well as an accurate analysis of the antenna is required to conduct a modified Kurokawa's nonlinear analysis to guarantee stable oscillations within its active region. Note that this analysis takes into account several harmonics in addition to the fundamental signal.

Also, in the development of hybrid methods, it is necessary to consider the use of partial differential equation (PDE) based numerical methods for solving Maxwell's equations which are especially useful in dealing with regions of a radiating object which are electrically small but highly inhomogeneous. The finite different time domain (FDTD) has become a rather popular numerical PDE technique despite some drawbacks such as, for example, its difficulties in handling curvilinear geometries; on the other hand, the computational fluid dynamics (CFD) community appears to have made significant strides in PDE based numerical methods which has led to the finite volume time domain (FVTD) approach that appears to be potentially more advantageous especially from the point of view of its versatility

in dealing with curvilinear boundaries, and its robustness. However, a thorough comparison of FDTD with FVTD does not appear to have been conducted making it unclear as to which method is better suited for what situations. Consequently, a study of one form of this potentially useful FVTD has begun to characterize its efficiency, stability, use in wide band and even non-liner regimes, and its behavior with respect to absorbing boundary conditions for truncation of FVTD regions. The initial studies are focusing on antenna phenomena in the presence of antenna excitation, and in presence of materials for optimizing the antenna performance. An elliptic body fitting grid generator has also been developed in 2-D to be used in the FVTD discretization. It is hoped that this study would provide more useful information on the FVTD and to also indicate areas of further study to possibly improve the efficiency of the FVTD procedure while still maintaining its versatility.

Work has also continued on the development of a hybrid method for dealing with material treatment of edged bodies in which the material can control the scattering characteristics of the edge. An area where this hybrid approach has an impact is in antenna design. Most antenna structures contain edges and the treatment of edge effects becomes crucial in many applications to obtain the desired antenna performance. The use of the special Green's function for the impedance wedge developed in the Diffraction Studies unit has been employed in this hybrid approach to demonstrate its usefulness in the design of a microstrip antenna where edge effects produce detrimental effects on the antenna performance, and where these undesired effects are nullified to obtain an excellent antenna performance by proper design of edge treatment using a hybrid numerical moment method asymptotic approach. In this hybrid approach, an integral equation formulation is employed which is solved by a numerical moment method (MM) procedure, but the number of unknowns to be solved in this MM is drastically reduced because of the special choice of the aforementioned wedge Green's function in the kernel of the integral equation.

Significant progress has also been made in the hybrid analysis of conformal antennas. This hybrid analysis employs an integral equation formulation for dealing with antennas and large antenna arrays mounted conformally on electrically large, perfectly-conducting convex surfaces with a uniform material coating (which can act as a radome or be used for impedance matching, or both). The integral equation is to be solved numerically via the

moment method (MM); however, the number of unknowns to be solved is reduced drastically by a special choice of a UTD form of the kernel (Green's function) in the integral equation. This analytical UTD Green's function for electric/magnetic point current sources on an "arbitrary" smooth convex conducting surface with a thin uniform material coating has been completed recently and constitutes a significant result which is to be used in this hybrid approach. The general UTD solution is developed from generalization of the canonical conducting sphere and circular cylinders with uniform material coating which was reported in the last year's JSEP annual report. Presently, a numerical computation of some of the special UTD transition functions is being conducted so that this analytical UTD Green's function can be computed efficiently for use in the hybrid method. It is noted that brute force numerical methods may become intractable for predicting the behavior of large scanning arrays mounted conformally on large smooth convex conducting bodies with or without material coating; in contrast the present hybrid method is expected to efficiently analyze such a radiating configuration in which the unknowns to be solved are restricted only to the fields on just the antennas and not to the rest of the large convex material coated platform. Demonstrations of the utility of this hybrid approach are planned for the next phase of this study.

Finally, work on the development of the hybrid procedure for analyzing the radiation/scattering from generic but realistic complex aircraft/missile shapes is progressing well. At this time, the required UTD solutions which will comprise the special Green's function for the fuselage region are being developed in the unit on Diffraction Studies. These UTD solutions are expected to be completed by early next year. They will subsequently be implemented as the kernel of an integral equation for this generic radiating configuration to reduce the region of the unknown fields to be solved via this integral equation to the horizontal/vertical stabilizers and fins, since the main fuselage is accounted for by the UTD. The unknowns over the regions of the stabilizers or fins will then be solved for fairly realistic but generic examples of aircraft/missile using the moment method (MM). The MM solution will be computed via an iterative approach to avoid problems associated with inversion of large MM matrices. In the future phase of this study, a super hybrid scheme will be incorporated

to include the effects of antennas, antenna windows, gaps, and jet engine cavities. Work is in progress to analyze the latter components by techniques best suited for each case.

A separate yet related study was undertaken to substantially speed up the fast multipole method (FMM) which has emerged recently as a very useful method for actually speeding up MM computations based on iterations. This acceleration of the FMM was demonstrated in the 2-D case by using a hybrid approach in the sense that the FMM numerical technique was made more efficient by introducing certain windowed operations based on asymptotic high frequency concepts. An analysis based on the asymptotic steepest descent method provided a rigorous framework for incorporating windows into the FMM scheme thereby substantially reducing computation times. In particular, an operation count $\mathcal{O}(N^{3/2})$ of the FMM was reduced to $\mathcal{O}(N^{4/3})$ in the accelerated FMM procedure developed in this study. Similar extensions to 3-D will be investigated in the future phases of this study.

2. Design and Analysis of Active Integrated Antennas

The field of "wireless communications" has experienced a tremendous growth in the last few years and it is projected that this growth will continue in the foreseeable future. Some of the key requirements for systems in this field such as cellular phones is that the components need to be low cost, small, reliable, etc. Active integrated antennas can play an important role because they satisfy some of the above requirements. The integration of solid-state devices (active) and antenna functions (passive) onto the same substrate to produce compact radiating structures is referred to as an active integrated antenna. The main advantages of such structures lie in their low cost, simplicity of design and small size. Therefore, they are well-suited for mass production and applications in radar, satellite and communication systems [1]–[4]. Some of the goals of this research are to develop analysis and design methods that are accurate and efficient as well as designs of active integrated antennas that satisfy the most important specifications in the area of wireless communications. A scheme that is currently being pursued to design/analyze this class of antennas is a hybrid combination of a full-wave solver (3-D FDTD code) with a non-linear circuit simulator (LIBRA, developed by EESOF). The full wave solver is used to obtain the S-parameters of the passive components,

while LIBRA is used to analyze the active nonlinear components. The full wave solver will also be used to calculate the radiation patterns of the antennas.

A prototype for a transistor-oscillator active antenna was developed in this study by integrating a three-terminal device (AT-42035, medium power Silicon Bipolar Transistor, produced by HP-AVANTEK) with a microstrip patch antenna which radiates the RF power, and acts like a resonator to set the operating frequency, and a resonant load to produce high DC-to-RF efficiencies. Before the fabrication process, the design is analyzed and verified with an improved form of Kurokawa's generalized analysis [5]–[6]. Note that Kurokawa's analysis is usually applied without taking into account the harmonics. The present scheme being considered here does take into account several harmonics and therefore yields more accurate designs.

The initial design can be done by the "negative resistance" and/or "reflection coefficient" techniques that are popular in the design of oscillators. We define Z_A and Γ_A as the impedance and the reflection coefficient of the "active" port, and similarly Z_L and Γ_L as the impedance and the reflection coefficient of the "load" port respectively. For the reflection coefficient technique, the oscillation conditions for start-up are:

$$| \Gamma_A || \Gamma_L | > 1 \tag{62}$$

$$\angle(\Gamma_A) + \angle(\Gamma_L) = 0. \tag{63}$$

While the steady-state conditions can be written as follows:

$$| \Gamma_A || \Gamma_L | = 1 \tag{64}$$

$$\angle(\Gamma_A) + \angle(\Gamma_L) = 0 \tag{65}$$

For the negative resistance technique, the oscillation conditions for start-up are:

$$Re(Z_A) + Re(Z_L) < 0 \tag{66}$$

$$Im(Z_A) + Im(Z_L) = 0 \tag{67}$$

and the steady-state conditions are given by:

$$Re(Z_A) + Re(Z_L) = 0 \tag{68}$$

$$Im(Z_A) + Im(Z_L) = 0 \tag{69}$$

Comparison of these two techniques indicates that the steady-state conditions for both techniques are equivalent, however the start-up conditions are not, and the negative resistance technique is much better for design purposes [7]. The reflection coefficient technique is useful for analysis, but from the view point of design, the oscillators designed based on this method either do not start at all or start far away from the predicted frequency. On the other hand, Equation (66) will start the oscillation and then the non-linearities will bring it into steady-state. Thus, following the negative resistance technique, the following steps are important:

- An NPN-active biasing circuit is precisely modelled in Libra and a non-linear model of AT-42035 is biased such that the transistor works in the active region. Some transistor parameters are compared with the experimental results and both the bias network and non-linear model of the transistor are tested.

- The transistor is forced to become potentially unstable at the frequency of oscillation by adding some stubs to the emitters and base.

- The length of the stubs are optimized in such a way that we will have a negative impedance ("active" port) at the desired frequency and the emitters have a balanced structure.

The output port of the active device is directly connected to a microstrip patch antenna via a microstrip line (see Figure 35) and the design of the load should satisfy (66) and (67) simultaneously.

The input impedance of the antenna at resonance is chosen to be exactly the same as the characteristic impedance of the microstrip line in order not to use any matching networks. Therefore, a notch is introduced and the width of the notch is optimized with a modified transmission line model. The design is verified, and both the time and frequency domain characteristics of the antenna are obtained by using a 3-D FDTD code.

As mentioned before, we are using an improved form of Kurokawa's generalized analysis of negative-resistance oscillators where the effect of harmonics, which has not been included

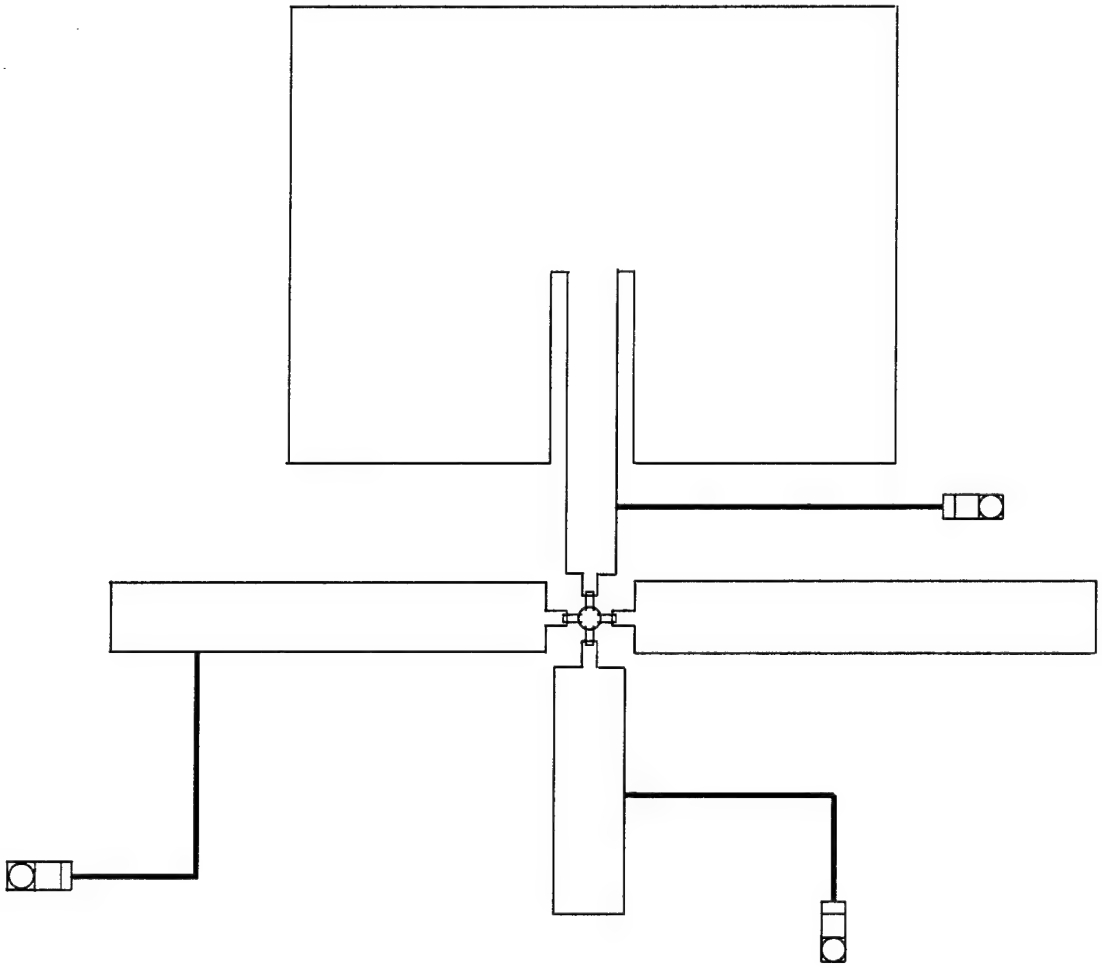

Figure 35: Configuration of active integrated microstrip antenna.

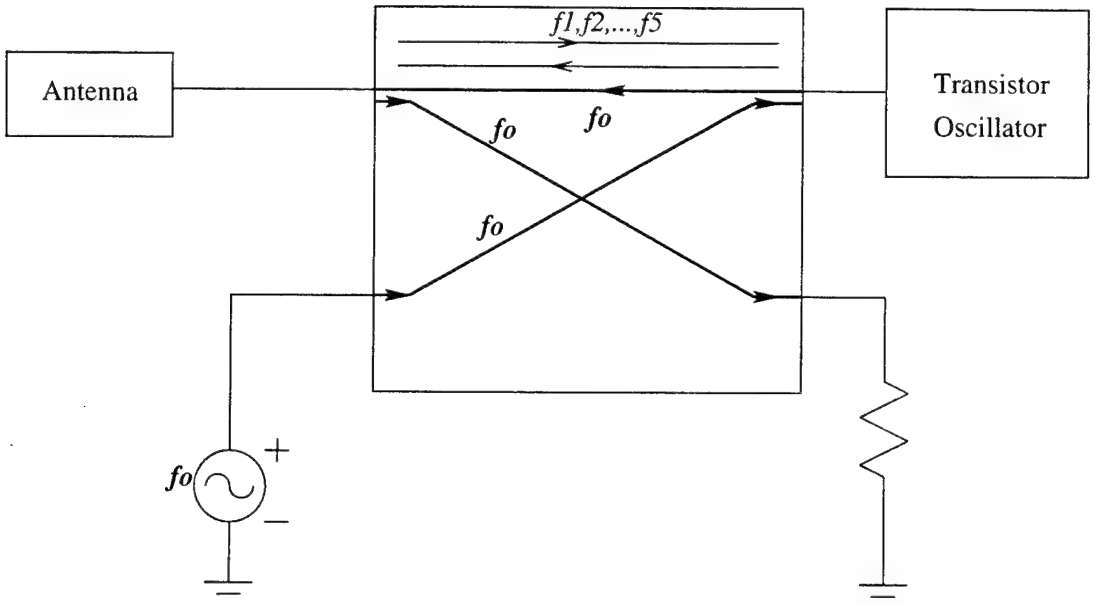

Figure 36: Schematic of an improved Kurokawa analysis which includes harmonics.

before, is taken into consideration. Besides the fundamental signal, the harmonics see the main load (antenna unit) and travel back and forth between the antenna and the oscillator units as depicted in Figure 36. Consequently, this is a very realistic representation of the actual circuit. In Kurokawa's generalized analysis, a stable operation point for a current waveform of the form $i(t) = A(t)\cos(\omega t + \phi(t))$ is given by ;

$$A_0[\frac{\partial R_A(A_0)}{\partial A}\frac{\partial X_L(\omega_0)}{\partial \omega} - \frac{\partial X_A(A_0)}{\partial A}\frac{\partial R_L(\omega_0)}{\partial \omega}] > 0 \tag{70}$$

where $Z_A = R_A + jX_A$ and $R_A < 0$ is the impedance of the active device, and $Z_L = R_L + jX_L$ is the load impedance. In our improved analysis the load impedance locus will not change, however, as seen from Figure 37, the harmonics (which see the true load and reflect back) will change the device impedance locus. With this analysis we can also predict the current, voltage and power levels at the fundamental frequency and harmonics.

Two different active antennas, one having microstrip line open circuits (MLOC) and the other having microstrip line short circuits (MLSC) at the emitters, were designed (for operation at 2.01GHz) and fabricated. Both designs have MLOC at the base. Figures 38 and 39 show the measured spectrum of the signals for both designs at the desired frequency. For these 2 devices the center frequency is seen to be 2.019 GHz and 2.047 GHz, respectively. The final step was to measure the radiation patterns in the compact range at The Ohio State University. Figs 40 and 41 show both the co-polarizations and the cross-polarizations in the

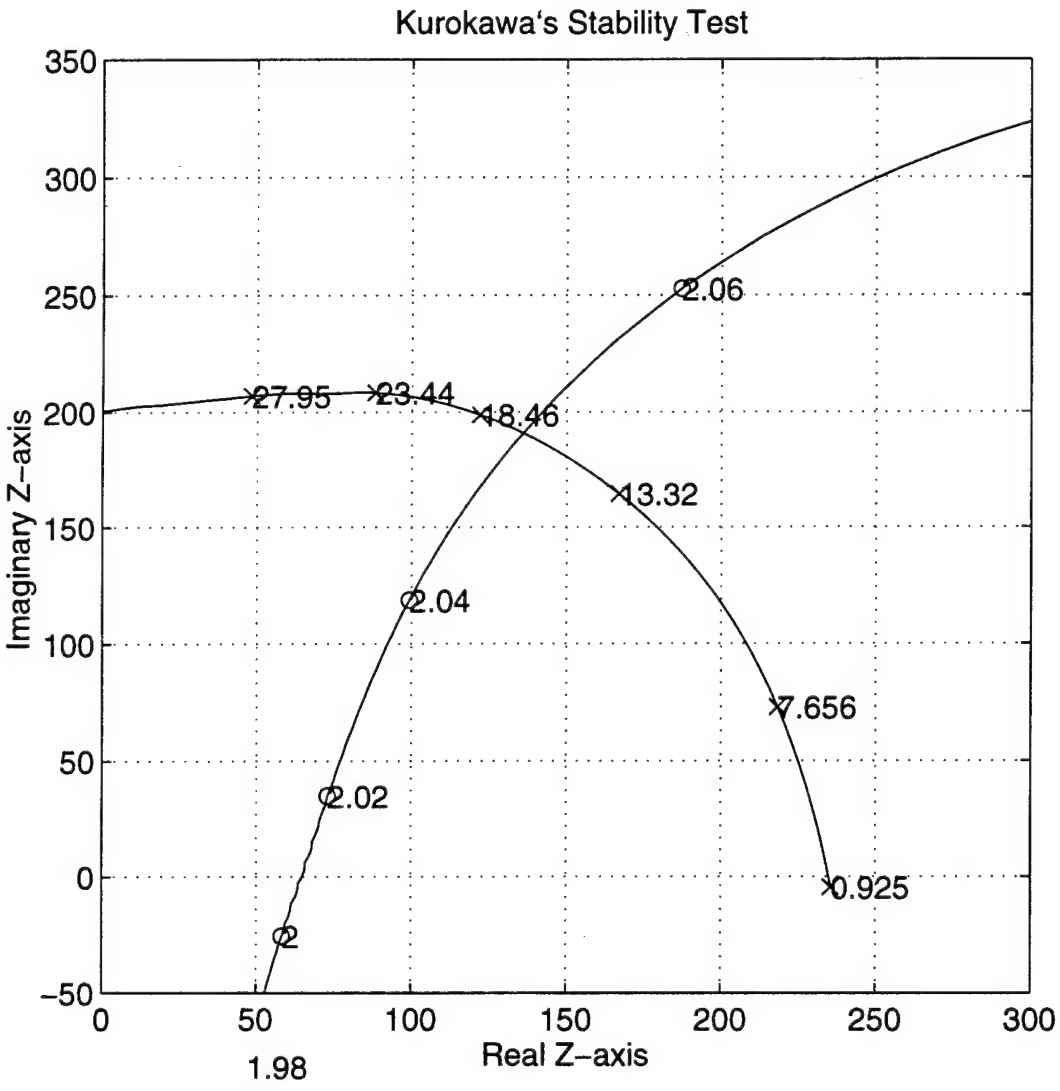

Figure 37: Locus of load impedance (antenna) (o–o–o) and negative of active device impedance (×–×–×) as a function of frequency. The load impedance is plotted for various values of frequency ranging from 2 to 2.06 GHz. The negative of the active device impedance is plotted for various values of collector current (AC) ranging from 0.925 to 27.95 mA.

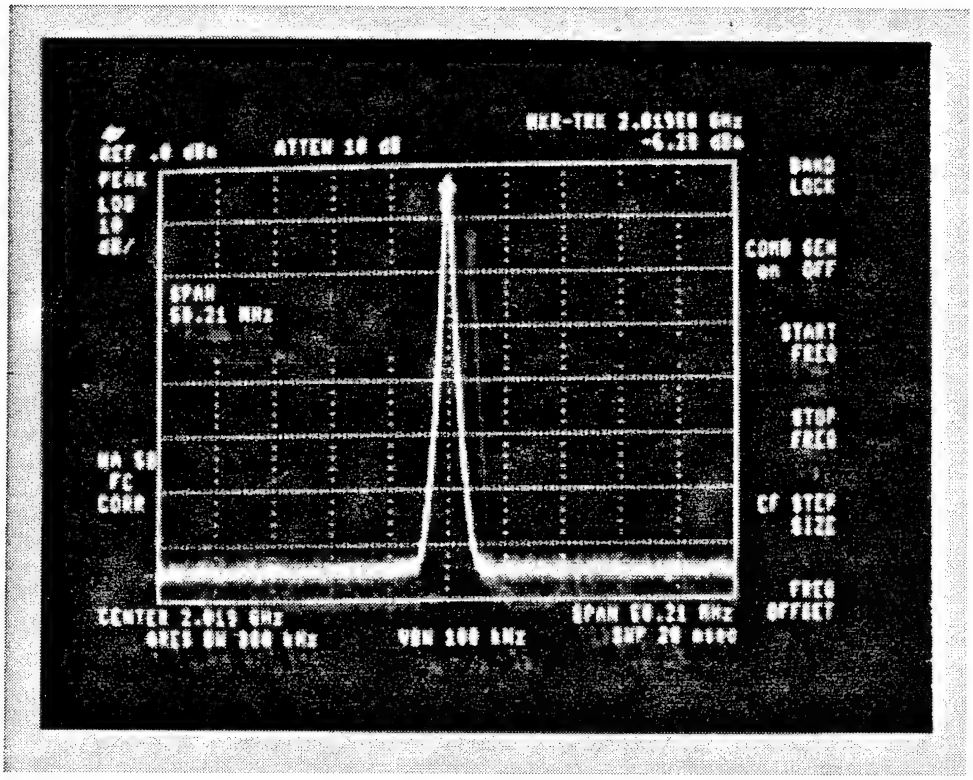

Figure 38: Spectrum of measured output signal for MLOC design.

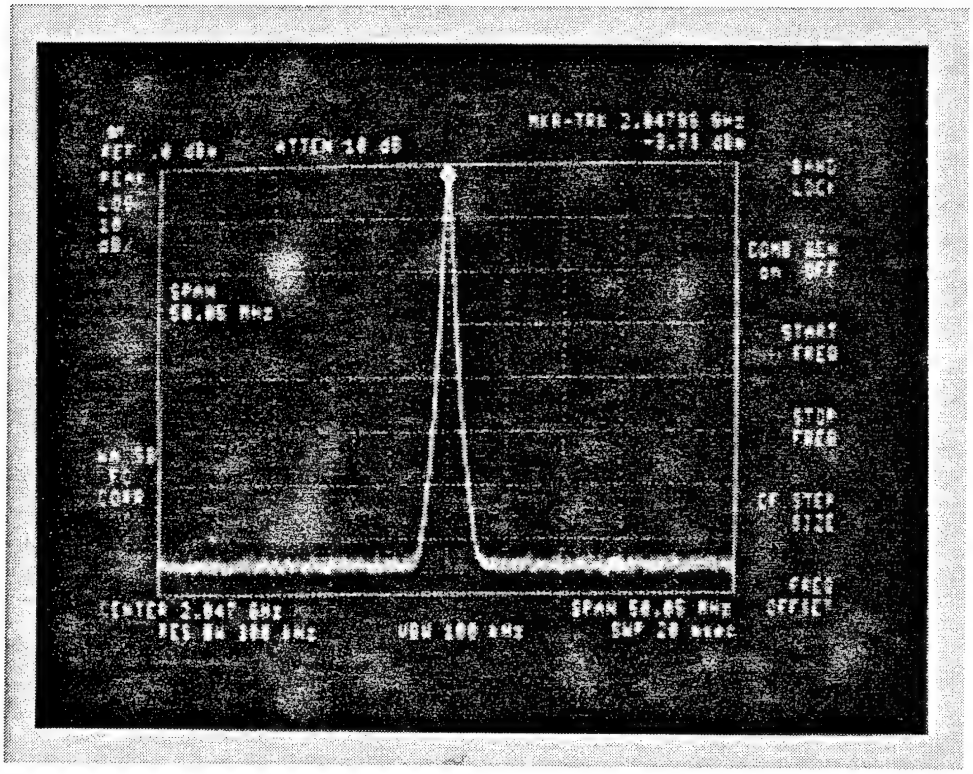

Figure 39: Spectrum of measured output signal for MLSC design.

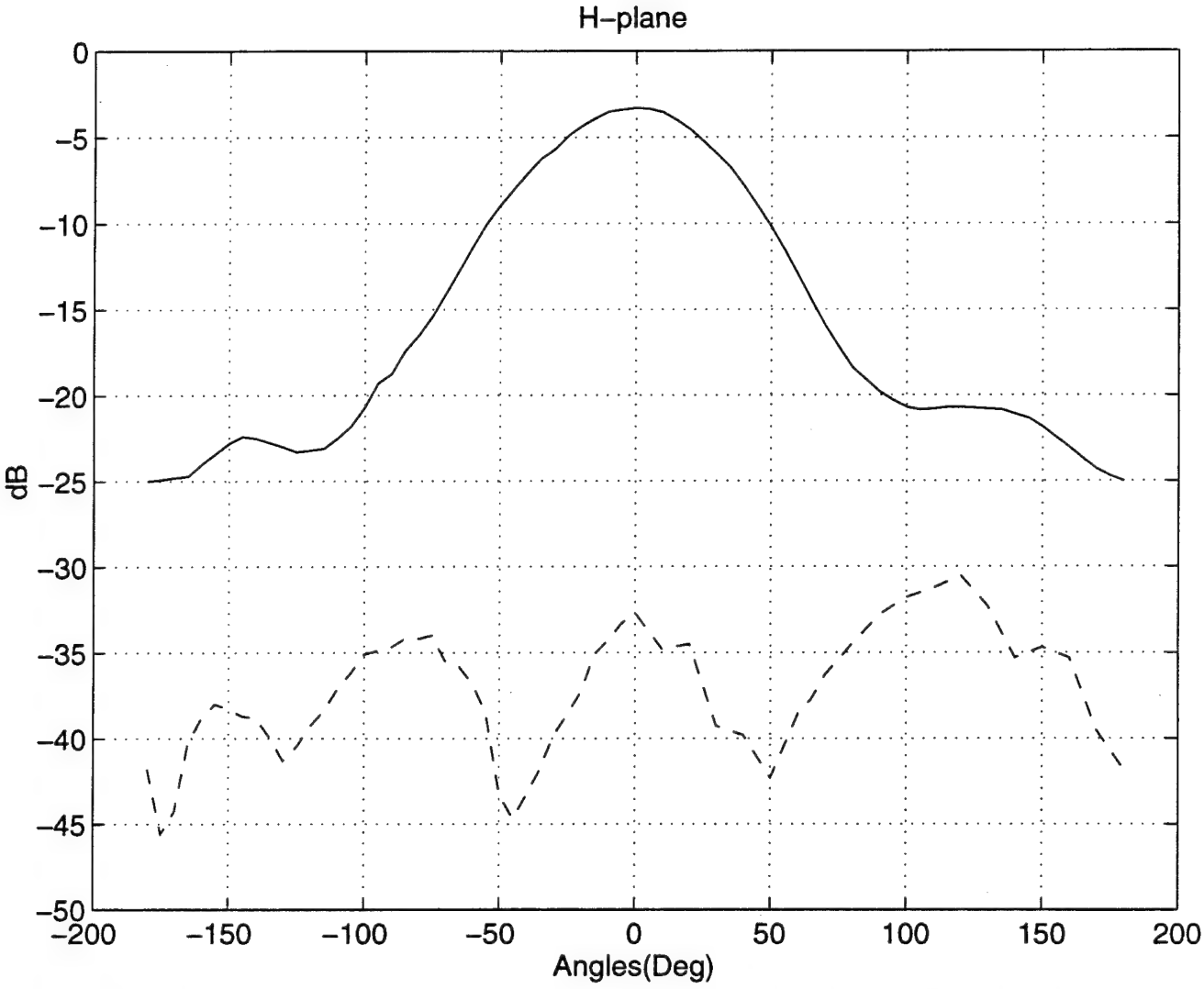

Figure 40: Measured H-plane pattern (co- and cross-polarized fields) for MLOC design.

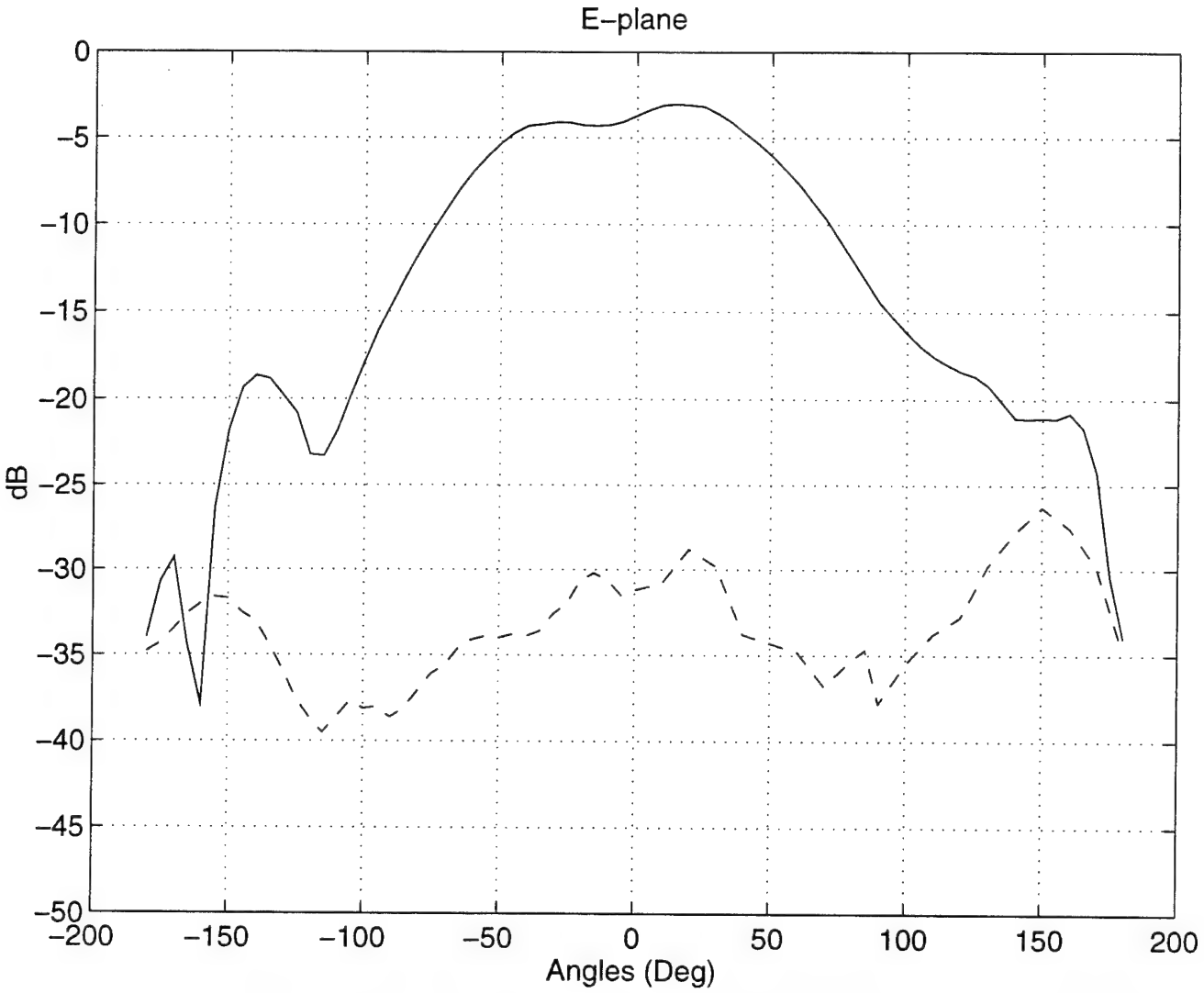

Figure 41: Measured E-plane pattern (co- and cross-polarized fields) for MLOC design.

E and H-planes. The patterns are very good and show very low cross-polarized components in the broadside region ($-90°$ to $90°$).

3. Characteristic-Based Finite Volume Time Domain (FVTD) Solver

Since the late 80's there has been a continuing effort in the Computational Fluid Dynamics (CFD) community to apply their numerical algorithms to solve Maxwell's equations in the time domain. Among the several methods developed so far, a Finite Volume Time Domain (FVTD) scheme, originated by Shankar's group [8, 9] has emerged as a viable scheme for its robustness and versatility. In the Computational Electromagnetics Community, the Finite Difference Time Domain (FDTD) [10] method, originally developed by Yee [11], has on the other hand already attained a dominant position as a time domain Maxwell solver despite some undesirable numerical characteristics. Thus, we began to investigate the FVTD method developed in [8, 9] to see what are the differences, advantages and disadvantages of this method over the well known FDTD. There are very few papers in the literature where there is a thorough analysis comparing the performance of these two methods in solving Maxwell's equations. It is important to mention that there are other FVTD schemes also being developed in the CFD community [12], however, at the present time we are only considering one of them.

The FVTD scheme being studied here is based on numerical algorithms used in Computational Fluid Dynamics. Maxwell's equations need to be written in conservation law form which is commonly done in the CFD community. Then the quantities we are dealing with are electric fluxes and magnetic fluxes following the concepts of fluid dynamics. The integral form of Maxwell's equations can be written in the form of a conservation law as follows

$$\frac{\partial}{\partial t}\iiint_V \bar{Q}dV + \iint_S \bar{\bar{\mathcal{F}}}\cdot d\bar{A} = \iiint_V \bar{S}dV \tag{71}$$

where $\bar{Q}$ is a vector quantity to be conserved, $\bar{\bar{\mathcal{F}}}$ is a dyadic flux going out of the volume V, and $\bar{S}$ is the source vector. For Maxwell's equations,

$$\bar{Q} = \begin{bmatrix} \bar{B} \\ \bar{D} \end{bmatrix} \quad , \quad \bar{\bar{\mathcal{F}}} = \begin{bmatrix} -\bar{\bar{\mathcal{I}}} \times \bar{E} \\ \bar{\bar{\mathcal{I}}} \times \bar{H} \end{bmatrix} \tag{72}$$

where $\bar{\bar{I}}$ is the identity dyadic. In rectangular coordinates, $\bar{\bar{I}} = \hat{x}\hat{x} + \hat{y}\hat{y} + \hat{z}\hat{z}$. Finally, the source vector $\bar{S}$ is given by

$$\bar{S} = \begin{bmatrix} \bar{0} \\ -\bar{J} \end{bmatrix} \tag{73}$$

The differential form of (71) is given by

$$\frac{\partial}{\partial t}\bar{Q} - \nabla \cdot (\bar{\bar{\mathcal{F}}}) = \bar{S} \tag{74}$$

Recall that for linear, isotropic, inhomogeneous media, $\bar{B} = \mu(\bar{r})\bar{H}$ and $\bar{D} = \epsilon(\bar{r})\bar{E}$. Equation (74) can be easily modified to incorporate general curvilinear coordinate system which enables us to handle complex curvilinear geometries in physical space. To utilize this body conformal feature we need to have a grid generator mapping complex geometries in physical space to a simple one in computational space. We developed and tested a preliminary version of a computer code for this purpose. Note that (71) can be used to develop a "unstructured" grid formulation, which has some advantages over the "structured" grid formulation that uses a curvilinear coordinate system.

To solve Partial Differential Equations (PDE) we need a time integration scheme. Unlike the FDTD, which uses the Leap-frog method in time integration, the FVTD we are considering uses a modified version of the upwind Lax-Wendroff scheme which is widely used in CFD problems [13]–[14]. Here the scheme is based on characteristic theory of signal propagation. For hyperbolic equations like Maxwell's equations, upwind-based schemes can be constructed to provide the right amount of numerical dissipation to achieve both stability and accuracy of computation.

Originally these upwind-based methods in CFD have been devised to handle discontinuities in solutions like shock phenomena. In Computational Electromagnetics these features may be useful in the study of wave propagation over multilayer materials with large change in the dielectric constants from one layer to the next. The conventional FDTD method might have difficulties handling this situation. A second advantage of FVTD over FDTD is its body conformal capability. FDTD uses spatially staggered grids that can only approximate curvilinear boundaries in stair case manner. Though there have been some efforts in the Computational Electromagnetics community to implement the FDTD using nonorthogonal and unstructured grids [10], their achievements at the present time cannot be compared

to those used in FVTD solvers in their flexibility and robustness. This is because the CFD community has a long tradition of treating general curvilinear geometries which arise in fluid dynamics [15]- [18] Of course, the use of curvilinear coordinates adds to the complexity of the solver. A third possible advantage that one can expect from FVTD is its feasibility in implementation of absorbing boundary conditions. The truncation of computational space is a basic dilemma to be addressed in Computational Electromagnetics. Much of the research effort in FDTD has been devoted to the development of appropriate numerical absorbing boundary conditions that can guarantee minimum reflections in the outer boundaries of computational spaces at a reasonable computational cost [19]. Since FVTD is based on characteristic theory of signal propagation, it has the direct control of outgoing waves. With the help of flexible curvilinear grid systems and simple absorbing boundary conditions, one may be able to reduce the reflection from outer boundaries with little extra computation. It should also be mentioned that the FVTD being considered here is suitable for wide band applications.

Some of the reasons that have made the EM community skeptical about this method are the following. First of all, the FVTD is fairly sophisticated both in theory and implementation and inevitably requires large computational resources. This comes from the fact that original algorithms were developed to treat basically nonlinear discontinuous situations in fluid dynamics. But today's demanding electromagnetic problems can include nonlinear and wide band applications which cannot be adequately handled by existing techniques. One possible application of this method is in Antenna problems especially ones with complex curvilinear geometries and high contrast dielectric loading. Currently we finished a simple one dimensional Maxwell solver in homogeneous media and are developing and testing a 2 dimensional solver in a rectangular grid system. As an example of the 1-D solver, Figure 42 shows the propagation of Gaussian pulses in homogeneous space with different Courant numbers (CFL) ranging from 2 to 1.5. Each Gaussian pulse shows no significant dispersion after 1000 time steps. We are currently carrying out a quantitative comparison of FVTD and FDTD in one and two dimensions.

In developing a FVTD code for antenna applications we have several problems to address in our research. The first one is the extension of the solver to 2-D and 3-D in general curvi-

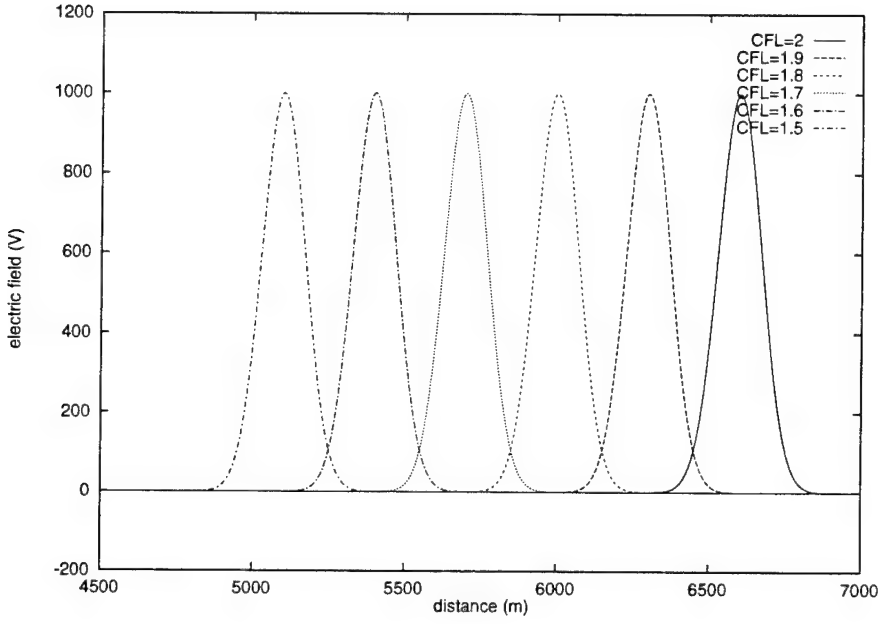

Figure 42: Gaussian pulse propagation for different Courant numbers (CFL) where $CFL = c \triangle t / \triangle x$.

linear coordinate systems. We are investigating several multi-dimension algorithms such as the Strang Type time splitting method. Once we have a FVTD solver in 3-D, we will need a robust 3-D grid generator which may take much more effort. Though there exists commercial 3-D elliptic generation software for Aerospace Engineering, we need to implement our own code to be specifically used in Antenna Radiation problems. Another important point is the problem of excitation which is an integral part of the antenna simulation process. Since the nature of the algorithms in FVTD are quite different from the conventional FDTD, we need to develop methods of field excitation for antenna applications. Note that most of the FVTD applications in the CFD community so far have been only in scattering problems like RCS predictions of aircraft; on the other hand, there have been few attempts to solve radiation problems.

Development of Elliptic Grid Generator for FVTD

As a pre-processor for the FVTD method discussed here there is a need for body-fitting grid generators to deal with curvilinear geometries. This feature is very important for the EM solver to accurately handle curvilinear boundaries in the given electromagnetic problems. Note that there have been extensive research on various aspects of numerical grid generation algorithms for the last two decades. Most of them were intended for use in Computational Fluid Dynamics where curvilinear boundaries are common such as air-foil problems. Among them, the elliptic grid generation algorithm is widely used in many engineering problems for its versatility. For example, for the two-dimensional case, in the elliptic grid scheme, we need to find the transformations $\xi = \xi(x, y)$ and $\eta = \eta(x, y)$ to satisfy Poisson's equation, namely,

$$\nabla^2 \xi = \xi_{xx} + \xi_{yy} = P \tag{75}$$

and

$$\nabla^2 \eta = \eta_{xx} + \eta_{yy} = Q \tag{76}$$

Inverting the above equations, yields,

$$g_{22} x_{\xi\xi} - 2 g_{12} x_{\xi\eta} + g_{22} x_{\eta\eta} = -g_{22} P x_{\xi} - g_{11} Q x_{\eta} \tag{77}$$

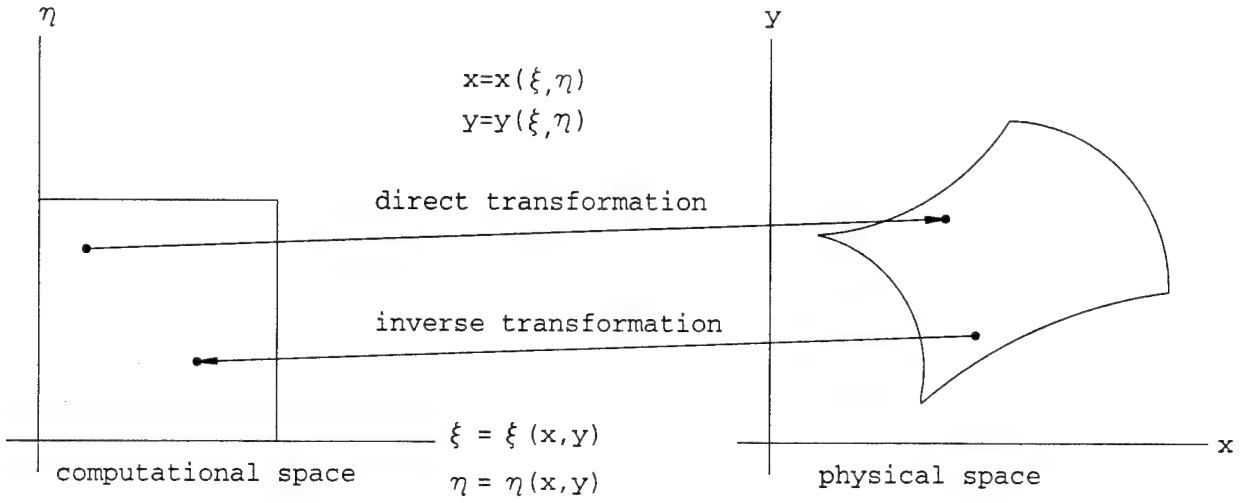

Figure 43: Mapping from computational to physical space.

and

$$g_{22}y_{\xi\xi} - 2g_{12}y_{\xi\eta} + g_{22}y_{\eta\eta} = -g_{22}Py_{\xi} - g_{11}Qy_{\eta} \tag{78}$$

where $g_{11} = x_{\xi}^2 + y_{\xi}^2$, $g_{12} = x_{\xi}x_{\eta} + y_{\xi}y_{\eta}$ and $g_{22} = x_{\eta}^2 + y_{\eta}^2$.

Fig 43 shows the map between the computational and physical spaces.

To generate elliptic grids we need to solve the quasi-linear elliptic equations (77) and (78) numerically. Here we chose the Successive Over Relaxation(SOR) method to solve the elliptic equations because it is relatively easy to implement it while the computational cost is still reasonable. Figure 44 shows the computer generated grid of the transformation represented by $\xi(x,y)$ and $\eta(x,y)$.

So far we finished the implementation of a preliminary version of a two dimensional body-fitting grid generator that can make several simple canonical geometries. Fig 45 shows one example of a body-fitted coordinate system in 2 dimensions. Since the quality and performance of a body-fitted grid for this FVTD method can be estimated properly after we incorporate the elliptic body-fitted grid system into the established EM solver code, we postponed further improvement and concentrated our efforts in the implementation of the EM solver. For a complete version of a 2-D grid generation code we need to make further improvements such as refined internal grid control capability, acceleration of computing speed

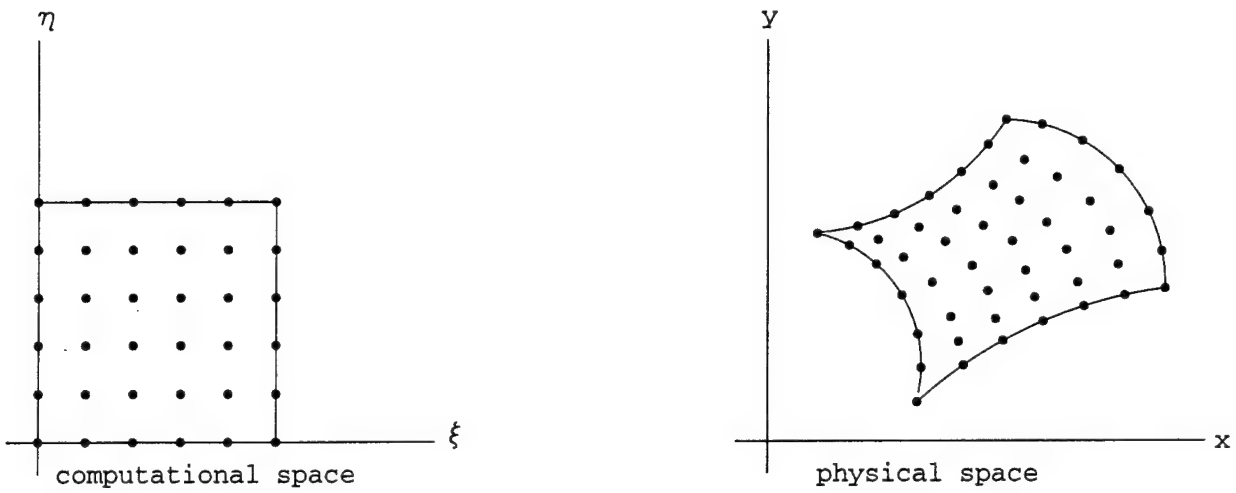

Figure 44: Grids in computational and physical spaces.

by adaptive parameter decision, user friendly interface subroutines for complex boundary definitions, multizone capability and extension to 3-dimensional grids.

4. Hybrid Analysis of the Scattering by Material Bodies and Antennas with Edges/Junctions

As indicated in Section III of the Diffraction Studies Unit, the study of diffraction by material bodies with edges and/or junctions is important due to the widespread use of composite materials in the construction of airplanes, satellites, antenna systems, etc. In the past few years, we have developed/improved analytical methods to study this class of diffraction phenomena in the Diffraction Studies Unit. Due to the complex nature of the field behavior near material surfaces with edges/junctions, the number of canonical shapes that can be studied analytically is very limited. In order to study a wider class of canonical shapes with arbitrary material properties, it is necessary to use some combination of analytical and numerical schemes. The scheme chosen here was the Method of Moments/Green's function approach [20], where the Green's function of a canonical shape is obtained analytically and the rest of the scatterer is handled by means of the Method of Moments (MM). The present study was done for a material cylinder in the presence of a wedge shaped object as depicted in Figure 46. An special case of the material cylinder is an inhomogeneous resistive card

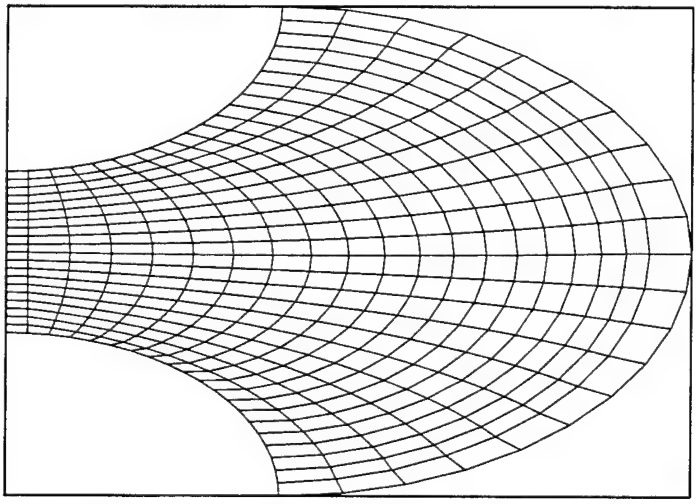

Figure 45: Curvilinear coordinates for two-dimensional body.

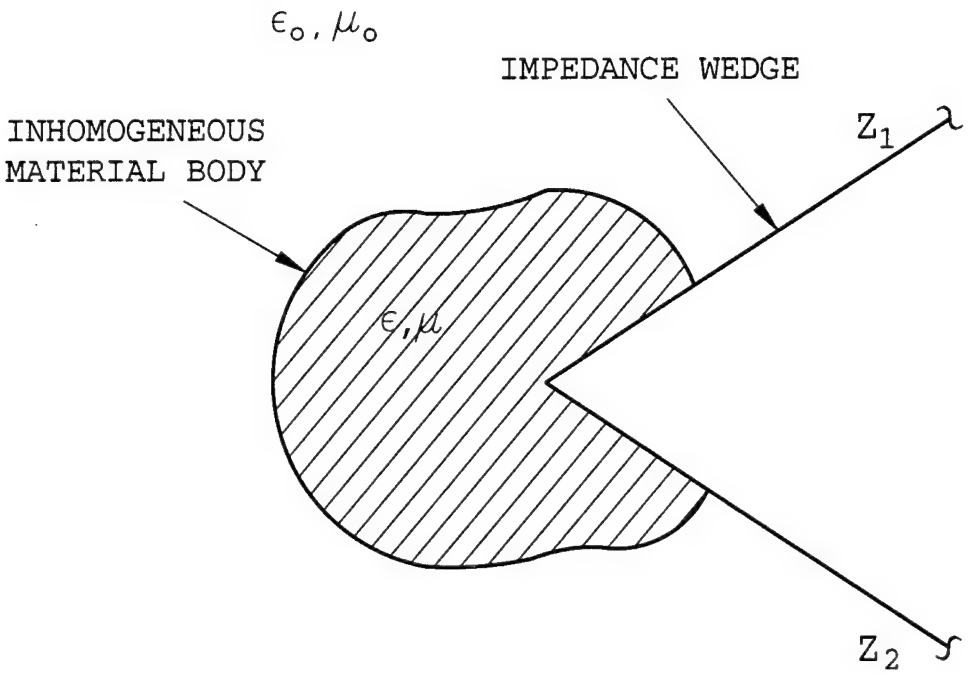

Figure 46: Configuration for a material cylinder in the presence of an impedance wedge.

attached to the edge of the wedge as shown in Figure 47. The faces of the wedge satisfy impedance (Leontovich) boundary conditions. This set of boundary conditions can be used to model coated conductors, rough surfaces or surfaces with corrugations. If necessary, the present Green's function can be modified to included Generalized Impedance Boundary Conditions (GIBC) [21]

The development of the Green's function for the wedge with impedance faces is discussed in the Diffraction Studies unit and will not be repeated here. Using this special Green's function, integral equations were developed for the geometries depicted in Figures 46 and 47. This integral equations are then solved by means of the Method of Moments. The number of unknowns is substantially reduced because the Green's function automatically takes into account the presence of the wedge. However, special care must be taken in solving the

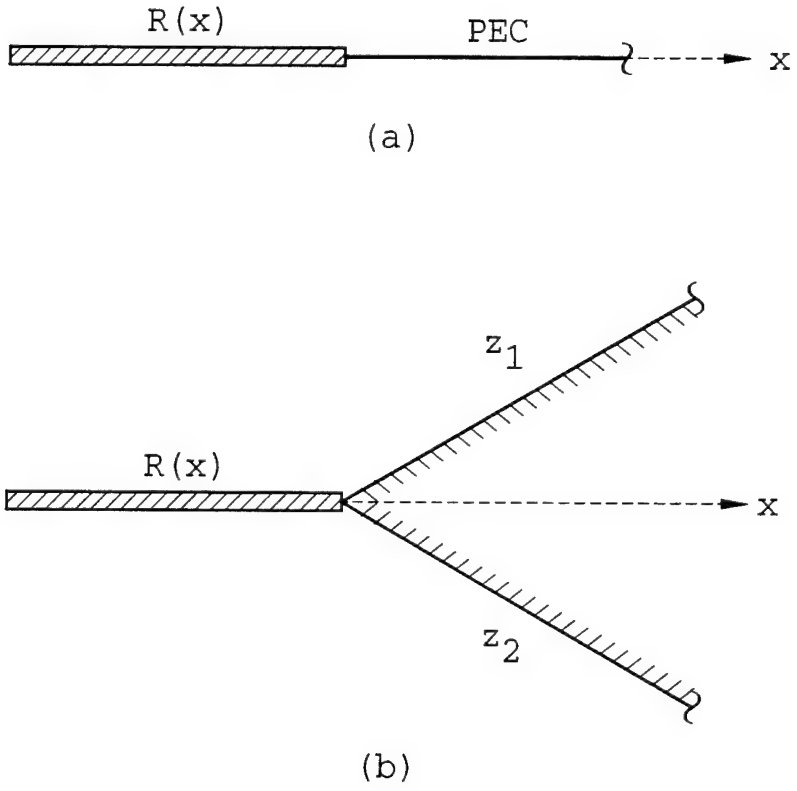

Figure 47: Applications for an inhomogeneous resistive card to reduce the scattering from: (a) a PEC semi-infinite half-plane, (b) an impedance wedge.

integral equation for Figure 47 for the TE_z polarization due to the highly singular nature of the derivative of the Green's function.

An important application of this study is the analysis of the radiation characteristics of antennas mounted on a finite ground plane. The radiated field will in general illuminate the edges of the ground plane from which it is diffracted over a wide angular sector. This diffracted field can then serve to corrupt the radiation pattern of the antenna. As an example, consider a microstrip antenna which is used in many applications. The two-dimensional models of this antenna which are valid in the E- and H-planes are shown in Figure 10 in the Diffraction Studies unit. One way the edge diffraction can be decreased is to attach an inhomogeneous resistive card to the edges of the ground plane. The present analysis can be used to design an optimum resistive taper because it is a very efficient scheme. Note that the design of the taper is a synthesis problem which in general has to be solved numerically due to the nonlinear nature of the cost function. The numerical scheme used in this study to optimize the resistive card is the Conjugate Gradient method (CGM) [22]. The profile of the resistive card is assumed to be exponential, quadratic or some other function. This reduces the number of unknowns to two or three variables. However, if no function is assumed for the taper, the number of unknowns is larger. We are currently planning to use the Genetic Algorithm [23] which is more efficient than the CGM when there are a large number of variables that are being optimized.

Although the MM/Green's function method developed here is applicable to a structure with a single edge, it can be easily adapted to study structures with two or more edges. This is accomplished by obtaining a numerical diffraction coefficient for a single edge and then using this diffraction coefficient to diffract from various edges. Consider the single-edge configuration shown in Figure 48(a); where the total radiated field consists of the two field components U_{go}, which is the geometrical optics field that would be radiated by an antenna that is mounted on an infinite substrate (shown in Figure 48(b)), and U_{d_1}, which is the field that diffracts from the first edge. The pattern for an antenna mounted on a structure with a single edge, and whatever material loading there may be, is generated using the MM/Green's function technique. Then, the pattern for the same antenna, but this time mounted on an infinite substrate, is then generated by using the wedge Green's function. By

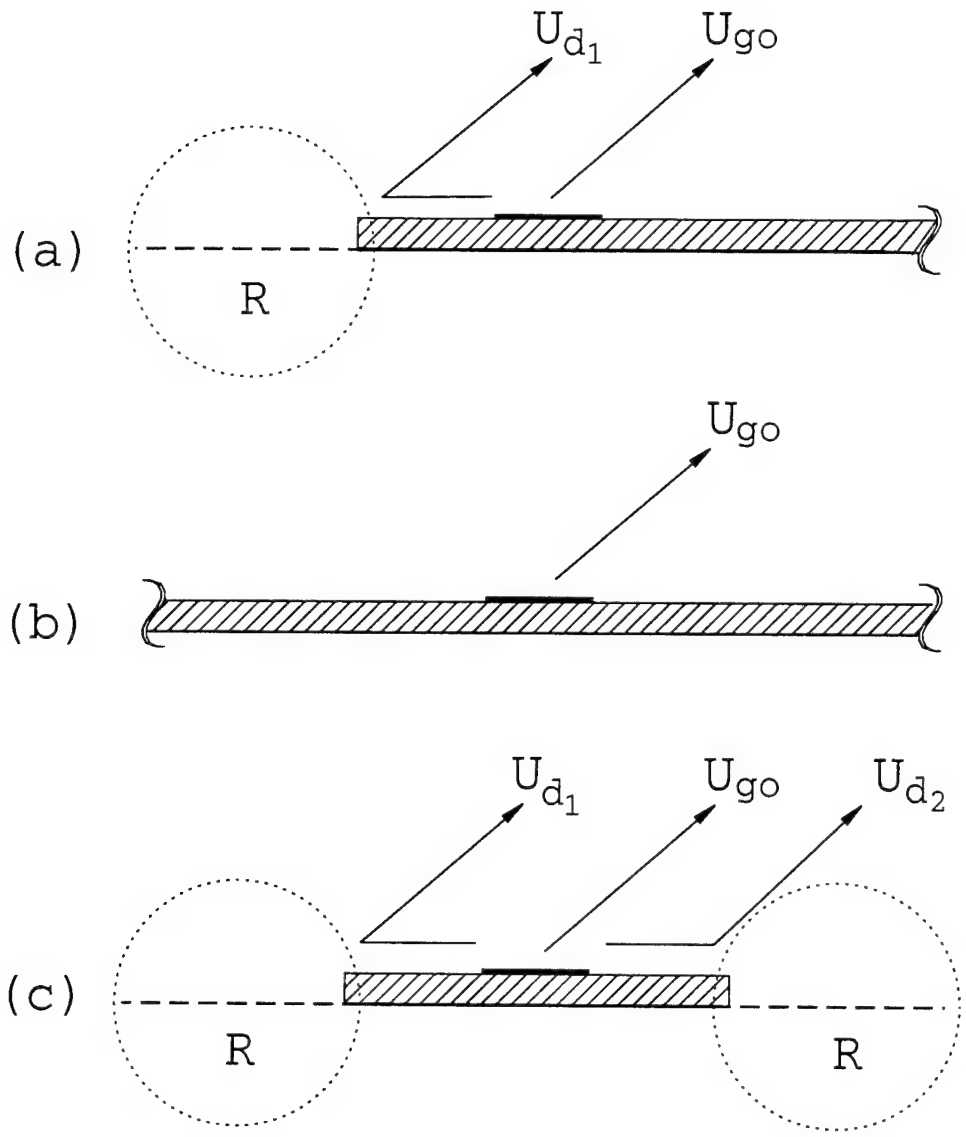

Figure 48: Development of the hybrid MM/GTD technique. The single-edge geometry consists of the fields U_{go} and U_{d_1} (a). The field U_{go} is determined from the infinite geometry (b). Combining the field term U_{d_2} to the single-edge geometry in (a) then gives the pattern for the double-edge geometry (c).

subtracting the pattern of the infinite structure from the pattern for the single-edge geometry, the diffracted field term U_{d_1} is obtained. By shifting the phase and angle reference, this term can then be used to obtain the field that diffracts from the second edge U_{d_2}, which is then superimposed onto the pattern for the single-edge geometry (Figure 48(a)) to give the pattern for the double-edge geometry (Figure 48(c)). This method will be referred to as the hybrid MM/GTD method. Although the pattern which has been generated by this method does not take into account multiple diffraction that can occur between the two edges, it will be shown that the single diffraction model is a very accurate one and can be extremely useful for developing methods to control the edge diffraction. The configuration for an actual antenna that has been examined using the present approach is depicted in Figure 49. The original antenna had an all ground plane and it was the goal of this design to replace a section of that ground plane by tapered resistive cards. The two dimensional model that is used for this finite configuration is shown in Figure 50. This 2-D model is valid in the E- and H-planes where the patch is replaced by the appropriate z-directed current source. Note that the grounded dielectric substrate is modeled by an equivalent impedance surface. One of the advantages of using the wedge Green's function in this analysis is that the different field components can be explicitly separated and studied individually. This can be a valuable tool for providing physical insight into the various mechanisms involved in the radiation and scattering from structures. In determining the radiation pattern of the patch in the presence of the edge, there are three field components that should be considered, which are shown in Figure 51. Usually, the direct space wave is the desired field and the other two, namely, diffracted space and surfaces waves are not desired because they distort the direct space wave. Radiation patterns will be shown for the antenna configuration depicted in Figure 49, where the entire ground plane is a PEC and when a portion of the ground plane is replaced by an optimized resistive card with a quadratic taper. For comparison, measured results as well as MM reference solution are also included. This MM reference solution utilizes a free-space Green's function.

A plot of the radiation pattern for the all PEC ground plane configuration comparing the hybrid MM/GTD and MM solutions for the 2-D model with measured data is shown in Figure 52. The agreement between the hybrid MM/GTD and MM solutions is very good,

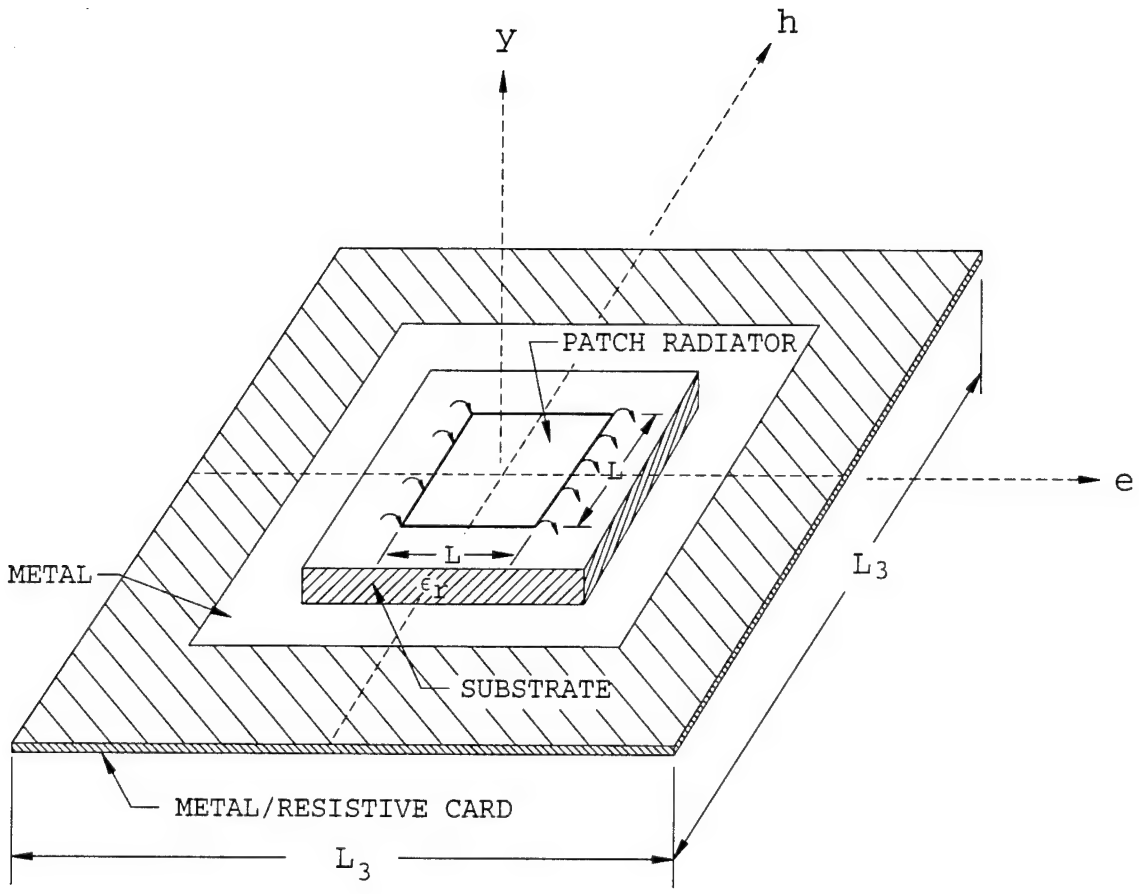

Figure 49: Three-dimensional configuration for a rectangular microstrip patch radiator mounted on a grounded, dielectric slab.

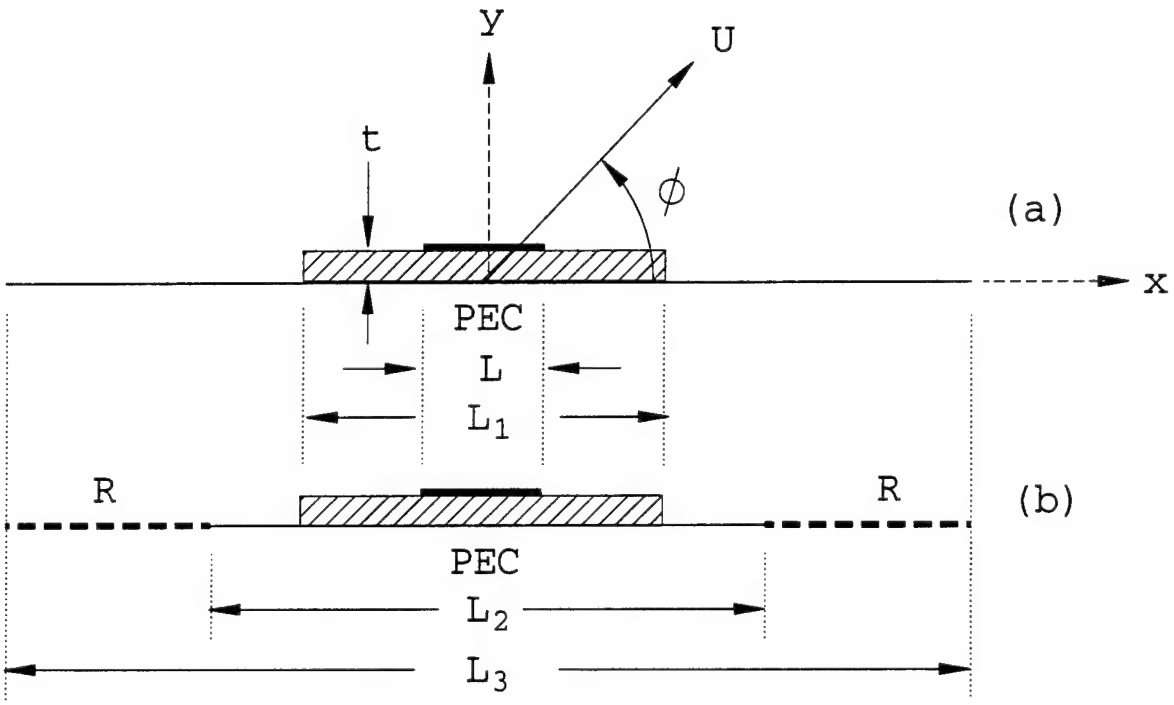

Figure 50: 2-D configuration for the finite antenna of Figure 49. Dielectric substrate can be mounted on an entirely PEC ground plane (a), or on a ground plane where part of the PEC is replaced by an R-card (b).

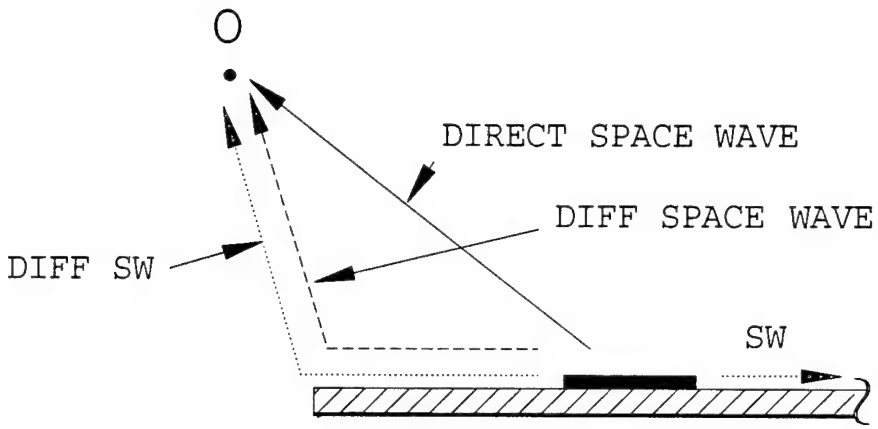

Figure 51: Various field components for a radiating patch on a substrate.

and the slight discrepancies can be mostly explained by the lack of multiple diffraction terms in the hybrid method. The patterns generated by the 2-D model compare reasonably well with the measured data, predicting the same characteristic shape and ripple in the mainbeam as well as the back region, with some noticeable level difference there. This is to be expected since there are some difficulties in measuring the radiation pattern in the back region, mainly due to the presence of the mounting structure and feed network for the antenna. There is also some asymmetry in the measured pattern, which indicates there could be some measurement error as well. A plot showing the same comparisons is next made for the case where the R-card with the quadratic profile replaces a section of the ground plane (see Figure 53). In this case, the agreement between the hybrid and MM methods is noticeably better. This is most likely due to the reduction in the amount of multiple diffraction because of the presence of the R-cards. The R-cards reduce the end point diffraction with the obvious benefit seen by the reduction of the ripple in the mainbeam, which is shown in both the 2-D model and the measurements, and it also decreases the amount of scattering in the back region. The improvement of the antenna performance in the mainbeam region is more clearly shown by the phase plot of Figure 54 for the measured pattern. The diffraction from the edges of the PEC ground plane introduces an oscillating phase variation that indicates an unstable

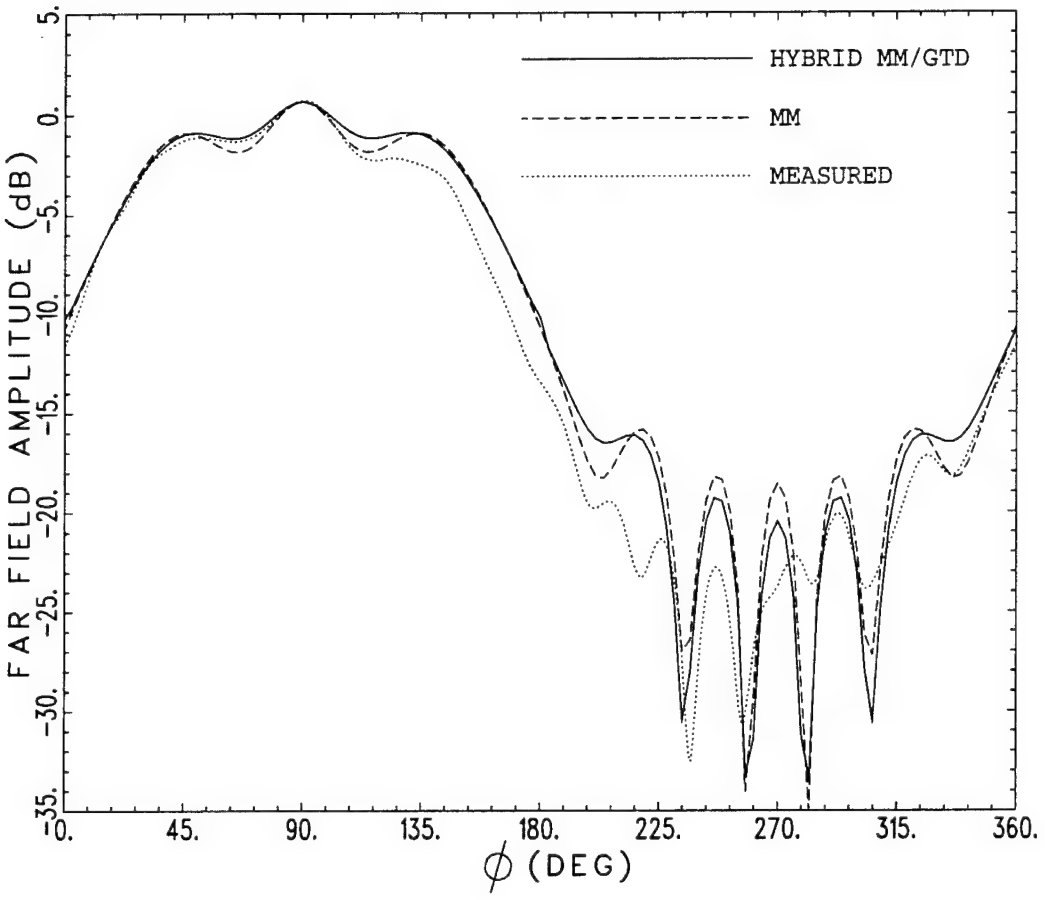

Figure 52: TE_z radiation patterns for the finite configuration of Figure 50(a) (with $L = .3\lambda$, $L_1 = .67\lambda$, $L_3 = 2.54\lambda$, and $t = .0184\lambda$), comparing the hybrid MM/GTD and MM solutions for the 2-D model with measured data for an all PEC ground plane.

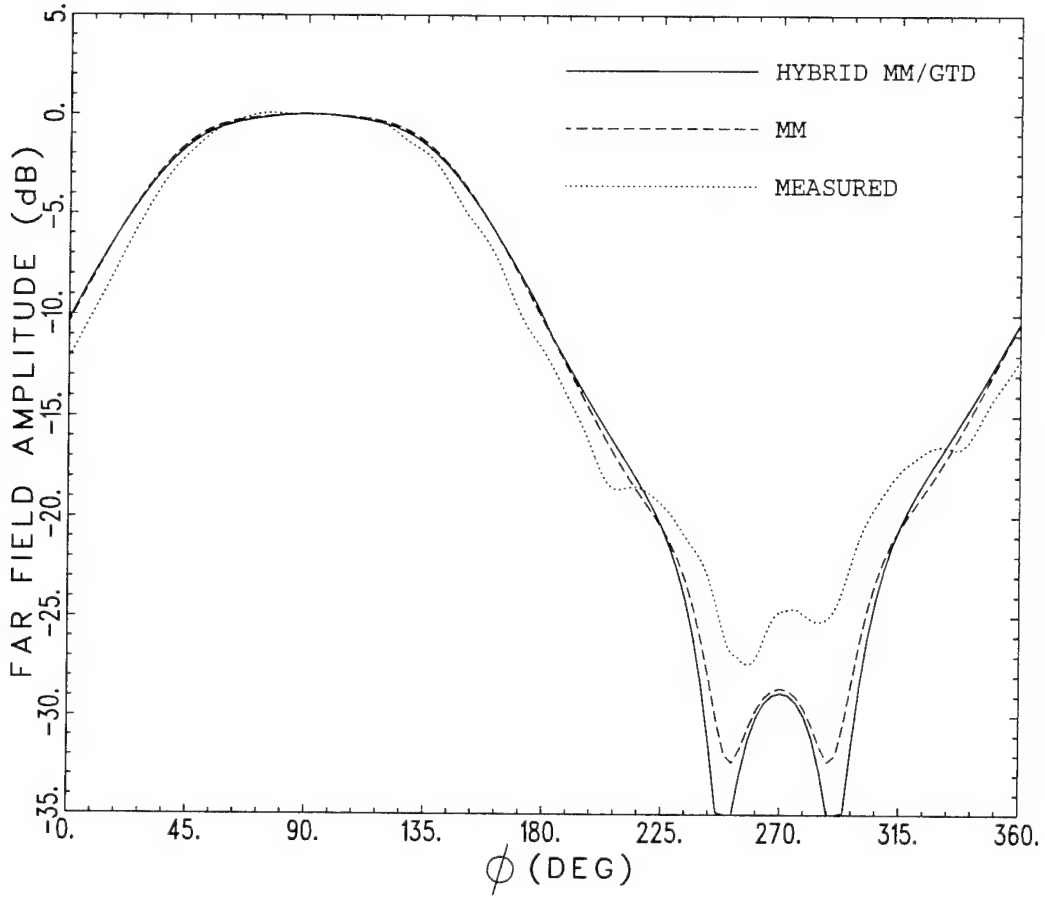

Figure 53: TE_z radiation patterns for the finite configuration of Figure 50(b) (with $L = .3\lambda$, $L_1 = .67\lambda$, $L_2 = 1\lambda$, $L_3 = 2.54\lambda$, and $t = .0184\lambda$), comparing hybrid MM/GTD and MM solutions for the 2-D model with measured data for an R-card with a quadratic profile.

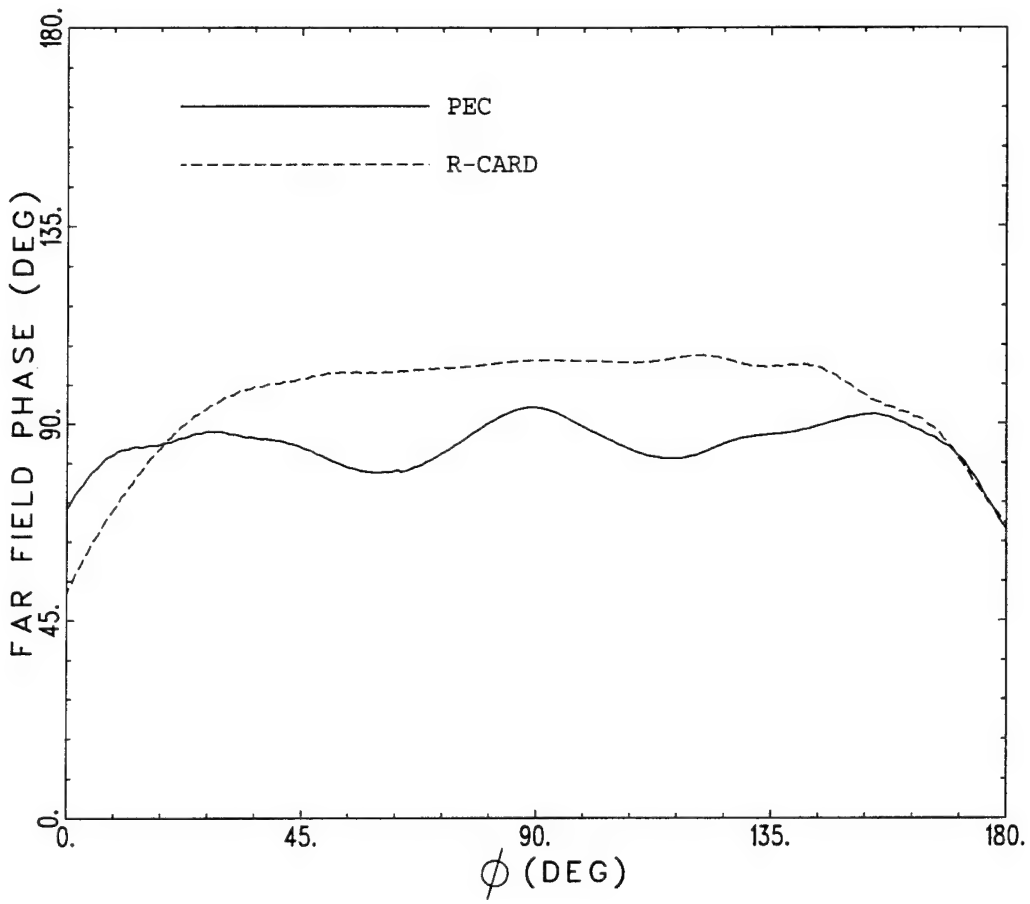

Figure 54: TE_z measured phase responses for the configurations of Figures 50(a) and (b) (with $L = .3\lambda$, $L_1 = .67\lambda$, $L_3 = 2.54\lambda$, and $t = .0184\lambda$), comparing the effect of replacing the PEC with an R-card.

phase center for the antenna, whereas the R-card provides for a very flat phase characteristic which indicates a more stable phase center. Similar patterns can also be calculated for the H-plane, however, they will not be shown here.

5. Conformal Antennas

A hybrid MM-UTD approach was developed previously under JSEP to efficiently analyze large microstrip or slot arrays on planar conducting surfaces with a plane material coating. This was made possible by including an asymptotic or UTD form of the special grounded material slab Green's function which occurs as the kernel of the governing integral equation for solving the unknown currents on the microstrip patches or the fields in the slots. The unknowns are then solved by the MM technique. Since the UTD form of the Green's function

is in closed form as opposed to the exact conventional Sommerfeld integral form which is poorly convergent, the hybrid MM-UTD makes the analysis/synthesis of truly electrically large arrays tractable, as opposed to the use of a conventional brute force numerical MM solution with the exact Sommerfeld integral form of the special Green's function to do the same. It is noted that infinite periodic array theory which is often employed to study such arrays is not strictly applicable because practical arrays are of finite extent and the effects of finiteness of the array are included only crudely in such a infinite array model. On the other hand, the present hybrid approach rigorously accounts for the finiteness of the array and predicts the array edge effects accurately. Work is now in progress to employ this UTD special Green's function, whose usefulness has already been demonstrated for analysis of one-dimensional arrays, to next deal with two-dimensional arrays containing feed networks, etc., to demonstrate the versatility, efficiency and usefulness of this hybrid approach for analysis/design of large finite arrays.

Yet another important hybrid MM-UTD solution is being developed to deal with arrays on non-planar convex surfaces of variable curvature. In particular, as a first step, a UTD form of the special Green's function has been developed for a fully 3-D material coated perfectly conducting convex surface, which for the first time would predict the performance of antennas in or on such configurations and show explicitly in relatively closed form, the effects on fields of such antennas arising from surface curvature and the presence of material coating. It is noted that infinite periodic array theory is not even applicable to such curved surface configurations because arbitrary curvature destroys periodicity in the fields; furthermore, it is note possible to obtain an exact analytical form of the special Green's function for this case. Hence, the importance of developing a special UTD based special Green's function for an arbitrary smooth convex surface with uniform material coating can hardly be overemphasized.

In the recent months, the UTD transition functions involving modified Fock type integrals that appear in the UTD form of the special Green's function, which has been developed for electric or magnetic point sources on an arbitrary perfectly conducting convex surface with a uniform material coating, are being computed numerically in an efficient manner. While some past researchers have evaluated some of the these types of Fock integrals, their procedure is

extremely time consuming. Several useful procedures have been incorporated to significantly speed up the evaluation of these integrals, and to also enhance the accuracy of computations. It is imperative that these special UTD transition functions be computed rapidly to maintain the overall efficiency and utility that are characteristic of the UTD method in general. There are four basic types of UTD Fock integral transition functions which are required in the analysis of radiation and mutual coupling associated with antennas on perfectly-conducting convex surface with uniform material coating. Unlike the Fock integral based UTD transition functions which are universal functions of only a single parameter for the perfectly conducting convex surface (and which hence can be tabulated), the ones for the material coated convex surface depend on at least two parameters. Furthermore, their behavior is more complicated than for the uncoated case. Three out of these four basic Fock type UTD transition functions have been coded efficiently using some useful procedures to sum the "tails" of these infinite Fock integrals in closed form. The remaining fourth basic Fock type function for the coated case is currently under investigation to study its properties carefully so that an intelligent choice of procedures can then be developed to evaluate this Fock type integral efficiently as well. It is expected that the efficient numerical evaluation of these special UTD transition functions will be completed by the end of this year or so. Subsequently, it is proposed to employ this UTD solution in a hybrid MM-UTD formulation to demonstrate its versatility and usefulness in the analysis/design of antenna arrays that truly conform to a general smooth doubly curved convex surface (e.g., the fuselage of an aircraft or missile, or the top of an automobile, etc.). The antenna elements can be relatively arbitrary (slots, monopoles, microstrip patches, etc.) in this hybrid MM-UTD approach. It is important to note that no such solution presently exists, other than this proposed hybrid MM-UTD approach, for the analysis/design of truly general convexly curved, large conformal antenna arrays.

6. High-Frequency Asymptotic Acceleration of the Fast Multipole Method

The fast multipole method (FMM) is a fairly recent development [24] which provides a means of accelerating iterative algorithms for solving large-scale integral equation problems. In our research, the FMM has been improved so that it is substantially faster as will be

explained below. This FMM approach may be applied to electromagnetic integral equation problems where the unknown currents are expanded into N subsectional basis elements. Iterative algorithms, such as the conjugate gradient method, solve for the unknown currents by repeatedly multiplying the $N \times N$ system matrix times the $\mathcal{O}(N)$ current vector. This matrix-vector product computation has an operational count of $\mathcal{O}(N^2)$, and many iterations may be required for convergence. The basic FMM accelerates the matrix-vector multiplication by dividing the N basis elements into M localized groups, and by expressing the matrix interactions between separated groups using multipole expansions. The matrix interactions between basis elements inside the same group and with elements of adjacent groups are expressed in the conventional manner, so singularities associated with certain integral equation formulations may be handled using existing methods. By optimally choosing M to minimize the number of computer operations, the FMM reduces the operational count of the matrix-vector product from $\mathcal{O}(N^2)$ to $\mathcal{O}(N^{3/2})$.

The matrix interactions between separated groups in the FMM are expressed via plane wave translations from the source group to the receiving group. In the basic FMM, plane waves propagate in all directions and all plane waves are translated from the source to the receiver. However, from a high-frequency asymptotic point of view, only plane waves propagating close to the direction from source to receiver should contribute strongly. A windowed version of the FMM has been developed which filters out plane waves propagating at wide angles with respect to the line connecting two separated groups. The windowing filter is derived from an asymptotic evaluation of the plane wave translation operator. The resulting reduction in plane waves further accelerates the FMM to an $\mathcal{O}(N^{4/3})$ operational count without increasing the complexity of the implementation. Figure 55 shows the CPU times for a single matrix-vector multiplication found using brute force, the basic FMM, and the new asymptotically windowed FMM. The solid lines are actual times on a Sun SparcStation IPX, and the dashed lines are estimated projections.

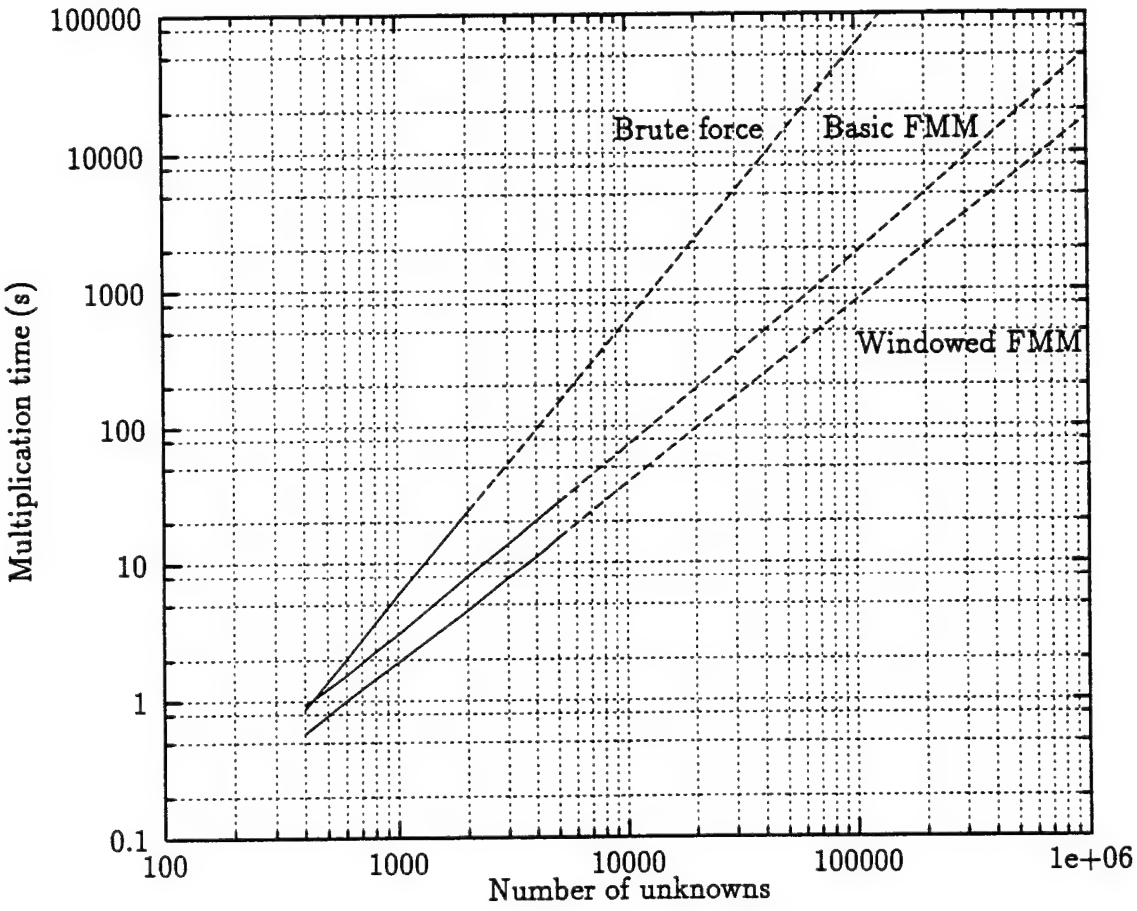

Figure 55: CPU time vs. number of unknowns N for a single matrix-vector multiplication. Solid lines are computed data points and dashed lines are estimated projections. Times are for a Sun SPARCstation IPX workstation.

7. Hybrid High-Frequency Asymptotic/Numerical Methods for Electrically Large Radiating Objects

An important EM phenomenon that needs to be predicted efficiently and accurately is the radiation/scattering of EM waves by electrically large realistic aircraft/missile geometry which obviously falls in the category of complex shapes. Such a complex realistic aircraft/missile configuration typically consists of a large smooth and generally convex fuselage except possibly for an end cap in the nose region to use a forward looking antenna inside a radome, and has large control surfaces (wings, fins, etc.) as well as other small and large perturbations such as antennas, antenna windows, jet inlet cavities, gaps etc. A brute force numerical EM solution of such an electrically large, complex radiating/scattering object can become tremendously inefficient and even intractable. On the other hand, a purely high frequency based EM solution may not be able to handle electrically small but nonetheless potentially important contributors to the overall radiation/scattering, and it also may not be able to handle some electrically large portions for which the pertinent asymptotic high frequency solutions (e.g., the UTD) are not available at the present time. Clearly, therefore, a hybrid MM-UTD approach appears to provide an attractive scheme for analyzing this complex EM configuration, where MM refers to the numerical moment method (MM) for solving the governing integral equation, and the kernel of the integral equation (pertinent Green's function) is to be approximated in this hybrid approach by UTD to a priori account for the basic convex aircraft/missile fuselage shape leaving the unknown induced surface currents to be found only over the remaining part of the aircraft/missile geometry. Such a hybrid MM-UTD approach is far more efficient than a brute force numerical MM solution of the integral equation for the whole geometry or a numerical solution based on the partial differential equations of EM, because the number of unknowns to be solved in the hybrid approach are drastically reduced in comparison to those that need to be found in the brute force numerical solution methods. However, one notes that even with this hybrid procedure, it is possible to still have a large number of unknowns, even though they may be far less than the number of unknowns required to be solved by conventional numerical based methods. It is for this reason one must not only find the best choice of the kernel (Green's function), which is to be represented asymptotically via a UTD approximation, in order to a priori limit the region

of the unknowns to be solved using the MM technique, but one must in addition also find ways to speed up the MM portion of the computations. In particular, the latter implies an efficient choice of basis or expansions functions for the unknown currents and an iterative solution of the MM equation rather than the conventional MM matrix inversion method of solution. Presently, it is planned that the UTD solutions being developed for the smooth convex surface (with or without an end cap) for arbitrary source and field point locations as described in Part IV of the section on Diffraction Studies, will be incorporated into a version of our existing aircraft geometry code which is also simultaneously undergoing additional improvement in its modeling capabilities. It is expected that the relevant UTD results will be incorporated by mid-1996 into this aircraft geometry code. This geometry code will also provide a discretization of the surface geometry as required for the MM part of this hybrid scheme. Once this basic hybrid MM-UTD scheme is demonstrated for a more sophisticated generic aircraft shape than one consisting of just plates and circular cylinders, it will later be extended through a super-hybrid scheme to include additional effects such as those resulting from the presence of an inlet cavity or antennas, etc. It is noted that separate procedures are being developed to deal with inlets, gaps/cracks and antennas, etc. This super hybrid scheme will be highly useful once it is fully developed, for it is expected that this may actually be one of the most tractable approaches for analyzing the radiation/scattering from generic and also actual aircraft/missile shapes.

References

[1] B. Robert, T. Razban and A. Papiernik, "Compact Amplifier Integration in Square Patch Antenna," *Electron. Lett.*, vol. 28, no. 19, pp. 1808–1810, Sept. 1992.

[2] J.A. Navarro, K.A. Hummer and K.Chang, "Active Integrated Antenna Elements," *Microwave Journal*, pp. 115–126, Jan. 1991.

[3] K. Chang, K.A. Hummer and G.K. Gopalkrishnan, "Active Radiating Element using FET Source Integrated with Microstrip Patch Antenna," *Electron. Lett.*, vol. 24, no. 21, pp. 1347–1348, Oct.1988.

[4] J. Lin and and T. Itoh, "Active Integrated Antennas," *IEEE Trans. Microwave Theory and Tech.*, vol. 42, no. 12, pp. 2186–2194, Dec. 1994.

[5] K. Kurokawa, "Some Basic Characteristics of Broadband Negative Resistance Oscillator Circuits," *Bell Syst. Tech. J.*, vol. 48, no. 6, pp. 1937–1955, July–August 1969.

[6] N.D. Kenyon, "A Lumped-Circuit Study of Basic Oscillator Behavior," *Bell Syst. Tech. J.*, vol. 49, no. 2, pp. 255–272, Feb. 1970.

[7] S. Savaria and P. Champagne, "Linear Simulators for Use in Oscillator Design," *Microwave Journal*, pp. 98–105, May 1995.

[8] V. Shankar, W.F. Hall and A.H. Mohammadian, "A Time Domain Differential Solver for Electromagnetic Scattering Problems," *Proc. IEEE*, vol. 77, p. 709, 1989.

[9] V.Shankar, W.F.Hall and A.H.Mohammadian, "A Time Domain, Finite-volume Treatment for the Maxwell Equations," *Electromagnetics*, vol. 10, p. 127, 1990.

[10] A. Taflove, Computational Electrodynamics, Artech House, Inc., 1995.

[11] K.S. Yee, "Numerical Solution of Initial Boundary Value Problems involving Maxwell's Equations in Isotropic Media," *IEEE Trans. Antennas and Propagation*, vol. 14, 1966, pp. 302–307.

[12] J.S. Shang, "Characteristic-Based Algorithms for Solving the Maxwell Equations in the Time Domain," *Ant. & Propagation Magazine*, vol. 37, pp. 15–25, June 1995.

[13] R. Lax and B. Wendroff, "System of Conservation Laws, " *Commun. Pure Appl. Math*, 13(1960) 217.

[14] R.F. Warming and R.M. Beam, "Upwind Second-order Difference Schemes and Applications in Aerodynamic Flows," *AIAA J.*, vol. 14, Sept. 1976.

[15] J.F. Thomson, F.C. Thames, and C.W. Mastin, "Automatic Numerical Generation of Body-fitted Curvilinear Coordinate System for Field Containing Any Number of Arbitrary Two Dimensional Bodies," *Journal of Computational Physics*, vol. 15, July 1974.

[16] G. Birkhoff and R.E. Lynch, "Numerical Solution of Elliptic Problems" SIAM,Philadelphia 1984.

[17] J.F. Thomson,ed. 1982a, Numerical Grid Generation. North-Holland, New York.

[18] J.L. Steger and R.L. Sorenson, "Automatic Mesh-point Clustering near a Boundary in Grid Generation with Elliptic Partial Differential Equations", *Journal of Computational Physics*, vol 33, Dec. 1979.

[19] J.P. Berenger, "A Perfectly Matched Layer for the Absorption of Electromagnetic Waves," *J. Computational Physics*, vol. 114, pp. 185–200, 1994.

[20] E. H. Newman, "An Overview of the Hybrid MM/Green's Function Method in Electromagnetics," *Proceedings of the IEEE*, Vol. 76, No. 3, pp. 270–282, March 1988.

[21] R.G. Rojas, Z. Al-hekail, "Generalized Impedance/Resistive Boundary Conditions for Electromagnetic Scattering Problems," *Radio Science*, Vol. 24, Number 1, pp. 1–12, Jan-Feb 1989.

[22] M. Athans, et al., Systems, Networks and Computation: Multivariable Methods, McGraw-Hill, Inc., pp. 132-136, 1974.

[23] R.L. Haupt, "An Introduction to Genetic Algorithms for Electromagnetics," *IEEE Ant. & Propagation Magazine*, vol. 37, pp. 7–15, April 1995.

[24] R. Coifman, V. Rokhlin and S. Wandzura, "The Fast Multipole Method for the Wave Equation: A Pedestrian Prescription," *IEEE Ant. & Propagation Magazine*, vol. 35, no. 3, pp. 7–12, June 1993.

Refereed Publications:

1. P. Munk and P.H. Pathak, "A Useful Approximate Analysis of the EM Scattering by a Rectangular Antenna Cavity containing an Array of Dominant Mode Waveguide Loaded Slots," *Journal of EM Waves and Applications*, (special issue on EM Scattering), vol. 8, no. 9/10, pp. 1351–1379, 1994.

2. L.M. Chou, R.G. Rojas and P.H. Pathak, "WH/GSMT Based Full-Wave Analysis of Planar Transmission Lines Embedded in Multilayered Dielectric Substrates," *IEEE Trans. on Microwave Theory and Techniques.* vol 43, pp. 119–130, January 1995.

3. F. Obelleiro, J.L. Rodriguez and R.J. Burkholder, "An Iterative Physical Optics Approach for Analyzing the Electromagnetic Scattering by Large Open-Ended Cavities," *IEEE Transactions on Antennas and Propagation*, vol. 43, no. 4, pp. 356–361, April 1995.

4. P. Munk and P.H. Pathak, "EM Scattering by a Dielectric Filled Rectangular Antenna Cavity Recessed in a Ground Plane and Backed with an Array of Loaded Dominant Mode Waveguides," *IEEE Transactions on Antennas and Propagation*, vol. , no. , pp. , 199.

Papers Accepted for Publication

1. P.R. Rousseau and R.J. Burkholder, "A Hybrid Approach for Calculating the Scattering from Obstacles within Large Open Cavities," *IEEE Trans. on Antennas and Propagation.*

2. T.T. Chia, R. Lee, and R.J. Burkholder, "The Application of FDTD in Hybrid Methods for Cavity Scattering Analysis," *IEEE Trans. on Antennas and Propagation.*

3. R.J. Burkholder, P.H. Pathak, H.T. Chou, and D. Andersh, "Generalized Ray Expansion with Elliptic Ray Tubes in Hybrid Analysis of EM Scattering by Open Cavities," Invited Paper, *IEICE Trans. Electronics.*

4. P. Munk and P.H. Pathak, "EM Scattering by a Dielectric Filled Rectangular Antenna Cavity Recessed in a Ground Plane and Backed with an Array of Loaded Dominant Mode Waveguides," *IEEE Transactions on Antennas and Propagation.*

Papers submitted for Publication

1. R.J. Burkholder and D.H. Kwon, "High-Frequency Asymptotic Acceleration of the Fast Multipole Method," submitted to *Radio Science,* Special Section on "Computational Electromagnetics."

Papers in preparation for publication

1. P.H. Pathak, A. Nagamune and R.G. Kouyoumjian, "An Analysis of Compact Range Measurements," submitted to *IEEE Transactions on Antennas and Propagation.*

2. M.F. Otero and R.G. Rojas, "Scattering of a Complex Material Cylinder of Arbitrary Shape in the Presence of an Impedance Wedge."

3. R.J. Burkholder and P.H. Pathak, "A Generalized Ray Expansion for Computing the EM Fields Radiated by an Antenna in a Complex Environment."

4. M.F. Otero and R.G. Rojas, "Application of a Resistive Card to Reduce the EM Scattering from Metallic/Material Edges,"

Conferences/Oral Presentations

1. R.J. Burkholder, "An Iterative Physical Optics Approach for the EM Analysis of Cavities and Other Multi-Bounce Geometries," 11th Annual Review of Progress in Applied Computational Electromagnetics, Monterey, California, March 1995.

2. R.J. Burkholder, P.H. Pathak, H.T. Chou, D. Andersh and J. Fath, "Improved Ray Basis in the Hybrid Analysis of EM Scattering by Large Open Cavities," 11th Annual Review of Progress in Applied Computational Electromagnetics, Monterey, California, March 1995.

3. R.J. Burkholder and D.H. Kwon, "High-Frequency Asymptotic Reduction of the Fast Multipole Method," URSI Radio Science Meeting, Newport Beach, California, June 1995.

4. C.W. Chuang, P.H. Pathak and R.J. Burkholder, "High Frequency Analysis of EM Scattering by Masts and Towers Present in Certain Propagation Environments," URSI Radio Science Meeting, Newport Beach, California, June 1995.

5. R.J. Burkholder, P.R. Rousseau and P.H. Pathak, "A Hybrid Approach for Computing the EM Scattering from Complex Terminations Inside Large Open Cavities," IEEE/APS International Symposium and URSI Radio Science Meeting, Newport Beach, California, June 1995.

6. R.G. Rojas, M.F. Otero, D. Colak and W.D. Burnside,"Synthesis of Tapered Resistive Ground Plane for a Microstrip Antenna," IEEE/APS International Symposium and URSI Radio Science Meeting, Newport Beach, California, June 1995.

7. M. Hsu and P.H. Pathak, "Hybrid Analysis (MM-UTD) of EM Scattering from Finned Convex Objects," IEEE/APS International Symposium and URSI Radio Science Meeting, Newport Beach, California, June 1995.

Ph.D. Dissertations

1. M. Hsu, "Hybrid (MM-UTD) Analysis of EM Scattering by Finned Objects," Winter 1995.

2. M.F. Otero, " Radiation and Scattering from a Complex Material Cylinder in the Presence of an Impedance Wedge," August 1995.

M.Sc. Theses

1. Do Hoon Kwon, "Asymptotic Acceleration of the Fast Multipole Method and its Application to Two Dimensional EM Scattering by Perfect Conductors," Summer 1995.